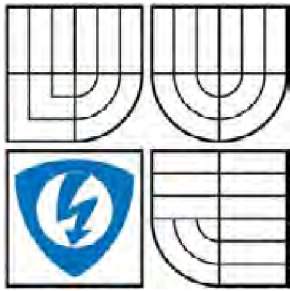# VYSOKÉ UČENÍ TECHNICKÉ V BRNĚ

BRNO UNIVERSITY OF TECHNOLOGY

FAKULTA ELEKTROTECHNIKY A KOMUNIKAČNÍCH TECHNOLOGIÍ
ÚSTAV AUTOMATIZACE A MĚŘICÍ TECHNIKY

FACULTY OF ELECTRICAL ENGINEERING AND COMMUNICATION
DEPARTMENT OF CONTROL AND INSTRUMENTATION

USING ACOUSTIC HOLOGRAPHY FOR VIBRATION ANALYSIS

ANALÝZA VIBRACÍ POMOCÍ AKUSTICKÉ HOLOGRAFIE

DIZERTAČNÍ PRÁCE
DOCTORAL THESIS

AUTOR PRÁCE   Ing. ZDENĚK HAVRÁNEK
AUTHOR

VEDOUCÍ PRÁCE   doc. Ing. LUDVÍK BEJČEK, CSc.
SUPERVISOR

BRNO 2009

Abstrakt

Disertační práce se zabývá bezkontaktní analýzou vibrací pomocí metod akustické holografie v blízkém poli. Akustická holografie v blízkém poli je experimentální metoda, která rekonstruuje akustické pole v těsné blízkosti povrchu vibrujícího předmětu na základě měření akustického tlaku nebo akustické rychlosti v určité vzdálenosti od zkoumaného předmětu. Konkrétní realizace této metody závisí na použitém výpočetním algoritmu.

Vlastní práce je zaměřena zejména na rozbor algoritmů, které využívají k rekonstrukci zvukového pole v blízkosti vibrujícího objektu transformaci do domény vlnových čísel (prostorová transformace), kde probíhá vlastní výpočet. V úvodu práce je vysvětlena základní teorie metody akustické holografie v blízkém poli s popisem základních vlastností a dále rozborem konkrétních nejčastěji používaných algoritmům pro lokalizaci a charakterizaci zdroje zvuku a pro následnou vibrační analýzu. Stěžejní část práce se věnuje pokročilým metodám zpracování, které se snaží určitým způsobem optimalizovat přesnost predice zvukového pole v blízkosti vibrujícího předmětu v reálných podmínkách. Jde zejména o problematiku použitého měřicího systému s akustickými snímači, které nejsou ideální, a dále o možnost měření v prostorách s difúzním charakterem zvukového pole. Pro tento případ byla na základě literárního průzkumu optimalizována a ověřena metoda využívající dvouvrstvé mikrofonní pole, které umožňuje oddělení zvukových polí přicházejících z různých stran a tedy úspěšné měření v uzavřených prostorách např. kabin automobilů a letadel. Součástí práce byla také optimalizace, rozšíření a následné experimentální ověření algoritmů publikovaných v posledních letech pro měření v reálných podmínkách a za použití běžně dostupných akustických snímačů.

Klíčová slova

Akustická holografie v blízkémem poli, analýza vibrací, lokalizace zdroje zvuku, mikrofonní pole, bezkontaktní měření, akustické snímače, měřicí systémy.

Abstract

The main aim of the thesis is application of near-field acoustic holography for non-contact vibration analysis. Near-field acoustic holography is an experimental technique for reconstruction of sound field close to the surface of the vibrating object based on measurement of sound pressure or acoustic particle velocity in certain distance from the examined object. Practical realization of this method depends on used calculation procedure.

The thesis is focused on analysis of acoustic holography algorithms with transformation into wavenumber domain (spatial transformation) where the reconstruction of the sound field near vibrating object is calculated. The introductory part of the thesis describes the theory of near-field acoustic holography with general characteristics and with analysis of most common algorithms used for localization and characterization of sound source and consequent vibration analysis. Principal part of the thesis deals with advanced processing methods where these methods try to optimize the accuracy of prediction of sound field near vibrating object in real environment. In this study, real measurement conditions represent the measurement system with non-ideal acoustic sensors and also areas with reverberant sound field. Based on literature study, there has been optimized and verified the new method which uses double layer microphone array to separate incoming and outgoing sound field, thus allows successful measurement in confined space e.g. cabins of cars and airplanes. Part of the thesis has been also focused on optimization, extension and successive experimental validation of selected classical algorithms published in last decade for possible measurement in real conditions and with common acoustic sensors.

Keywords

Near-field Acoustic Holography, Vibration Analysis, Sound Source Localization, Microphone Arrays, Non-contact Measurement, Acoustic Sensors, Array Measurement Systems.

Bibliographic reference

HAVRÁNEK, Z. *Using acoustic holography for vibration analysis.* Brno: Brno University of Technology, Faculty of Electrical Engineering and Communication, 2009. 115 p. Supervisor: doc. Ing. Ludvík Bejček, CSc.

Declaration

"Prohlašuji, že svou disertační práci na téma "Analýza vibrací pomocí akustické holografie" jsem vypracoval samostatně pod vedením školitele a s použitím odborné literatury a dalších informačních zdrojů, které jsou všechny citovány v práci a uvedeny v seznamu literatury na konci práce.

Jako autor uvedené disertační práce dále prohlašuji, že v souvislosti s vytvořením této disertační práce jsem neporušil autorská práva třetích osob, zejména jsem nezasáhl nedovoleným způsobem do cizích autorských práv osobnostních a jsem si plně vědom následků porušení ustanovení § 11 a následujících autorského zákona č. 121/2000 Sb., včetně možných trestněprávních důsledků vyplývajících z ustanovení § 152 trestního zákona č. 140/1961 Sb."

V Brně dne: Podpis:

Acknowledgement

I would like to thank everybody who helped me during my doctoral studies and with realization of this dissertation. Especially I would like to thank:

- my supervisor Assoc. Prof. Ludvík Bejček for assign this interesting theme and possibility to study the methods of untraditional vibration analysis,

- Assoc. Prof. Finn Jacobsen for helpful consultations during research fellowship at Denmark Technical University,

- Dr.Tech. Jørgen Hald from Brüel & Kjær for deep understanding of the holography methods and the SONAH algorithm implementation,

- my parents and my girlfriend for their support and tolerance during my studies.

Contents

List of Tables

List of Figures

Introduction

Measurement of noise and vibration is one of the basic area of measurement of non-electrical quantities in technical practice [57]. Influence of noise and vibration on environment and humans and systematic pressure on their reducing or limiting causes demands for fast and accurate measurement of acoustic quantities and localization of sources of noise or vibration.

With classical methods of vibration measurement with accelerometers there are difficulties with placement and fixing of the sensor to the measured object which is obviously the problem of all contact measurement methods. Also the weight of the sensor plays its role and can cause large measurement error when the examined object is very small. And the measurement with contact sensors on moving parts (e.g. rotating machines) is more complicated and sometimes impossible [57].

Therefore the non-contact methods have been developed systematically in last decades. Their main advantage is basically in zero influence of measurement object without affecting the object surface or its acoustic parameters. There can be used many principles of measurement starting with pure acoustic, where the acoustic quantities is evaluated (e.g. sound pressure, sound intensity, etc.) and ending with methods for measurement surface displacement of the vibrating object based on laser interferometry [15, 48].

There are usually used intensity probes, calibrated microphones or microphone arrays during measurement of acoustic quantities. The microphone arrays (arrays of acoustic sensors generally) is very useful for localization of source of vibration which produces noise and for creation of noise maps above vibrating objects. For processing of measured data from microphone arrays the acoustic holography methods are used. Acoustic holography is an experimental technique for processing the input data obtained by measurement in hologram area. Input information have to be processed effectively to obtain accurate values of acoustic quantities which describe generated sound field from vibrating surfaces of analyzed objects and consequently could describe the vibrating source itself (energy, location, etc.). For that reason the algorithms and methods for processing input holographic data are developed. With the rising demands on accuracy and speed of calculation of acoustic quantities the new algorithms have to be developed or existing algorithms need to be optimized for new applications or environments [44, 16].

This doctoral thesis thus deals with optimization of existing and development of new acoustic holography algorithms for areas where existing algorithms fails or they are less accurate (confined space, cabins, etc.). The algorithms published in last two decades were taken in account and the main orientation of this thesis was selected to focus on acoustic holography methods based on transformation into wavenumber domain and with measurement systems using novel double layer microphone array. The next chapter describes general theory of acoustic holography method and presents the main approaches in processing of data with existing algorithms and measurement systems.

Future research should be focused on methods using double layer microphone array where there could be applied iterative procedure of prediction of sound fields between

layers to enlarge the originally measured hologram area to open the possibility of better measurement with "patch" to "patch" principle. Also future development of measurement systems based on MEMS sensors could be valuable.

State of the Art 2

The main objective of this thesis is a localization and characterization of sound sources and vibration analysis with non-contact methods, especially with near-field acoustic holography (NAH). In this chapter, the basic theory and state-of-the-art of the acoustic holography methods is described.

2.1 Basic Theory of Near-field Acoustic Holography

Near-field acoustic holography is an experimental technique for localization and quantification of sound sources. In general the holography is a technique carrying large amount of information recorded in a plane (holography plane) to reconstruct three-dimensional wave field and thus compose 3D picture of any observed quantity.

In acoustics, the time record of an acoustic quantity (usually sound pressure) in holography plane carries all information about 3D sound field near the plane. The 3D sound field can be expressed with pressure sound field, acoustic particle velocity vector field or field of sound intensity vectors. From these acoustic quantities the mechanical quantities of sound (vibration) source surface could be determined consequently (surface velocity, location and strength of driving mechanical force). The information in the acoustic hologram are an amplitude and phase of measured acoustic quantity (usually sound pressure) and the variation in time.

Acoustic holography also removes the wavelength resolution limit of reconstructed picture of classical holography, where the length of the radiating wave defines the overall resolution in the 3D space. This feature can be achieved in near field by including special part of the sound field in holography calculation. This statement will be described in next paragraphs.

The wave field near sound source can be expressed as infinite number of waves in defined geometry (planar, cylindrical, spherical) as expressed in Fig. 2.1. The most common geometry used in the acoustic holography calculation is planar, thus wave field is expressed as a composition of plane waves.

The sound field generated by the source as propagating in space can be expressed differently based on distance to the source. If the observation point is closer to the source surface than the half of the wavelength ($\lambda/2$) of the radiating wave then we talk about near-field. Otherwise the observation point is in far-field. The difference between these two domains is in the composition of wave field existing in the domains. The near-field domain contains two types of waves, the propagating waves and the evanescent waves. The propagating waves as title describes propagates from the source through the space without changing their amplitudes (neglecting the losses in the medium), but their phase is changing. On the other hand the phase of the evanescent waves remains constant, but the amplitude is changing.
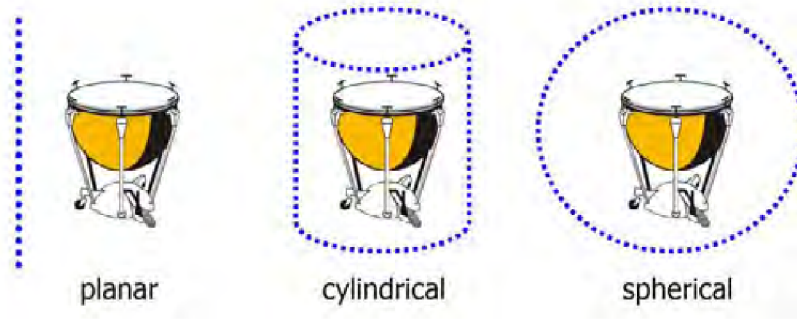
Figure 2.1: Common geometries used in acoustic holography [33].

Spatial angular frequency k (wavenumber) of the plane wave is defined in Eq. (2.1).

$$k = \frac{2\pi}{\lambda} = \frac{\omega}{c}, \tag{2.1}$$

where λ is the wavelength [m],
 ω is angular frequency in time domain $[rad.s^{-1}]$,
 c is a speed of sound $[m.s^{-1}]$, in air $c = 343\ m.s^{-1}$.
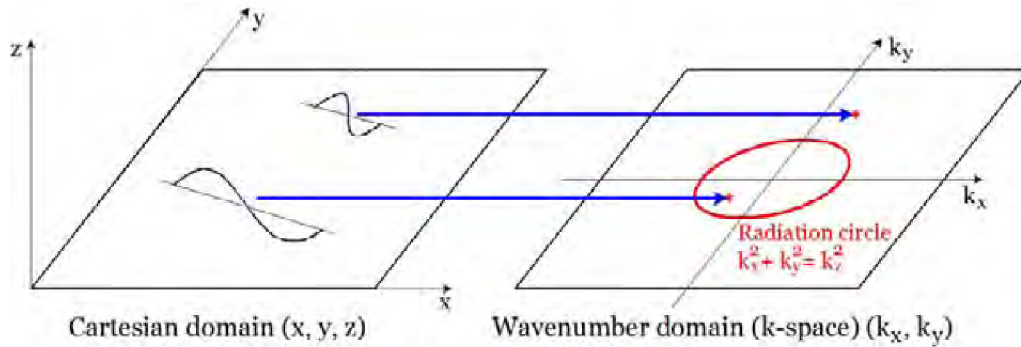
Figure 2.2: Relation between spatial domain and wavenumber domain in acoustics [15].

For calculation of sound quantities near vibrating surface or near acoustic sound source determination of propagation of sound waves should be determined. The governing equation for wave propagation in near field is homogenous wave equation as described in Eq. (2.2). The pressure sound field in time domain $p(\mathbf{r}, t)$ near source is determined by this wave equation.

$$\nabla^2 p - \frac{1}{c^2} \frac{\partial^2 p}{dt^2} = 0, \tag{2.2}$$

where c is speed of sound $[ms^{-1}]$,
 ∇^2 is Laplace operator $\frac{\partial^2}{\partial x^2} + \frac{\partial^2}{\partial y^2} + \frac{\partial^2}{\partial z^2}$.
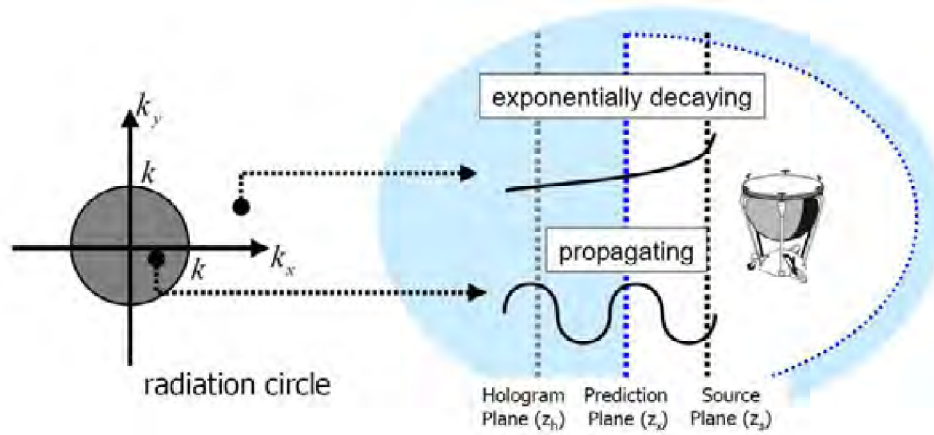
Figure 2.3: Propagating and evanescent waves in k-space and holograms' configuration in spatial domain [33].

2.1.1 Acoustic Holography Based on Transformations to k-space

Classical NAH is based on spatial transformation, where the most used is Fourier transform. The transformation pair is described in Eq. (2.3) and Eq. (2.4).

$$P(k_x, k_y, z, \omega) = \int_{-\infty}^{\infty} \int_{-\infty}^{\infty} \int_{-\infty}^{\infty} p(x, y, z, t) e^{j(k_x x + k_y y - \omega t)} \, \mathrm{d}x \, \mathrm{d}y \, \mathrm{d}t \qquad (2.3)$$

$$p(x, y, z, t) = \frac{1}{(2\pi)^3} \int_{-\infty}^{\infty} \int_{-\infty}^{\infty} \int_{-\infty}^{\infty} P(k_x, k_y, z, \omega) e^{-j(k_x x + k_y y - \omega t)} \, \mathrm{d}k_x \, \mathrm{d}k_y \, \mathrm{d}\omega \qquad (2.4)$$

The usefulness of using transformation into the wavenumber domain is easier calculation of convolution in wavenumber domain. After the transformation, recalculation of sound pressure to any parallel plane near or far from the source can be processed by simple multiplication of the image pressure by the propagator. There can be defined two general approaches based on configuration of prediction and measurement (holography) planes. The brief look on the possible configurations can be expressed in Fig. 2.4.

If all sound sources is located on or below vibrating surface each transformation equation can be expressed accordingly in Eq. (2.5), Eq. (2.6).

- Forward transformation of sound fields (for $z_x > z_h$)

$$P(k_x, k_y, z_x, \omega) = P(k_x, k_y, z_h, \omega) e^{j\sqrt{k^2 - k_x^2 - k_y^2}(z_x - z_h)}. \qquad (2.5)$$

- Backward transformation of sound fields (for $z_x < z_h$)

$$P(k_x, k_y, z_x, \omega) = P(k_x, k_y, z_h, \omega) e^{-j\sqrt{k^2 - k_x^2 - k_y^2}(z_h - z_x)}. \qquad (2.6)$$

Exponential part of the Eq. (2.5) is called direct transformation function (propagator) and is constituted with Green's function G_p, which can be rewritten in Eq. (2.7).
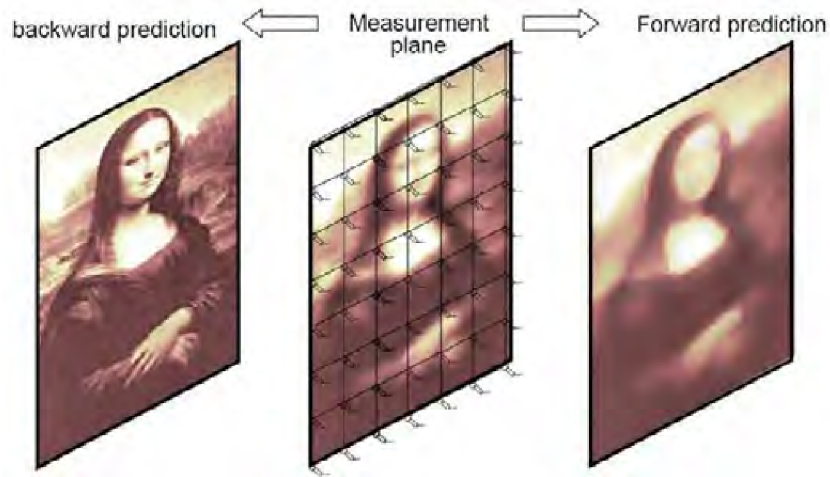
Figure 2.4: Possible predictions with acoustic holography method [33].

$$G_p\left(k_x, k_y, z\right) = e^{jk_z z} \tag{2.7}$$

where $k_z = \sqrt{k^2 - k_x^2 - k_y^2}$.

In the backward transformation the propagator is defined with indirect transformation function (indirect Green's function). The only difference between direct and indirect Green's function is in the sign of the exponent.

The resulting pressure image can be transformed to spatial domain by using inverse Fourier transformation. The whole equation describes the above mentioned procedure can be written by this simple notation in Eq. (2.8).

$$p_{z_x}\left(x, y, z_x\right) = F_x^{-1} F_y^{-1} \left[F_x F_y\left[p\left(x, y, z_h\right)\right] G_p\left(k_x, k_y, z_x - z_h\right)\right] \tag{2.8}$$

The Fourier transform represents the plane wave decomposition where to types of waves can be expressed as described in previous chapter. The recalculation of propagating waves, which don't change their amplitudes while propagating while changing their phase, closer to sound source surface (backward transformation) can be described in Eq. (2.9).

$$P(k_x, k_y, z_x, \omega) = P\left(k_x, k_y, z_h, \omega\right) e^{-j\sqrt{k^2 - k_x^2 - k_y^2}(z_h - z_x)} \tag{2.9}$$

The evanescent waves, which change their amplitude during the propagation, but phase remains stable, are strongly amplified when the distance to the source surface decreases. This can be represented in Eq. (2.10).

$$P(k_x, k_y, z_x, \omega) = P\left(k_x, k_y, z_h, \omega\right) e^{\sqrt{k_x^2 + k_y^2 - k^2}(z_h - z_x)} \tag{2.10}$$

2.1.2 Spectral Leakage, Spatial Sampling and Aliasing, Hologram Aperture

While using 2D Fourier transformation from spatial to wavenumber domain, common characteristics of the transformation should be taken in account. There are dependencies in sampling distance, aperture size and continuity of the signal in original (spatial) domain with spectral bandwidth, resolution and leakage in projection (wavenumber) domain. Some of the parameters of input sound pressure signal could not be neglected to obtain corresponding wavenumber spectrum and correctly predict the sound field.

Spectral Leakage

The first common characteristic of transformation from spatial to wavenumber domain is a spectral leakage. The spectral leakage is caused by discontinuity on the edges of the 2D input data signal (measurement plane), because Fourier transform suppose the periodicity of input signal. To reduce the errors caused by Fourier transformation which creating unwanted high wavenumber components, the smooth periodicity of original measured data has to be fulfilled. This can be done by windowing of the original hologram aperture. The usual shape of the spatial window is rectangular cosine window (Tukey window) with the transfer function written in Eq. (2.11) [44].

$$w(x) = 0.5 - 0.5 \cos \left[\pi(x - \frac{L_x}{2})/x_w \right] \tag{2.11}$$

The procedure to minimize the spectral leakage is expressed in Fig. 2.5. The discontinuity on the edges is removed, but anyway some of the input signal information is lost. In literature there are few studies on how to construct the ideal shape of the window to minimize errors in reconstruction, especially on the edges of the reconstruction plane [34, 39].

original spatial data   window function   windowed spatial data
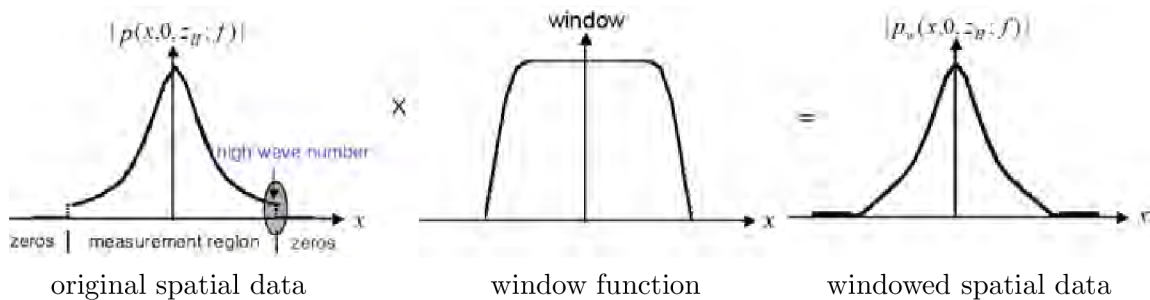
Figure 2.5: Procedure to minimize spectral leakage by windowing in spatial domain [33].

Spatial Sampling and Aliasing

The spatial sampling, in other words discrete measurement in hologram plane, defines the bandwidth of the wavenumber spectrum (the size of 2D k-space). Thus it defines how many evanescent waves (plane waves outside radiation circle) are present in the spectrum. The amplitude of evanescent waves with high wavenumber is rising reversely with the distance from the sound source. From this assumption there should be satisfied

the rule for spacing between discrete measurement point Δ and distance from the source surface d (Fig. 2.6). The rule of thumb is that $\Delta < d$ [33].
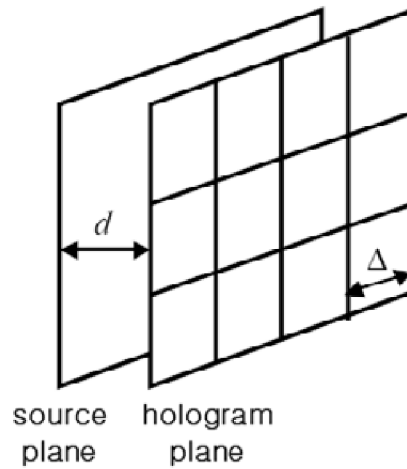
Figure 2.6: Spatial sampling interval and standoff distance in acoustic holography [33].

The effect of changing the distance d between source surface (prediction plane) and measurement (hologram) plane is described in Fig. 2.7. There is demonstrated the situation when the distance to the source is small, thus many high wavenumber (evanescent) components are present in the measured pressure spectrum, but the spacing of discrete measurement points (microphone positions) is not sufficient and spatial aliasing occurs.
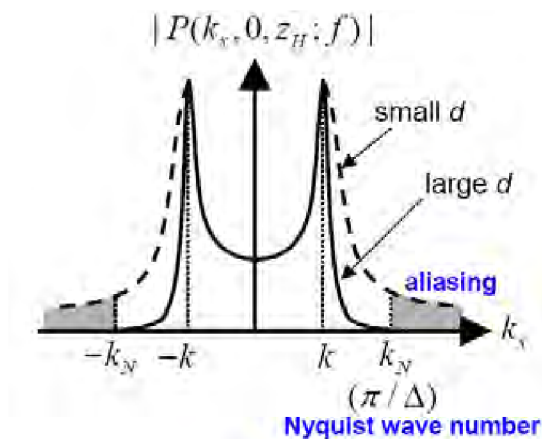
Figure 2.7: Definition of spatial aliasing in k-space with respect to sampling interval and standoff distance [33].

Hologram Aperture

The hologram aperture is a dimension of the 2D area where the discrete spatial sampling of the input sound field is carried out. After inverse Fourier transformation of wavenumber spectrum back to the spatial domain due to the circular convolution in transformation, ghost images of the original aperture are present as expressed in Fig. 2.8.
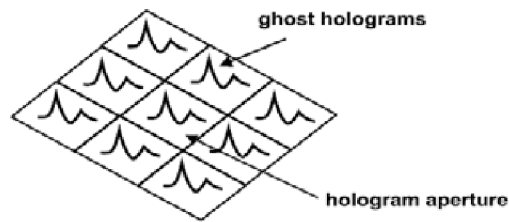
Figure 2.8: Ghost images of original hologram in spatial domain after 2D Fourier transformation [33].

To enhance the resolution in wavenumber domain and move ghost images faraway there can be used the treatment of the original hologram which includes enlargement of the hologram by zero padding in spatial domain. The resulting situation in spatial domain after direct and inverse 2D Fourier transformation of the zero padded original hologram is in Fig. 2.9.
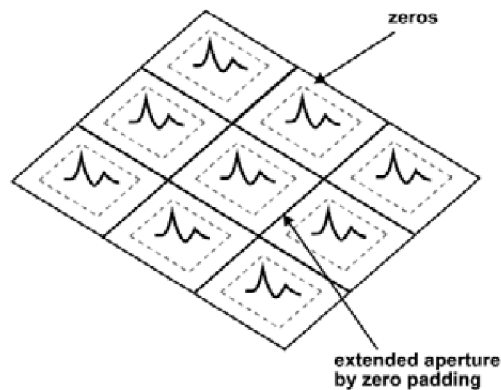
Figure 2.9: Resulting spatial domain after 2D inverse Fourier transformation of zero padded original hologram [33].

2.1.3   NAH with Simple k-space Filter

The reconstruction of the acoustic quantities near examined source is provided by simple basic acoustic holography calculation, where the measured pressure or velocity field in the hologram position is multiplied with propagator. This multiplication is ill-posed problem because the propagator amplifies evanescent components (waves lying outside radiation circle) and can also amplify noise and all distortion caused by imperfections of the measurement path must be taken in consideration. Presence of noise signal in the measurement can not be avoided thus some kind of filtration in wavenumber domain (k-space) should be realized. If there is no filtration in k-space the resulting sound field in prediction plane could be totally damaged and important information usually obtained with backward prediction will be lost. Filtration is applied to wavenumber spectrum of an acoustic quantity obtained in holography plane as expressed in Eq. (2.12).

$$P_{zx} = P_{zh}G_{pi}K(k_x, k_y) \qquad (2.12)$$

where G_{pi} is the backward propagator (Green's function),
         $K(k_x, k_y)$ is a low-pass filter in wavenumber domain.

The low-pass filter in k-space is usually realized with using Harris exponential two-dimensional window defined in Eq. (2.13) [44].

$$K(k_x, k_y) = \begin{cases} 1 - \frac{1}{2}e^{(\left|\sqrt{k_x^2+k_y^2}\right|/k_c - 1)/\alpha} & \text{for} \quad \left|\sqrt{k_x^2 + k_y^2}\right| < k_c, \\ \frac{1}{2}e^{(1-\left|\sqrt{k_x^2+k_y^2}\right|/k_c)/\alpha} & \text{for} \quad \left|\sqrt{k_x^2 + k_y^2}\right| > k_c, \end{cases} \qquad (2.13)$$

where α is a parameter defining the steepness of the filter shape,
         k_c is a spatial wavenumber determining the cut-off frequency of the wavenumber filter.
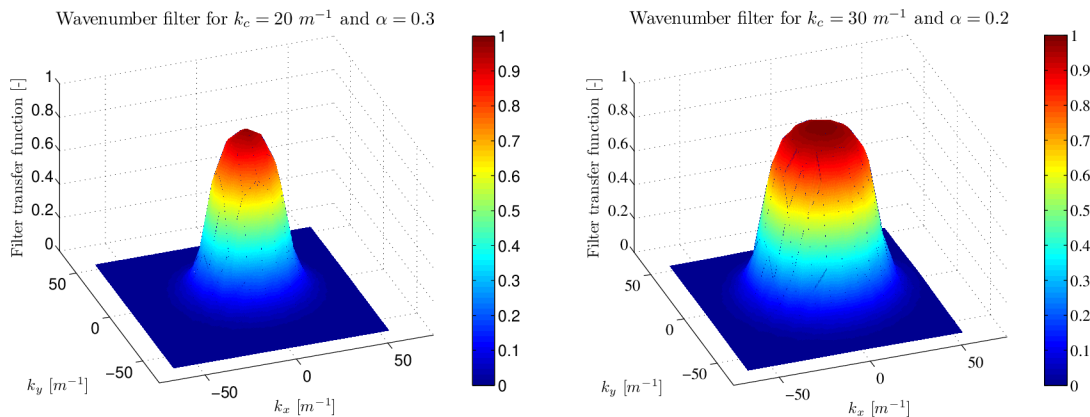
Figure 2.10: Shape of the transfer function of the wavenumber domain filter for $k_c = 20$, $\alpha = 0.3$ (left) and $k_c = 30$, $\alpha = 0.2$ (right).

The setup of filter parameters depends on amount of noise presented in the measurement. This information could be obtained through an experiment or set with some general knowledge about the measurement system and their characteristics. The cut-off frequency is usually set from 0.3 to 0.8 times the Nyquist frequency (wavenumber) of the measured input wave spectrum and the steepness of the filter α is selected at about 0.2.

2.1.4   Iterative NAH with Recursive Filtration

Improved variant of the algorithm with k-space filter is iterative NAH algorithm. The principle of the algorithm is using forward prediction of the first estimation of the sound field from reconstruction plane z_x to measurement (holography) plane z_h and comparison of the forward prediction result with originally measured values. All prediction calculation is performed in wavenumber domain. The difference between the wavenumber spectrum of sound pressure field values calculated with forward prediction and the spectrum of true pressure values measured in holography plane represents the prediction error which is subtracted from original spectrum estimation of sound pressure field in reconstruction plane and the whole procedure is repeated [15, 3]. The core part of the iterative calculation procedure of sound field in prediction plane can be defined in Eq. (2.14) [17].

The first estimation of the reconstructed field is made with simple setting of wavenumber filter (see chapter 2.1.3), where the cut-off frequency is selected to one half of the maximum frequency of measurement, equals to stepping in spatial domain (distance between microphones). This estimation is later used in iterative technique based on recursive Wiener filtering algorithm.

$$P_{zx} = P_{zx-1} + S \cdot (P_{zh} - G_p \cdot P_{zx-1}) \qquad (2.14)$$

where P_{zx} is a wavenumber spectrum of sound pressure field in prediction plane,

P_{zx-1} is a wavenumber spectrum of sound pressure field in prediction plane determined on previous iteration result or during the first step with initial estimation of sound field based on simple algorithm with k-space filter,

S is a feedback operator,

P_{zh} is a wavenumber spectrum of sound pressure field measured in the holography plane,

G_p is a direct (forward) transformation function (Green's function).

As a feedback operator S there can be used Wiener optimal filter which oneself guarantees the convergence of the whole iterative procedure. The Wiener filter in wavenumber domain can be expressed in Eq. (2.15) [17].

$$W(k_x, k_y, z_h - z_x) = \left(\frac{G_p^*}{\left|G_p\right|^2 + \varepsilon^2} \right) \qquad (2.15)$$

where G_p^* is a complex complement to the wavenumber spectrum of direct transformation function ,

ε is a level of unwanted disturbing signal (e.g. noise) which defines the dynamic range of the measurement of sound field values in holography plane.

Wiener filter incorporates regularization parameter ε to adjust transfer function of the filter. This parameter reduces very high evanescent wave amplification in recursive Wiener filtering, thus eliminates influence of the noise and imperfections in the measurement (non-ideal transducers). The regularization coefficient in the transfer function of Wiener filter can be represented in Signal-to-Noise Ratio (SNR), describing the expected difference between measured values and overall noise in the measuring path.

$$W(k_x, k_y, z_h - z_x) = \frac{G_p^*}{|G_p|^2 + 10^{-\frac{SNR}{10}}}$$ (2.16)

where SNR is Signal-to-Noise ratio of the input measured pressure signal [dB].

The whole iterative calculation procedure with Wiener filter application is on the diagram in Fig. 2.11.
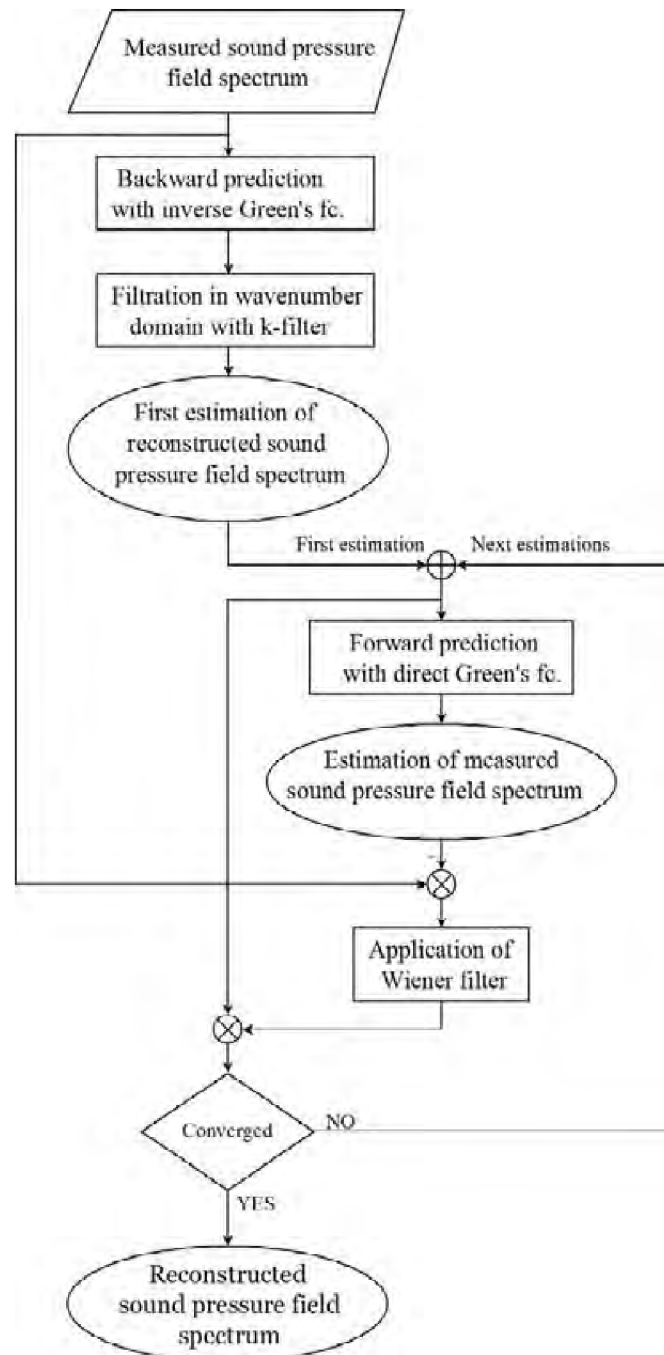
Figure 2.11: Diagram of calculation procedure of iterative NAH algorithm.

2.1.5 Acoustic Holography with Direct Calculation in Spatial Domain

In this section there are presented the acoustic holography algorithms which predict the sound field near source with direct calculation of backward propagation in the spatial domain without using transformation into wavenumber domain. These methods are usually called "patch" methods because there are no disturbing effects on the hologram edges in compare with algorithms based on Fourier transformation.

Statistically Optimized Near-field Acoustic Holography (SONAH)

Statistically optimized near-field acoustic holography (SONAH) is one of the so-called patch holography algorithms which doesn't use spatial transforms and thus avoid leakage. SONAH assumes that if there can be found the appropriate wave spectrum, it means sufficient set of elementary waves in Eq. (2.18), which creates the sound field propagated from the source to the microphone positions, the coefficients which describes this elementary wave set, can also in similar way describe the pressure set which is in measured and examined points in the sound field.

In the mathematical expression the above theory assumes that one can determine a transfer matrix for backward propagating sound pressure data measured at N points in the hologram plane to the prediction plane [18, 19] as can be represented in Eq. (2.17).

$$p(x, y, z_x) \approx \sum_{n=1}^{N} c_n(x, y, z_x) p(x_n, y_n, z_{\mathrm{h}}) \tag{2.17}$$

where c_n is a coefficient representing the contribution of each elementary wave to the total sound field.

The above equation requires an infinite set of elementary waves of the form defined in Eq. (2.18).

$$\Phi_{\mathbf{K}}(x, y, z) = e^{j(k_x x + k_y y + k_z z)} \tag{2.18}$$

This set of elementary waves composes the total radiated sound field and satisfies the similar equation as Eq. (2.17). The mathematical expression of finite sum of elementary waves is written in Eq. (2.19).

$$\Phi_{\mathbf{K}_m}(x, y, z) \approx \sum_{n=1}^{N} c_n(x, y, z_{\mathrm{x}}) \Phi_{\mathbf{K}_m}(x_n, y_n, z) \tag{2.19}$$

With assumption of infinite number of elementary waves the resulting system of equations is over-determined, but it can be solved for c_n in the least squares sense. In matrix and vector notation the regularized solution is [18, 19] expressed in Eq. (2.20).

$$\mathbf{c}(x, y, z_x) = (\mathbf{A}^{\mathrm{H}} \mathbf{A} + \theta^2 \mathbf{I})^{-1} \mathbf{A}^{\mathrm{H}} \mathbf{b} \tag{2.20}$$

where $\mathbf{A}^{\mathrm{H}}\mathbf{A}$ is n_x by n_y autocorrelation matrix of elementary wave set obtained in the hologram plane, superscript H denotes the Hermitian transpose,

  $\mathbf{I}$ is the identity matrix,

  θ is a regularization parameter related to the signal-to-noise ratio,

  $\mathbf{A}^{\mathrm{H}}\mathbf{b}$ is a cross correlation matrix of elementary waves between hologram and prediction plane.

In the limit of infinitely many elementary waves the elements of the matrices in Eq. (2.20) become integrals described in Eq. (2.21, 2.22) [19].

$$\left[\mathbf{A}^{\mathrm{H}}\mathbf{A}\right]_{n_x n_y} = \frac{1}{\pi k_0^2} \int \int_{-\infty}^{\infty} \Phi_K^* \left(r_n\right) \Phi_K \left(r_{n'}\right) \mathrm{dK} = \frac{1}{\pi k_0^2} \int \int_{-\infty}^{\infty} e^{j(k_z^* - k_z)z_h} e^{-jK\left(r_{xy,n} - r_{xy,n'}\right)} \mathrm{dK} \tag{2.21}$$

$$\left[\mathbf{A}^{\mathrm{H}}\mathbf{b}\right]_{n_x n_y} = \frac{1}{\pi k_0^2} \int \int_{-\infty}^{\infty} \Phi_K^* \left(r_n\right) \Phi_K \left(r\right) \mathrm{dK} = \frac{1}{\pi k_0^2} \int \int_{-\infty}^{\infty} e^{j(k_z^* d - k_z z)} e^{-jK(r_{xy} - r_{xy,n})} \mathrm{dK} \tag{2.22}$$

where k_0 is a wavenumber of the input pressure time domain signal,

  Φ_K is an elementary wave defined in Eq. (2.18),

  Φ_K^* is a complex conjugate of the elementary wave Φ_K.

The resulting sound pressure in the prediction plane z_x is defined in Eq. (2.23).

$$\mathbf{p}_{zx} = \mathbf{p}_{zh}^{\mathrm{T}}(\mathbf{A}^{\mathrm{H}}\mathbf{A} + \theta^2\mathbf{I})^{-1}\mathbf{A}^{\mathrm{H}}\mathbf{b} \tag{2.23}$$

The main challenge in using this algorithm is to determine the correct value of regularization parameter θ in this so called Tikhonov regularization. For the calculation of autocorrelation and cross correlation matrixes it is necessary to use numerical integration and the evaluation have to be done for all discrete points in the prediction plane where the knowledge of pressure field values is required.

From the above derivation it is straightforward that SONAH algorithm can as opposite to classical NAH (with discrete 2D Fourier transform) predict sound field values outside the (x, y) positions in prediction plane z_x where sound pressure is measured in holography plane z_h.

In the classical algorithms the limitation is based on 2D Fourier transform where there have to be constant interval between positions in measurement plane and consequently the same (x, y) positions in prediction plane [18, 43].

The SONAH algorithm has been initially developed for planar acoustic holography, but after successful application and evaluation of this principle it has been used after certain extension to another geometries, like cylindrical [6].

The comprehensive description of the theory and properties of SONAH algorithm has been published recently in [20].

Helmholtz Equation Least Squares - HELS

The HELS method assumes that radiated sound pressure can be expressed by formulation with extended basis function as written in Eq. (2.24) [48].

$$\hat{p}(\vec{x}, \omega) = \sum_{j=1}^{J} C_j(\omega)\Psi_j(\vec{x}, \omega) \tag{2.24}$$

where $\hat{p}(\vec{x}, \omega)$ is a complex amplitude of acoustic pressure at field point,

Ψ_j are basis functions obtained with Gram-Schmidt orthonormalization of particular solutions of Helmholtz equation with respect to surface of the sound source.

The equation is very similar to that one used in SONAH algorithm and it is also based on assumption that sound pressure in the field point can be defined with the sum of contribution of each elementary function defining the radiation from the vibrating object.

In the SONAH algorithm the elementary functions are elementary plane waves and the contribution of the pressure caused by each wave is summed to the total pressure at field point. On the other hand in the HELS algorithm the elementary function is defined as Ψ_j and they are obtained by Gram-Schmidt orthonormalization process of particular solution of Helmoltz integral. The particular solution can be easily expressed in spherical coordinates where there are known spherical Hankel and continous Legendre functions [48].

Unknown coefficients C_j connected to the basis functions Ψ_j in Eq. (2.24) can be determined by connecting of the expected solution forms to the M measured acoustic pressure values $\hat{p}_m$ where $m = 1, 2, \cdots, M$ leading to the linear system of equations written in matrix form in Eq. (2.25).

$$[\Psi]_{M \times J} \{C\}_{J \times 1} = \{\hat{p}_m\}_{M \times 1} \tag{2.25}$$

It is evident that number of measurements M have to be larger than number of basis functions J. The solution of this system of equations can be similarly solved by least square sense to determine appropriate set of coefficients C_j in respect to measured values in Eq. (2.26).

$$\{C\}_{Jx1} = \left([\Psi]_{J \times M}^{T} [\Psi]_{M \times J}\right)^{-1} [\Psi]_{J \times M}^{T} \{\hat{p}_m\}_{M \times 1} \tag{2.26}$$

After successful determination of unknown coefficients C_j it is possible to reconstruct or predict the acoustic field (sound pressure values) in any point above or very near the sound (vibration) source surface with evaluation of Eq. (2.26) [48].

The procedure of sound pressure prediction by the HELS method is described in Fig. 2.12.

The main advantage of the HELS method is its mathematical simplicity, effectiveness of the calculation and adaptability to the specific application. The method is working also in the field where there are reflecting surfaces present and requires low number of measurement points than planar NAH or inverse Boundary Element Method in the same measurement conditions [48] . The reason is given by the HELS method itself where the face of the sound pressure wave radiating from the defined object usually corresponding
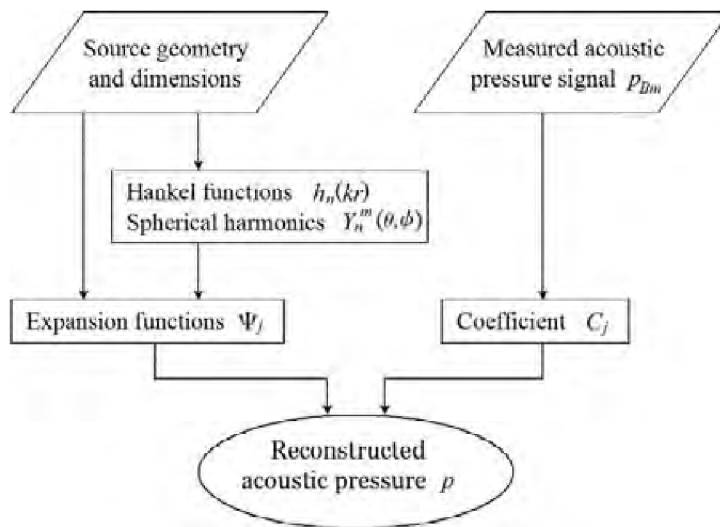
Figure 2.12: Flow chart of the computer program for the HELS method [49].

with or could be approximated with finite number of shape function used by the HELS method [48].

The HELS method has been already described mathematically in detail and it has been used for successful reconstruction of sound field radiating from arbitrary shaped objects in interior and exterior [41]. Also some new formulation and extensions of the original HELS method (combined HELS [50], hybrid NAH [51]) have been published in last decade.

There has been also comparison of HELS and SONAH algorithm for reconstruction of surface velocity through simulations and experimentally made by Gomes and Jacobsen [11]. The conclusions from their study is mainly linked to the regularization, where used Tikhonov regularization and parameter choice method GCV (Generalized Cross Validation) worked well with SONAH (for planar and also spherical sources), but the HELS algorithm has been obviously less robust with the non-spherical sources. There were also studied regularization with "L-curve" analysis with the same results as with GCV. Generally both algorithms perform good for spherical sources at low frequencies, but GCV has often found an unfavourable regularization parameter for HELS.

2.1.6 Acoustic Holography Based on Boundary Element Method

For reconstruction of acoustic quantities radiated by object with arbitrary surface geometry there can be used the theory of Helmholtz integral which defines relation between sound pressure field above vibrating object and normal component of surface velocity on the sound source surface. This theory is valid for outer and also for inner space. For arbitrary geometry there is not clear solution of Helmholtz integral. From that reason it was necessary to find numerical solution of the integral. Most common method for numerical solution of Helmholtz integral is Boundary Element Method (BEM) which divides the arbitrary surface of sound source to small elements and afterwards calculates the acoustic quantities at specified discrete points on that elements [36, 29].

The characteristics of sound source is found based on information about generated sound field, thus this procedure is called as backward acoustic problem and its numerical evaluation is realized with inverse boundary element method (IBEM) [36, 40].

Boundary element method is based on direct calculation of Helmholtz integral which is expressed by Eq. (2.27) with the direct propagator (Green's function, Eq. (2.28)) [36].

$$p_F = -\int_S \left(j\rho\omega G v_n + p_s \frac{\partial G}{\partial n} \right) \mathrm{dS} \tag{2.27}$$

where p_F is a complex sound pressure value at field point above vibrating object,

   G is a free space Green's function,

   n is a vector normal to the surface of vibrating object S with direction outside from acoustic field,

   v_n is a normal surface velocity at source surface S,

   p_s is a sound pressure on the surface S.

$$G(r) = \frac{e^{-jkr}}{4\pi r} \tag{2.28}$$

For N points on the source surface, Eq. (2.27) can be rewritten to discrete form represented in Eq. (2.29).

$$[\mathbf{H}] \{p_s\} = [\mathbf{G}] \{v_n\}, \tag{2.29}$$

where $[\mathbf{H}]$ and $[\mathbf{G}]$ are NxN matrices and $\{p_s\}$ and $\{v_n\}$ are vectors of sound pressure and normal particle velocity respectively. In case of knowledge of v_n Eq. (2.29) can be solved by standard matrix evaluation. When the values of p_s are known, after solving the integration in Eq. (2.27) the sound pressure at any field point can be determined.

Sound pressure field points can be related to normal surface velocities as expressed in Eq. (2.30).

$$\{p_F\} = [\mathbf{ATM}] \{v_n\}, \tag{2.30}$$

where $[\mathbf{ATM}]$ is acoustic transfer matrix. Thereafter Eq. (2.29) can be rewritten for one field point in Eq. (2.31).

$$p_{F,i} = \left[\underline{ATV}_i^T \right] \{v_n\}, \tag{2.31}$$

where $\left[\underline{ATV}^T_i\right]$ is i^{th} row of the matrix $[\textbf{ATM}]$.

Vector $\left[\,\underline{ATV}\,\right]$ is often called as acoustic transfer vector, vector of acoustic contributions or acoustic sensitivities. Thus it represents the set of acoustic transfer functions which describes relation between normal velocity at each point on the vibrating object surface and sound pressure value at one microphone position as shown in Fig. 2.13.
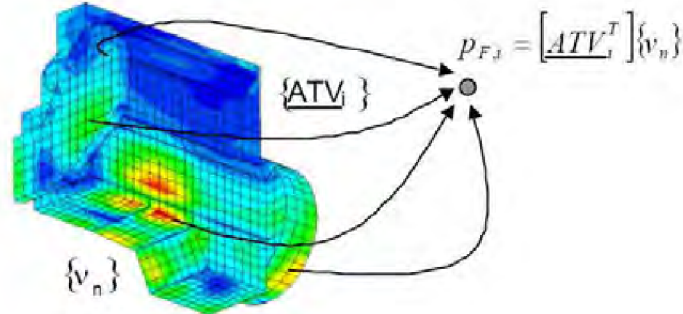
Figure 2.13: Diagram of the calculation procedure of sound pressure at field point with contribution from surface velocities on the whole surface of the vibrating object (direct transformation of sound fields) [36].

In inverse numerical acoustics (including IBEM) the goal is to solve Eq. (2.30) with respect to normal surface velocities $\{v_n\}$ and if measured sound pressure at field points $\{p_F\}$ is known. The number of field points N_F are usually lower in practice than number of surface points N (mesh points) where there are reconstructed the surface velocity [36, 29]. There are also certain types of the boundary elements used in BEM calculation (quadratic quadrilateral, quadratic triangular) as referenced in [4].
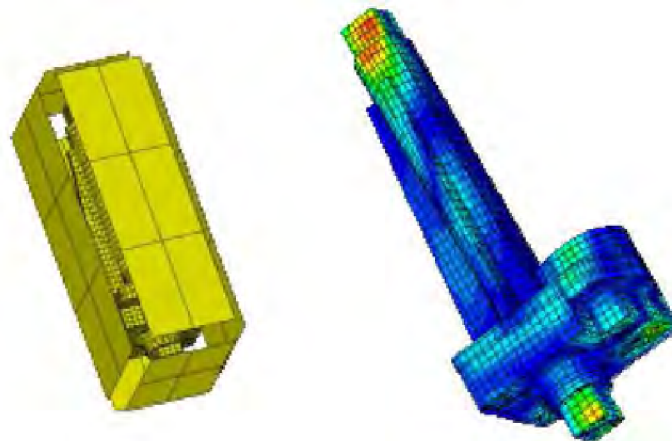
Figure 2.14: Surface mesh points N and field (measurement) points N_F in parallel planes at defined distances from the object surface (left) and surface velocities (right) [36].

As describe in literature the main advantage of the Inverse Boundary Element Method (IBEM) is reduction of problem dimension by one and its versatility to definition of measurement point locations [41]. There are also some substantial disadvantages.

Well-known disadvantage of IBEM is the capability to find unique solution if the examined frequency is close to any natural frequency of vibrating object. The resolution

of this problem can be done with the significant increase of complexity of numerical calculation [36, 41].

Another main disadvantage of IBEM is the requirement of surface mesh of the vibrating object which could not be always available in technical practice. Considering the rule of six mesh points of surface mesh per wavelength of radiated sound field to obtain true reconstruction of sound field the surface mesh of the vibrating object for IBEM calculation should be created. Based on the selection of upper critical frequency the number of discrete points in surface mesh is determined. To preserve the integrity of the reconstructed sound field the number of measurement points should be approximately the same as discrete nodal points in the surface mesh. This procedure could be sometimes problematic in practice due to the high number of discrete nodal points of arbitrary surface while vibrating from low to middle frequencies. Thus the procedure of reconstruction could be too complicated and lengthened [41].

The extensive comparison of IBEM algorithm and SONAH algorithm for reconstruction of the surface velocity of the vibrating object has been made by Juhl and Gomes [32]. For both methods there have been used Tikhonov regularization. On their test case (rectangular box) it seems that in some cases (measurement array very close to the box) the regularization method with IBEM algorithm leads to not sufficient reconstruction of surface velocity due to under regularization.

2.2 Measurement Systems for Near-field Acoustic Holography

For measurement of acoustic field quantities (acoustic pressure, particle velocity, sound intensity) there can be selected many different type of sensors working on different principles. The main usual measurement procedures should be:

- Measurement of sound pressure - microphones

- Measurement of sound intensity - intensity $p-p$ probe (calibrated microphone pair),

- Measurement of particle velocity - intensity $p-u$ probe (Microflown sensor).

2.2.1 Microphones

For measurement of sound pressure field values at discrete points above the vibrating object (sound source) there are often used classical microphones with capacitive transducers. The important parameters of the microphones are amplitude and phase frequency response and self noise (including potential amplifier). These parameters should be very similar for all sensors used in the measurement (it there is more than one) because the acoustic holography methods are very sensitive to amplitude and phase mismatch of the microphones. For this reason the sensors (microphones) are usually calibrated and the frequency response is stored in data file or directly (as TEDS - Transducer Electronic Data Sheet) in the smart sensor (in nonvolatile memory). The phase matching of typical array microphone (B&K Type 4958 in Fig. 2.15) is $< \pm 3°$ at a frequency range from 100 Hz to 3 kHz.

Figure 2.15: 20 kHz Precision Array Microphone - Type 4958, manufacturer Brüel & Kjær [2].

The other parameters of the array microphone from Brüel & Kjær is below and the free-field frequency response is in Fig. 2.16.

Features of 20 kHz Precision Array Microphone - Type 4958 [2]:

- Sensitivity: 12.5 mV/Pa (0.38 dB re 1 V/Pa),

- Frequency range: 10 - 20000 Hz,

- Dynamic Range: 28 - 140 dB,

- Built-in DeltaTron® preamplifier with TEDS IEEE 1451.4 V.1.0,

- Excellent amplitude and phase-matching,

- Dimensions: 34 mm long, 7 mm diameter,

- Temperature: -10 to +55°C.
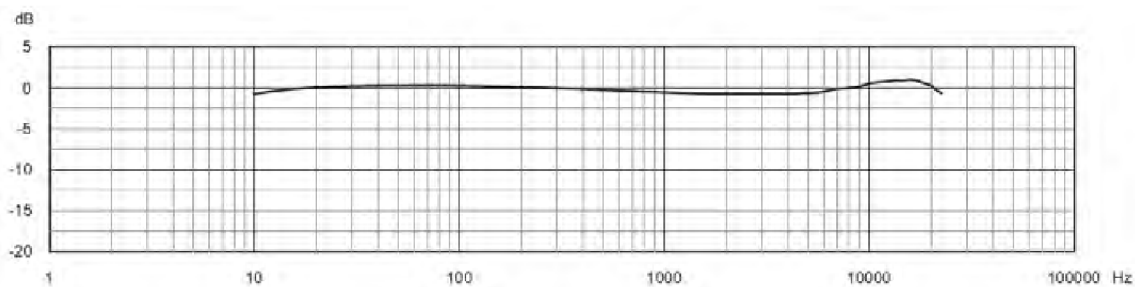
Figure 2.16: Free-field frequency response of the array microphone B& K Type 4958 [2].

2.2.2 Sound Intensity Probes

The intensity probes are devices (sensors) for vector measurement in compare with microphones which measure scalar sound pressure. They can give the value of the sound intensity including the direction of the intensity vector. The sound intensity could be calculated based on measurement with two microphones ($p - p$ probe) or with one microphone and one particle velocity sensor ($p - u$ probe).

Sound Intensity $p - p$ Probe

The standard intensity probe consists of two closely spaced identical pressure microphones which are placed "face to face". From the difference in measured pressure, the pressure gradient is determined, which, by Newton's law, is proportional to the time derivative of the velocity. The average pressure is determined from the sum of the two microphone signals. Then the sound intensity can be calculated from the imaginary part of the crossspectrum between the two microphone signals using a dual-channel audio analyzer. The frequency range of the $p - p$ probe is defined with the spacing between microphones in the pair. Common used spacers are 8.5 mm, 12 mm and 50 mm long [42].

Typical construction of intensity probe with two microphones is Type 3599 from Brüel & Kjær in Fig. 2.17. The probe contains two pressure microphones Brüel & Kjær Type 4197.

Phase matching of used 1/2" microphone pair B & K Type 4197 is better than 0.05° between 20 Hz and 250 Hz, and is better than $f/5000$ degrees at higher frequencies, where f is the frequency. Superior phase matching is given by the integral microphone phase-corrector units which are fitted to the microphones. The normalized microphone frequency responses differ by less than 0.2 dB up to 1 kHz and by less than 0.4 dB up to 7.1 kHz [42].

Figure 2.17: Sound Intensity Probe - Type 3599, manufacturer Brüel & Kjær [42].

Features of Sound Intensity Probe - Type 3599 [42]:

- Two 1/2 palce microphone pair Type 4197,

- Frequency range (8.5 mm spacer): 250 Hz to 6.3 kHz,

- Frequency range (12 mm spacer): 250 Hz to 5.0 kHz,

- Frequency range (50 mm spacer): 20 Hz to 1.25 kHz,

- Pressure-residual intensity index: $\delta_{pI0} > 15.3 \ dB$ for 8.5 mm spacer,

- Dimensions: 42 cm length, 43 mm width.

In real environment the sound pressure level is usually higher than the sound intensity level. The ability of a sound intensity instrument to measure intensity levels much lower than the pressure level depends on the probe and analyzer phase matching. The difference between pressure and intensity levels is called the Pressure-Intensity Index which is denoted by δ_{pI} and is normally a positive quantity. This difference also defines the useful frequency range of the intensity probe [42].

To verify the intensity probe parameters (phase matching of microphone pair) the pressure-residual intensity index is measured. The pressure-residual intensity index is obtained during calibration where same sound signal is applied to both microphones in

the pressure coupler. It is a difference between sound pressure level in the coupler and residual intensity measured with the probe (intensity in coupler should be zero) [42]. The typical pressure-residual intensity index for sound intensity probe from Brüel & Kjær is in Fig. 2.18.
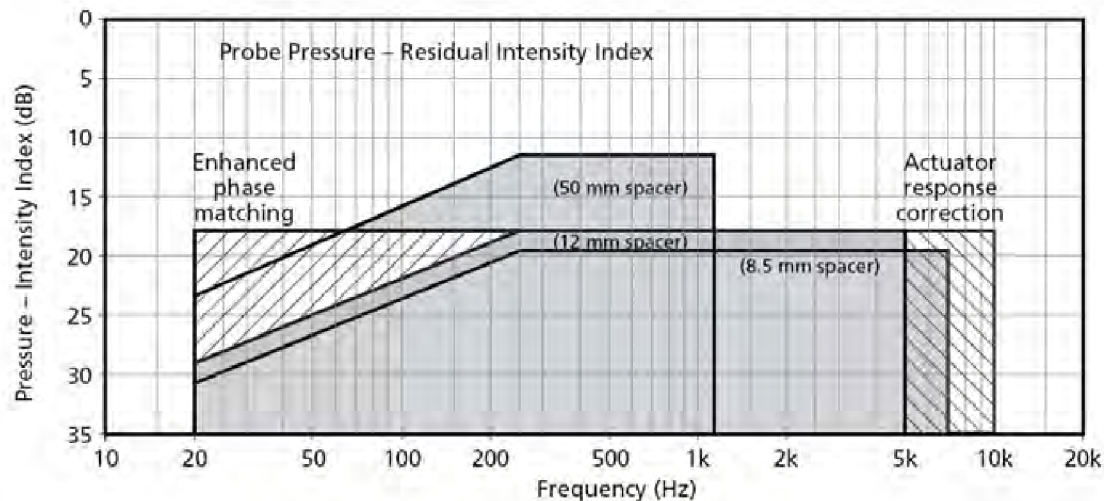
Figure 2.18: Specified frequency and Pressure-Residual Intensity Index ranges for the intensity probe B& K Type 3599 [42].

Sound Intensity $p - u$ Probe

The intensity probe based on measurement of sound pressure and acoustic particle velocity in one complex sensor has been developed by Microflown. The pressure sensor is common electret transducer and the particle velocity transducer (the Microflown sensor) is a micromachined silicon based sensor and operates on a thermal principle.

The Microflown particle velocity transducer consists of two short, thin, closely spaced wires of silicon nitride coated with platinum and heated by a dc current to about 300°C. The resistance of the wires depends on the temperature. An acoustic particle velocity signal in the perpendicular direction changes the temperature distribution due to the airflow, where one of the wires will be cooled more than the other, and this difference in resistance of wires is measured with a bridge circuit that provides a signal proportional to the particle velocity [30]. The size of the Microflown transducer is one millimeter in length, forty micrometer apart from each other and the thickness of both wires is half a micrometer. The Microflown transducer itself can be seen in Fig. 2.19 on the solid cylinder to the right, the electret microphone for pressure measurement is mounted inside the other cylinder.

Comparison of $p - u$ probe and $p - p$ probe measurement of sound intensity has been carried out by Jacobsen [31, 30]. A Microflown $p - u$ sound intensity probe has been examined experimentally in this study and results demonstrates that it is possible to measure sound power reliably with the device if reactive near fields are avoided. If the phase can be calibrated with sufficient accuracy it may be possible to expand the range of measurement to near field conditions [31].

Figure 2.19: The Microflown 1/2-inch. sound intensity probe [31].

Parameters of Microflown element (particle velocity sensor) [7]:

- Frequency range: 1Hz – 20kHz,

- Upper sound level 125dB (PVL re. 50nm/s),

- Sensitivity: 50mV/(mm/s),

- Directivity: figure of eight,

- Signal to noise ratio (at 1kHz in 1Hz bandwidth): 107dB.

2.2.3   Measurement Procedure

The measurement of the field acoustic quantities could be done using one sensor with scanning robot (measuremen point-by-point) or with line array of sensors also with scanning robot or with matrix array where all the field points are measure simultaneously. The usual configuration of measurement systems for near-field acoustic holography is in Fig. 2.20.

Step-by-step scanning   Continous scanning   Simultaneous measurement
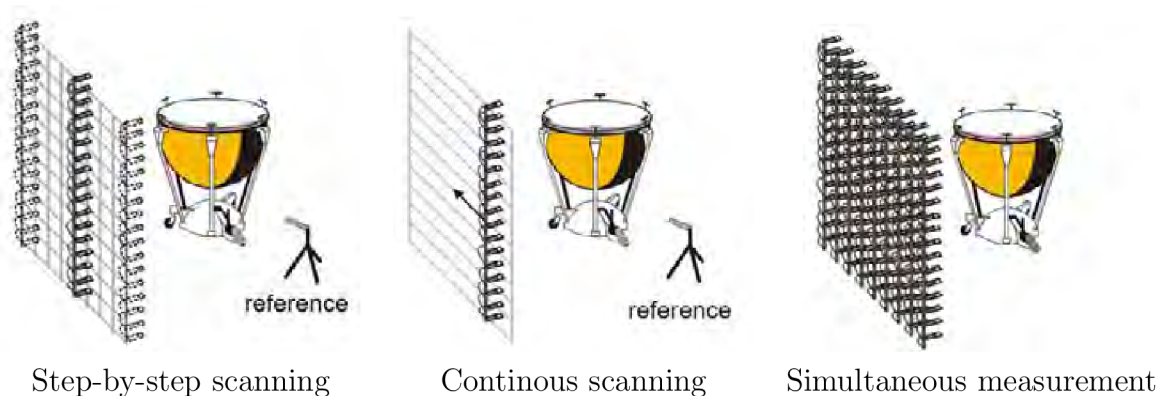
Figure 2.20: Usual acoustic holography measurement system configuration [33].

The first two methods require using of the reference sensor to obtain the information about phase shift between subsequent measurements. These two methods can be used only for stationary sound field, where the sound radiating from the vibrating source is not changing its frequency and energy (amplitude and phase of sound intensity vectors) and also its position. Description of using reference sensor during measurement with linear microphone array can be explain in Fig. 2.21.
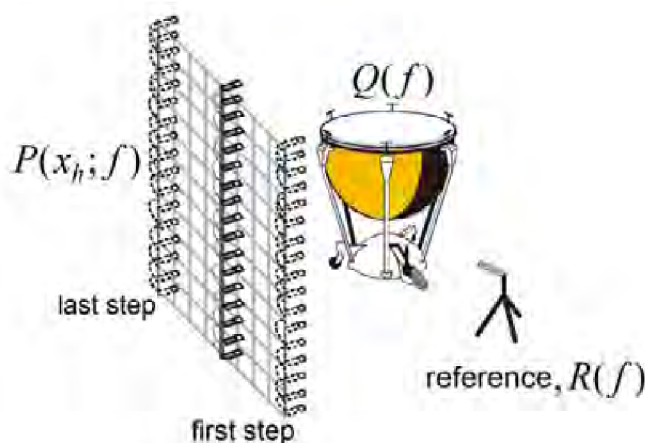
Figure 2.21: Using reference sensor in measurement with scanning linear array [35].

Sound pressure values obtained in each step (one column) $P(x_h; f)$ can be defined in relation to sound pressure values $Q(f)$ produced by the examined vibrating source in Eq. (2.32).

$$P(x_h; f) = H(x_h; f)Q(f), \tag{2.32}$$

where $H(x_h; f)$ is transfer function between radiating sound field with the vibrating object $(Q(f))$ and measured sound field at microphone positions. We can assume that transfer function $H(x_h; f)$ is invariant for each measurement step. Eq. (2.32) can not be solved due to unknown sound field radiation of the examined object, thus we have to introduce reference sensor signal $R(f)$. For the reference sensor pressure signal $R(f)$ we can write similar relation to measured pressure values at microphone positions as with original sound field and the new relation can be expressed in Eq. (2.33).

$$P(x_h; f) = H'(x_h; f)R(f). \tag{2.33}$$

If there is more than one sound source present in the measured field, the resulting sound field can be expressed in Eq. (2.34) and it requires multiple reference signal to determine proper input pressure signal at microphone position for each measurement step.

$$P(x_h; f) = H_1(x_h; f)Q_1(f) + H_2(x_h; f)Q_2(f). \tag{2.34}$$

In some cases, the vibrating object can be measured while it moves during the measurement. The similar situation is in the case where the linear array move continuously while vibrating object remain stable. The procedure of moving frame has been introduced in litearture [35] and lately extended with new improvements [38]. The processing algorithm expects that movement is with constant speed u_m and moving frame (linear microphone array) measures Doppler shifter spectrum of the original sound field as expressed in Eq. (2.35).

$$f' = f_{h0} - u_m \frac{k_x}{2\pi}, \tag{2.35}$$

where f' is the Doppler shifted spectrum of original sound field, f_{h0} is original frequency of the sound field and k_x is wavenumber spectrum in x direction (direction of movement).

The proposed method [35] is using de-Dopplerization based on shifting of measured spectrum to its original position based on reference sensor signal spectrum. The example application of using acoustic holography technique with moving microphone array is presented in Fig. 2.22. In this case the reversed procedure is used (array is still, object is moving).
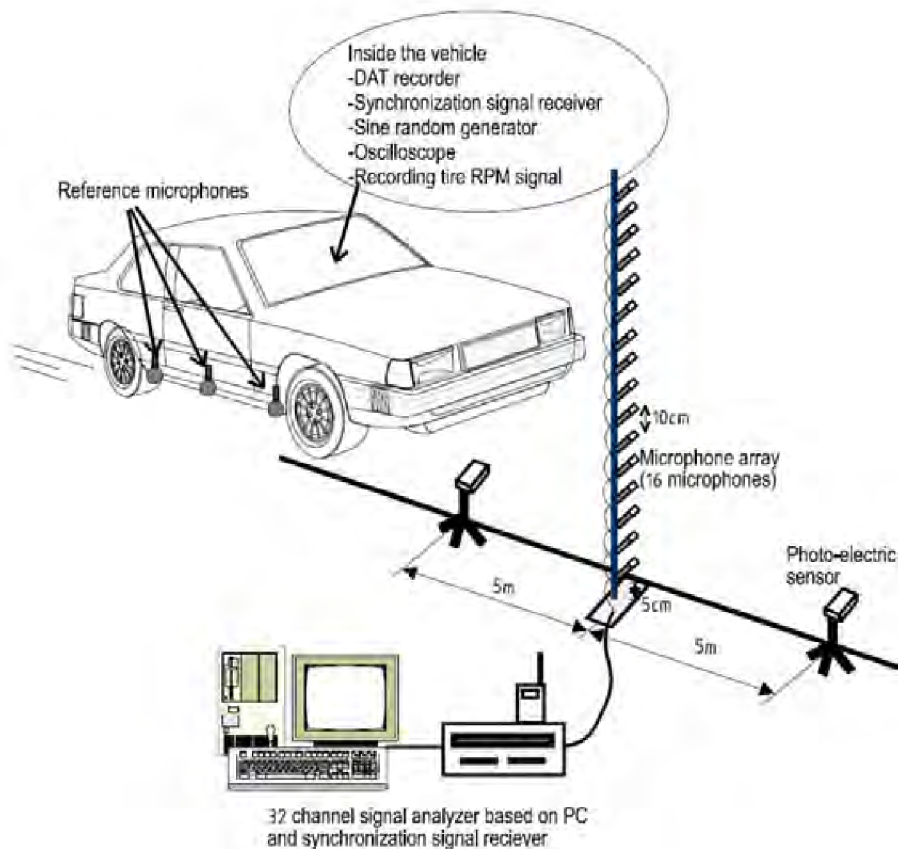
Figure 2.22: Example application of using moving array technique in acoustic holography [35].

2.3 Regularization Procedures for Near-field Acoustic Holography Algorithms

Ill-conditioned transfer matrices of the NAH algorithms (especially in algorithms which calculate predictions directly in spatial domain) are usually present and for inverse calculation, some kind of regularization should be used. Basically there are two mostly used methods for regularization and two methods for determination of regularization parameter.

2.3.1 Tikhonov and TSVD Regularization

As the methods for regularization of the inverse solution, the Tikhonov regularization and Truncated SVD are often used in connection with treatment of inverse matrixes of near-field acoustic holography algorithms.

In the Tikhonov regularization method we must minimize the general Tikhonov functional J_α for fixed parameter α. Detailed derivation of Tikhonov regularization can be found in literature [45, 12]. The term $\mathbf{R}_\alpha$ is called regularized inverse of $\mathbf{H}$ and is expressed in Eq. 2.36 [45].

$$\mathbf{R}_\alpha = (\alpha \mathbf{L}^H \mathbf{L} + \mathbf{H}^H \mathbf{H})^{-1} \mathbf{H}^H = (\alpha \mathbf{I} + \mathbf{H}^H \mathbf{H})^{-1} \mathbf{H}^H, \tag{2.36}$$

for $\alpha > 0$.

The TSVD method is based on the singular value decomposition (SVD) of the transfer function $\mathbf{H}$ described in Eq. (2.37).

$$\mathbf{H} = \mathbf{U} \sum \mathbf{V}^H, \tag{2.37}$$

where $\mathbf{U}$ and $\mathbf{V}$ are left and right unitary (orthonormal) matrices, respectively, and $\sum$ is a diagonal matrix of real singular values. Usually there can be assumed that the number of reconstruction points N and the number of measurement points M are equal. $\mathbf{V}^H$ is the conjugate transpose of $\mathbf{V}$ [45].

The truncated SVD method is setting all but the first k largest singular values equal to zero and using only the first k columns of $\mathbf{U}$ and $\mathbf{V}$ matirces, thus reducing the size of $\mathbf{U}$ and $\mathbf{V}$. It is also called reduced rank approximation of $\mathbf{H}$. The selection of appropriate k value (the number of remaining singular values) is a challenge while using this regularization method.

2.3.2 Parameter Identification Methods

There are two automated regularization parameter identification methods that are usually used in connection with acoustic holography. They are "L-curve" analysis/criterion and Generalized Cross Validation (GCV).

The so called "L-curve" criterion (L-C) is a heuristic method using LOG-LOG representation of two norms, the solution norm $\parallel \mathbf{x}_\lambda \parallel_2$ (corresponds to resulting unknown input values in inverse calculation) and residual norm $\parallel \mathbf{p} - \mathbf{K} \mathbf{x}_\lambda \parallel_2$ corresponds to difference between known output values and calculated output values from determined inputs and transform matrix (e.g. **ATM** in case of IBEM method). The analysis procedure

finds the corner of the L-curve, where the ratio between solution norm and residual norm is optimal, thus balances the regularization and perturbation errors in the solution [13].

The "L-curve" criterion can give regularization parameter for methods based on Tikhonov regularization (lowest singular value - λ) or Truncated Singular Value Decomposition (TSVD) (position of lowest singular value in transfer matrix - index k). Typical shape of L-curve is in Fig. 2.23.
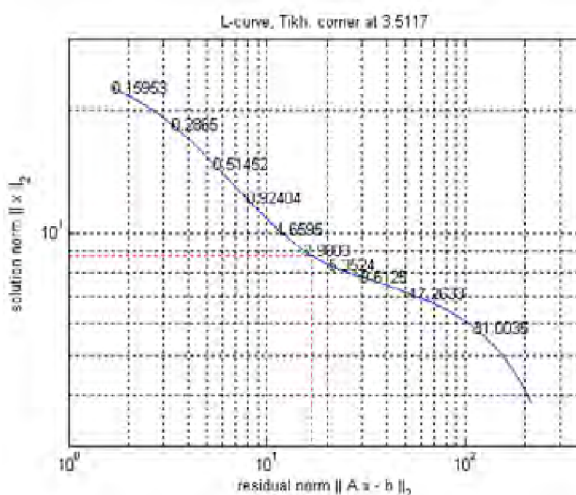
Figure 2.23: Regularization parameter identification with L-curve criterion.

As the second possible method for determination of the right regularization parameter for sound field prediction with SONAH algorithm, HELS algorithm and all BEM based NAH algorithms Generalized Cross Validation (GCV) can be used. The GCV function represents the error norm dependent on smallest singular value in the inverse calculation. The minimum of the $G(\lambda)$ function determines the lowest singular value usable in transfer matrix to avoid escalation of the solution error due to the singularities. GCV is a statistically based method that seeks to minimize the prediction error $\parallel \mathbf{p}^{\mathrm{t}} - \mathbf{K}\mathbf{x}_\lambda \parallel_2$ between the exact sound pressure $\mathbf{p}^{\mathrm{t}}$ and the predicted sound pressure. This is achieved by minimizing the GCV function defined in Eq. (2.38) [13].

$$\parallel \mathbf{p} - \mathbf{K}\mathbf{x}_\lambda \parallel_2 / \mathrm{trace}(\mathbf{I} - \mathbf{K}(\mathbf{K}^{\mathrm{H}}\mathbf{K} + \lambda^2\mathbf{I})^{-1}\mathbf{K}^{\mathrm{H}}), \qquad (2.38)$$

where $\mathbf{x}_\lambda$ is the regularized solution,
         $\mathbf{p}$ denotes the measured data,
         $\mathbf{K}$ is the coefficient/system matrix.

The typical result from GCV can be seen in Fig. 2.24, where the minimum of the function is found and corresponding lowest singular value λ determining amount of regularization to be used in any regularization method.

With two regularization parameter identification methods and two regularization procedures all this leads to four possible identification of regularization parameter and consequently four results of prediction of sound field near examined sound source.

The best combination of identification method and regularization procedure depends on acoustic holography method where the selected regularization procedure has been used. For example, the IBEM with truncated SVD and "L-curve" analysis offer better
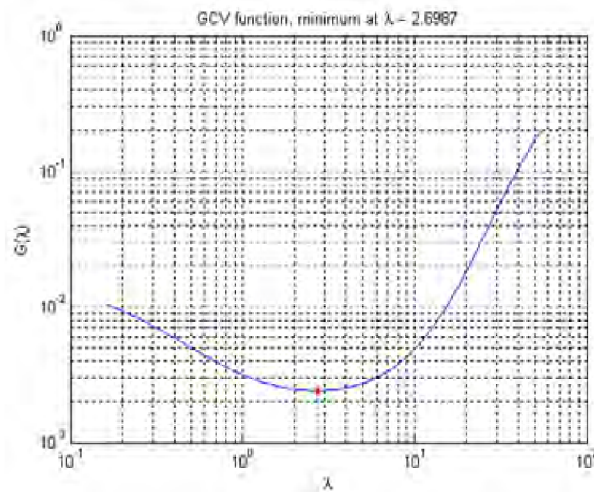
Figure 2.24: Regularization parameter identification based on GCV.

calculation stability (reduction of the prediction errors) than other combinations. There are also some cases where all methods work sufficiently and produce very similar results.

There are also another methods for determination of regularization parameters (e.g. NCP), but they are not used so often.

Goals of the Thesis 3

Analysis of vibration and visualization of sound fields with acoustic holography is very interesting for technical diagnostics due to high amount of information that can be acquired and also for the nature of non-contact measurement. The algorithms for acoustic holography calculation has been developed for more than 25 years and recently the algorithms for prediction of acoustic quantities to describe structural vibration of analyzed surfaces are growing. It can be allowed with improvement of computer systems for processing measure data, where there is a possibility to acquire input signal very fast with many measurement channels and precess it numerically. Current research in the field of acoustic holography is focused on development of new or optimization of existing algorithms. Sustained requirement of more accurate prediction and characterization of sound fields near the surface of vibrating object is rising the complexity of measurement system to obtain sufficient amount of input data, but such systems ale less applicable in technical practice. Analysis of vibration of large scale structures (larger than measurement array) is also required. Researchers try to solve this task with the new numerical methods which in most cases avoiding spatial transformation which has been usually used in classical algorithms. Involving spatial transformation into calculation procedures yields to the problems with preparation of input data for transformation (windowing function). On the other hand, the calculation procedure with spatial transformation is very fast.

Applicability of classical methods (with transformations) for near-field acoustic holography calculation is still relevant and their optimization and detailed characterization of each possible parameter in relation to prediction accuracy of sound field near vibrating surface have not been sufficiently performed yet. There can be some future improvements in prediction based on combination of different approaches and their optimization.

The main objective of this thesis is development, implementation and optimization of near-field acoustic holography algorithms based on spatial transformations with respect to increasing of prediction accuracy in real measurement conditions. The procedure with spatial transformations has been selected with assumption that these algorithms can calculated the predictions rapidly while using 2D Fourier transformation. There are also many improvements already published in last decade which have not been combined and could bring new ideas into future research. The promising procedure is measurement with double layer microphone array (in two plan-parallel planes with small distance between layers) for prediction of sound fields in complex environments, because from the theory of holography, amount of information in two parallel planes should be larger than with only single plane measurement. This procedure certainly has an advantage similar to measurement with intensity probes, where also the direction of the propagation of waves in sound field can be examined.

The reconstruction of whole sound field above vibrating surface with more than one measurement step is also prospective research task and has been studied within this research. The commercial research in this field is focused mainly to numerical methods.

The classical approaches could be also successful if there will be some treatment of input data to obtain better prepared preprocessed data before spatial transformation.

Development of new methods leads to construction of new improved measurement systems. This is also scope where the research can be done and is also described in this thesis. The procedure with double layer microphone array requires twice the number of acoustic sensors (microphones) to measure the sound field. With commonly used special array sensors (very precise and stable), these methods will be very expensive. The research in this field is focused on using common sensors (electret microphones, commercially available high volume sensors - MEMS microphones) incorporated with some additional information (e.g. stored frequency response of the sensor) which can be used during the measurement to correct the input data acquired with such sensor. Also the manufacturing precision of high volumes of acoustic sensors (e.g. microphones for cell phones) is increasing and these sensors can be used now for holography measurement where strict requirements are applied.

Finally, experimental validation of acoustic holography method for non-contact vibration analysis is expected to confirm applicability of the method for such vibration analysis.

Advanced Acoustic Holography Methods

<div style="text-align:right;">4</div>

This chapter describes development and enhancement of planar near-field acoustic holography algorithms which has carried out as a main goals of this thesis. The presented algorithms try to minimize prediction errors caused mainly by real measurement conditions (non-ideal transducers, presence of noise in measurement path, non-free field conditions, etc.). Also comparison with currently published algorithms has been made on simulated test cases. The results of the algorithm's accuracy and applicability is summarized in the end of each section. The short description of similar methods published in last years and used in comparison have been done too.

4.1 Simulation Model of Vibrating Panel

Based of literature study [15] there were designed simple model of vibrating surface in Matlab environment. The basic idea of this approach is the modeling of the vibrating surface by matrix of elementary point sources which are placed on the surface. Displacement w of the surface of that designed vibrating panel in points of fictitious point sources and driven with harmonic force F can be calculated in Eq. (4.1) [15].

$$w(x,y,\omega) = -\frac{2F}{\rho h \sqrt{L_x L_y}} \sum_{s=1}^{\infty} \sum_{t=1}^{\infty} \frac{\left[\sin\left(\frac{s\pi x}{L_x}\right)\sin\left(\frac{t\pi y}{L_y}\right)\right]\left[\sin\left(\frac{s\pi x_0}{L_x}\right)\sin\left(\frac{t\pi y_0}{L_y}\right)\right]}{\omega^2 - \omega_{s,t}^2} \tag{4.1}$$

where F is an amplitude of harmonic point force driving the panel,
$\quad\quad\quad x_o, y_o$ are x and y coordinates of driving force F,
$\quad\quad\quad \omega$ is angular frequency of driving force F,
$\quad\quad\quad s, t$ are natural angular frequencies of the panel (modal frequencies).

$$\omega_{s,t} = \pi^2 \sqrt{\frac{Eh^2}{12\rho(1-\mu^2)}\left[\left(\frac{s}{L_x}\right)^2 + \left(\frac{t}{L_y}\right)^2\right]} \tag{4.2}$$

where x, y are cartesian coordinates of the fictitious point source on the surface of the panel,
$\quad\quad\quad E$ is the Young's module of the panel's material,
$\quad\quad\quad \rho$ is density of the material of the panel,
$\quad\quad\quad \mu$ is Poisson constant,
$\quad\quad\quad h$ is a thickness of the panel,
$\quad\quad\quad L_x, L_y$ are dimensions of the panel,
$\quad\quad\quad s, t = 1, 2, \ldots$ are natural frequencies (modes) of the panel in x and y direction.

Results of the simulation of surface displacement of the panel based on above designed model in Matlab environment is are presented in Fig. 4.1.
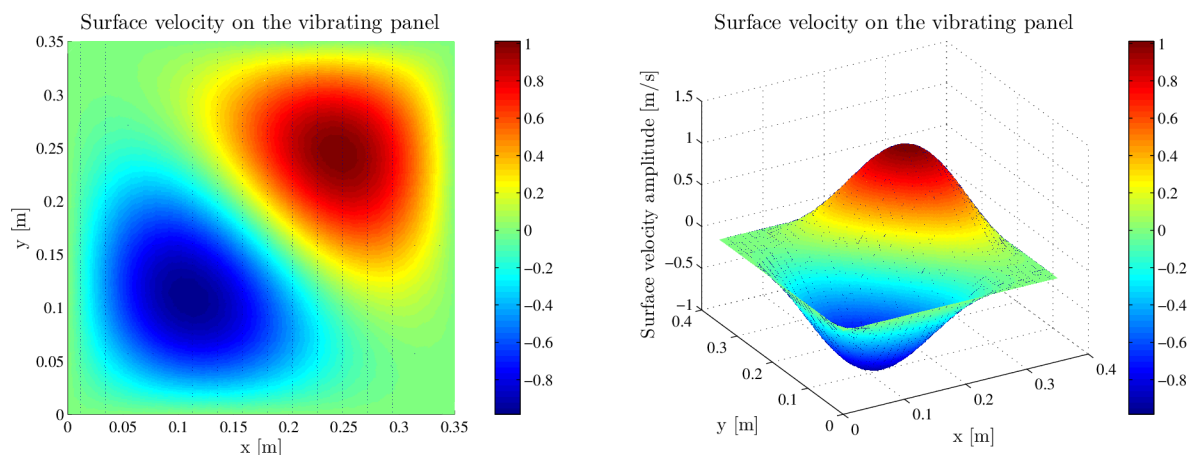
Figure 4.1: Amplitudes of surface velocity of the vibrating panel with driving force of 10 N and frequency of 100 Hz.

For development and optimization of acoustic holography algorithms it is necessary to know the true sound pressure field values at certain distances from the vibrating surface. To the specified spatial points there we can place virtual microphones and then calculate the contribution of each fictitious vibrating point of the surface to the total sound pressure at defined spatial point. The sound pressure values at the spatial points r where there are virtual microphones placed above vibrating surface can be calculated in Eq. (4.3) [15].

$$p_m = \frac{-j\omega\rho_0}{2\pi} \sum v_n S_n \frac{e^{jkr_{mn}}}{r_{mn}} = \frac{-\omega^2\rho_0}{2\pi} \sum w_n S_n \frac{e^{jkr_{mn}}}{r_{mn}} \qquad (4.3)$$

where r_{mn} is a distance between fictitious point source n on the panel surface and the spatial point m above the surface, where sound pressure value is calculated,

k is a wave-number,

v_n is a surface velocity of the fictitious point source,

w_n is a surface displacement of the fictitious point source,

S_n is an area of the baffle of the fictitious point source,

ρ is a density of air.

These values have to be calculated for at least two z distances from the source surface. These distances are at prediction plane position z_x (usually very close to the source surface) where we would like to know the pressure field and at measurement plane z_h where the sound pressure field values are usually measured with microphones or another acoustic sensors in real environment. If there are two measurement planes, the closer plane is marked z_{h1} and second plane is marked z_{h2}. The evaluation of the accuracy parameters (mostly the prediction error of sound pressure very close to the surface) of acoustic holography algorithms are proceed with the knowledge of true sound pressure field at
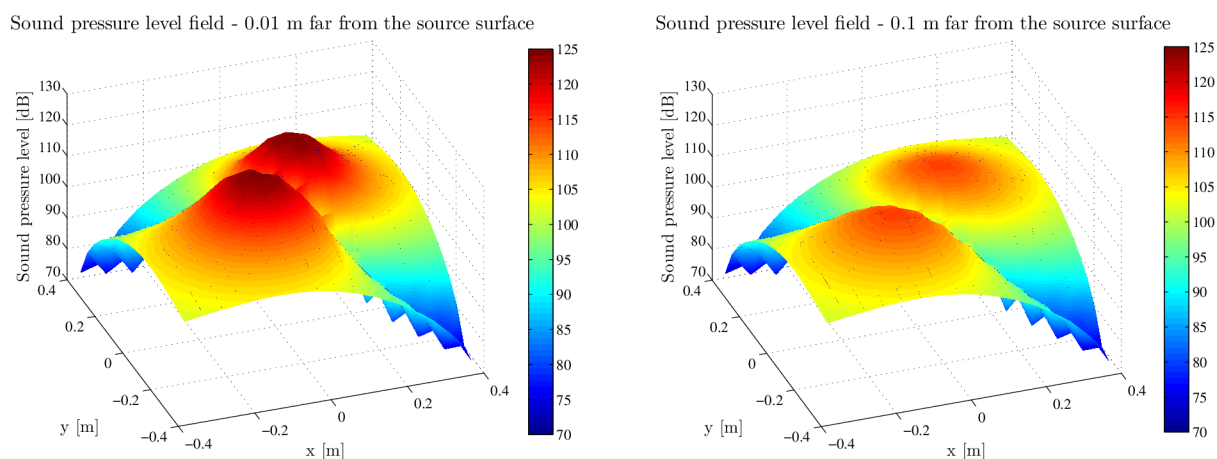
Figure 4.2: Sound pressure level field at the distance of 0.01 m (left) and 0.1 m (right) from the vibrating panel driven with force of strength of 10 N and frequency of 100 Hz.

prediction plane obtained in Eq. (4.3) and that calculated with acoustic holography algorithm where the input data (pressures at measurement plane(s)) are calculated similarly. Thus, the difference between true calculated pressure values and backward holography calculated values are evaluated. More specification about error evaluation of acoustic holography algorithms is defined lately in this chapter. The results from simulations of sound pressure field values at certain distances from the source surface (vibrating panel) calculated based on Eq. (4.3) is in Fig. 4.3.
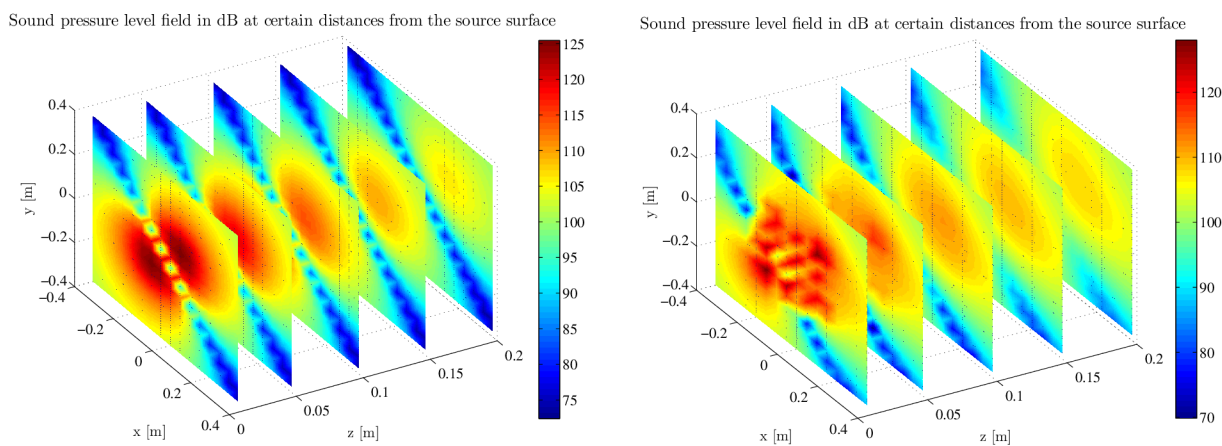
Figure 4.3: Sound pressure level field distribution from the vibrating panel driven with force of strength of 10 N and frequency of 100 Hz (left) and 500 Hz (right).

4.2 Simulation Test Cases for Evaluation of Acoustic Holography Algorithms

4.2.1 Test Case for Single Layer Holography

This simulation test case is outlined in Fig. 4.4. The examined source is a thin steel panel with dimensions 0.35 m x 0.35 m and a thickness of 3 mm mounted in an infinite baffle. The panel is driven by a harmonic point force near one of the corners to produce high number of natural modes. In this simulation, the plate was driven with force of strength in units of Newton (from 1 N to max. 10 N), at the point 0.05 m x 0.05 m far from one of the corners. The resulting surface velocity is calculated as a conventional modal sum. The number of modes included in the sum corresponds to modal indices from 1 to 15 in both the x- and y-direction. The sound pressure at the microphone positions is calculated from a numerical approximation to Rayleigh's first integral [44] as described in previous chapter.
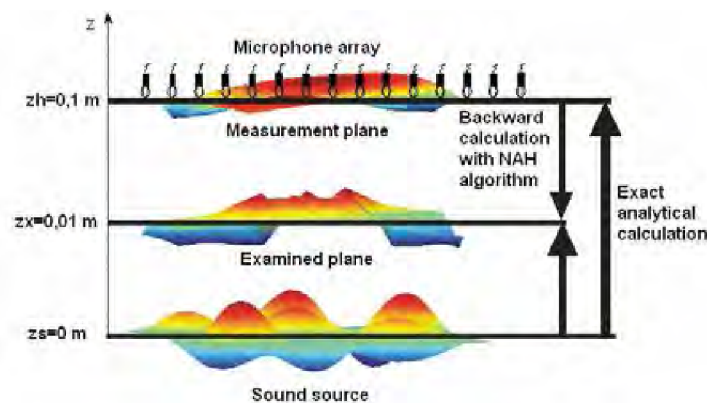
Figure 4.4: Outline of the simulation case with single layer holography (sources only below (in front of) the array.

There are 16 x 16 microphones in the microphone array, the dimensions of which are 0.75 m x 0.75 m, corresponding to a distance of 5 cm between the microphones. For detailed understanding see Fig. 4.5.

The "true" sound field in the prediction (calculation) plane is also determined by Rayleigh's integral.

For the algorithms with transformation into wavenumber domain the effect of the finite aperture size was reduced before 2D Fourier transform by 16-point Tukey window, the wrap-around error was reduced by zero padding to twice the measurement area, k-space filtering was done with an exponential window with a cut-off frequency of 0.3 times the Nyquist frequency and a value of α set to 0.2. If there is a regularization parameter involved (with Wiener filter) it has been set to 0.001 (signal-to-noise ratio 60 dB).

4.2.2 Test Case for Double Layer Holography

The simulation test case with double layer measurement array is outlined in Fig. 4.6 and with this case the second sound source is present. The second source is modeled
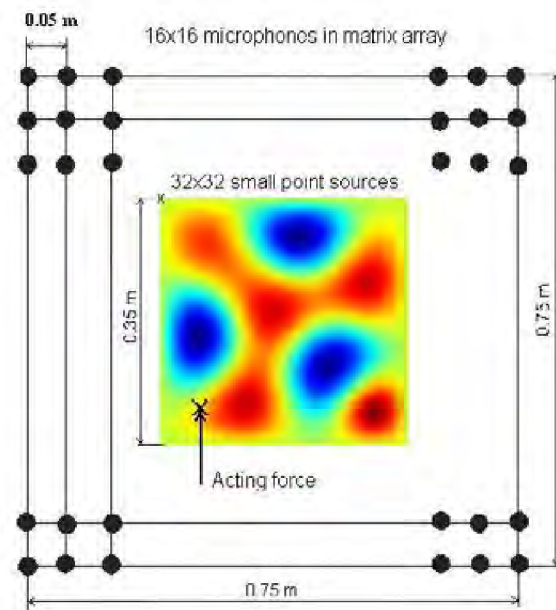
Figure 4.5: Position of the microphone array and the panel representing the sound source.

similarly as the first (primary) source with vibrating panel at higher distance from the measurement positions. This setup simulates background sound source which disturbs the original sound field. For the sake of simplicity the reflections from the first and second panel is neglected - the absorption coefficient of the panels is infinity in all directions. The two layers of microphones are spaced with same distance as spacing between microphones, in this case 5 cm.
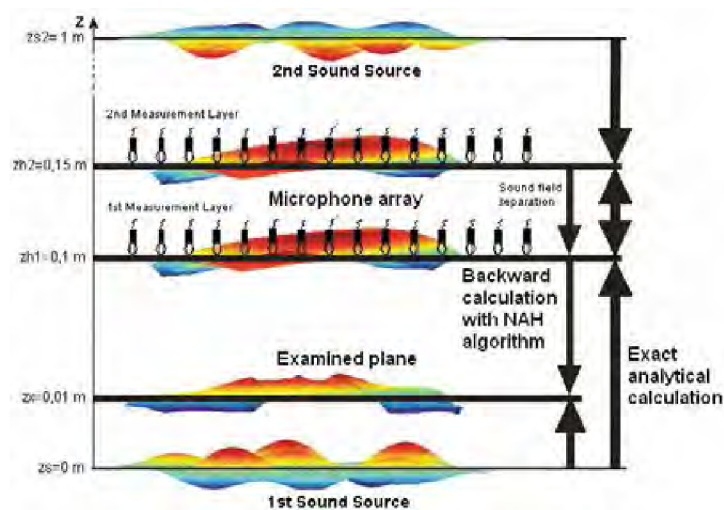
Figure 4.6: Outline of the simulation case with sources on both sides of the microphone array.

4.2.3 Error norms and representations for determination of accuracy of the algorithms

Two error norms can be applied to evaluate the effectiveness of the algorithms under test. The core of the both error representation is the same, but there is a difference in scaling. Both norms compare difference between true acoustic quantity values (analytical calculation of Rayleigh's integral) and values calculated by indirect NAH algorithm and total true square values at all discrete points on the examined plane.

For algorithms involving Fourier transform the calculation can be limited only for discrete points which lie directly above the source. This modification reduces the error caused by finite aperture calculation and results are better comparable with algorithms which aren't using Fourier transformation. When this procedure is applied the range of indexes i and j in Eq. (4.4) and Eq. (4.5) are reduced and they represent only points which are strictly above the source region. The first norm is logarithmic, calculating relative average error level and can be more transparent when there is a big difference between minimal and maximal error of compared algorithms and in the selected frequency range [19].

$$L_{err_p} = 10 \cdot \log_{10} \left(\frac{\sum\limits_{i} |p_i^{true} - p_i|^2}{\sum\limits_{j} \left|p_j^{true}\right|^2} \right) \quad (4.4)$$

The second norm in Eq. (4.5) represents the mean square average error in percent.

$$MSE = \sqrt{\frac{\sum\limits_{i} |p_i^{true} - p_i|^2}{\sum\limits_{j} \left|p_j^{true}\right|^2}} \cdot 100 \quad (4.5)$$

For more precise evaluation of error, there could be also used the direct acoustic quantity representation on the diagonal of the calculated plane or only above the vibrating plate (especially for algorithms with Fourier transformation), and a difference between true and calculated values are shown directly in figure. This representation can detect big errors in isolated points, but it is limited only on the diagonal, but usually this region determines the errors for the whole plane. Above mentioned error methods calculates the global average error and can't handle big errors in few points.

4.3 Advanced Methods for Single Layer Array NAH

The main goal of this thesis is development, evaluation and testing of new acoustic holography algorithms with focus on algorithms based on transformation to wavenumber domain. Within this scope the improvement of accuracy of existing algorithms, which have been published in the last two decades, and expansion of their usability and applicability into new areas are also the objectives of this thesis. The section about single layer acoustic holography algorithms (algorithms using input data from measurement in one plane parallel to examined source) mainly describes some important improvements and evaluates the properties of the algorithms.

4.3.1 Iterative NAH with Wiener Filtering

This method has been described in detail in chapter 2.1.4, but comprehensive study on the adjustable parameters in this method has not been presented. As mentioned in chapter 2.1.4, the main purpose of this method is an adaptive filtration of evanescent waves with high wavenumber to reduce the influence of noise presented in the measured input data. With constant setting of $k - space$ filter and one direct calculation of prediction field it is not possible to obtain good pressure or particle velocity backward prediction. Huge amplification of evanescent waves in backward calculation usually prevents good reconstruction accuracy with this simple setup. The iterative method with Wiener filter incorporates regularization parameter ε in Wiener filter which can be tuned to efficiently filtrate noise in the measurement. The algorithm itself converges to the right solution, but the number of iterations could not be the same for all frequencies in the selected frequency range. It is not efficient to spend time with more iterations if there is no more improvement in accuracy.

The general mathematical formulation has been already mentioned in state of the art, but for completeness is expressed here also. The recursive process is described in Eq. (4.6) with applied Wiener filter for wavenumber domain, described mathematically in Eq. (4.7).

$$P_{zx} = P_{zx-1} + W \cdot (P_{zh} - G_p \cdot P_{zx-1}) \tag{4.6}$$

$$W(k_x, k_y, z_h - z_x) = \frac{G_p^*}{|G_p|^2 + \varepsilon^2} \tag{4.7}$$

Representation of correct selection of number of iterations and speed of convergence can be seen in Fig. 4.7. In this case idealized measurement path is assumed (signal-to-noise ration of 60 dB).

In Fig. 4.7 there can be seen the valley where the ideal number of iterations with respect to overall accuracy can be found. The number of iterations arises with the frequency of examined sound field component.

If the measurement system has signal-to-noise ratio lower than 60 dB then some amount of regularization should be used in Wiener equation. In Fig. 4.8 there is a situation where measurement system is affected with transducer mismatch of ± 0.5 dB and the recursive algorithm is set to 500 iterations. There can be seen that higher regularization value (higher expected SNR) improves significantly the prediction accuracy.
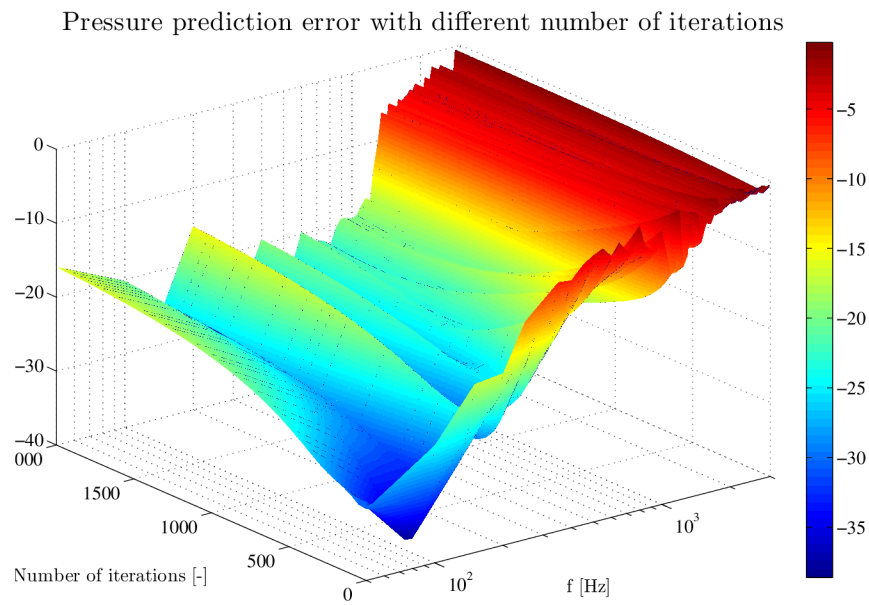
Figure 4.7: Pressure prediction error with differen number of iterations for whole frequency range calculated with algorithm involving recursive Wiener filteration.
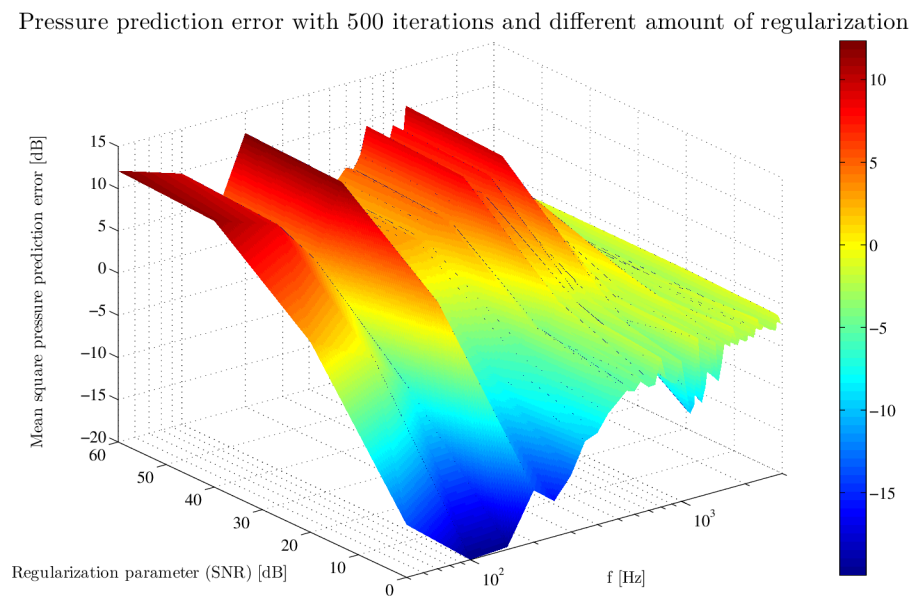
Figure 4.8: Pressure prediction error with differen amount of regularization for 500 iterations of recursive algorithm with Wiener filter.

4.3.2 Adaptive Enlargement of Hologram Aperture in NAH

This method tries to avoid windowing in spatial domain before transformation into wavenumber domain. If the spatial window (mostly Tukey shape) is applied, some of the information directly measured in examined sound field near source surface is lost. If the smooth shape of the measured pressure field is required (due to subsequent Fourier transformation) the sound field information on the edge of the measured hologram is damaged (the values on edges should be zero). It rapidly reduces the area of successful reconstruction of sound field near vibrating source. Avoiding of using spatial window, but ensuring the continuation of sound field beyond the original hologram is the main purpose of the method with adaptive enlargement.

The procedure is similarly to recursive Wiener filtering based on iterative process, but in compare with Wiener filtration, adaptive enlargement of hologram aperture optimizing original input data in spatial domain. This technique is based on procedure described in literature [46, 39] and the core of the method is described in next paragraph.

In the first step, original hologram aperture is enlarged with zero padding. The next step involves direct and indirect spatial transformation while filtering in k-space is applied. The resulting pressure data in spatial domain is then corrected with true measured (original) pressure data. The procedure is finished when the difference between transformed spatial pressure data and original measured pressure data is minimal. This procedure can be expressed in Eq. (4.8).

$$p_{zh}^{n(2Mx2N)} = F_{k_x,k_y}^{-1} \left[F_{x,y} \left[p_{zh}^{n-1(2Mx2N)} \right] K_f \right] \quad \Leftarrow \quad p_{zh}^{orig(MxN)} \tag{4.8}$$

where $F_{x,y}$ denotes direct 2D Fourier transformation,

$F_{x,y}^{-1}$ is 2D inverse Fourier transformation,

$p_{zh}^{orig(MxN)}$ is original pressure field (hologram) measured with the array of size M by N,

$p_{zh}^{n(2Mx2N)}$ is twice enlarged original hologram (2M x 2N),

K_f is a k-space filter,

n is an iteration number.

The whole calculation procedure of adaptively enlarge hologram aperture is in diagram in Fig. 4.9.
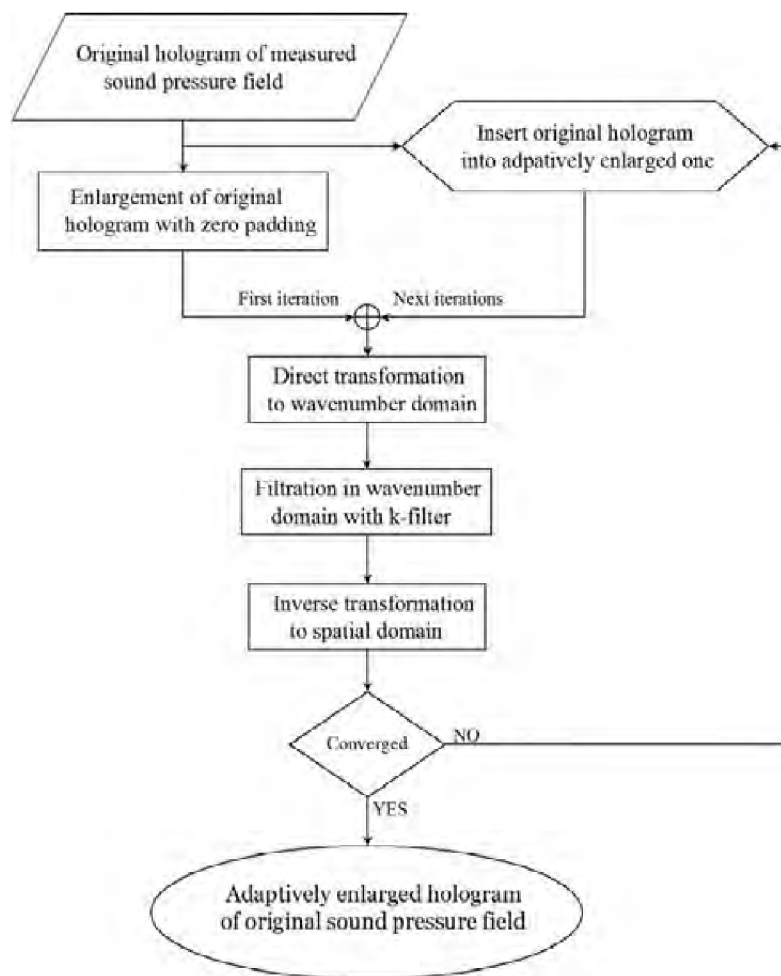
Figure 4.9: Diagram of calculation procedure of iterative NAH algorithm.

4.3.3 SONAH with Lower Computational Cost

One new computer implementation of the SONAH algorithm [19] has been proposed in the scope of this thesis and is presented in this chapter. The new implementation uses, as compared with recent classical calculation with numerical integration described in chapter 2.1.5, simplified but faster calculation of infinite integrals. In the followed paragraphs the detailed description of the calculation procedure for both implementations is presented.

Classical Implementation with Numerical Integration

Classical implementation of SONAH algorithm is based on original derivation by Hald [19] and described in more details in Master thesis by Gomes [14]. Infinite integrals are solved by numerical integration with Gauss-Laguerre and Gauss-Legendre quadrature. Autocorrelation matrix $\mathbf{A}^{\mathrm{H}}\mathbf{A}$ and cross-correlation matrix $\mathbf{A}^{\mathrm{H}}\mathbf{b}$ can be then determined using equations Eq. (4.9) and Eq. (4.10) [14].

$$\left[\mathbf{A}^{\mathrm{H}}\mathbf{A}\right]_{n_x n_y} = \frac{J_1\left(k_0 \mathbf{R}(x,y)_{n_x n_y}\right)}{k_0 \mathbf{R}(x,y)_{n_x n_y}}$$
$$+ \frac{1}{(2k_0 z_h)^2} \sum_{u=1}^{N_{Laguerre}} \left[w_u \, J_0\left(k_0 \mathbf{R}(\mathbf{x},\mathbf{y})_{\mathbf{n_x n_y}} \sqrt{1 + \left(\frac{\mathbf{x_u}}{\mathbf{2k_0 z_h}}\right)^{\mathbf{2}}}\right)\right] \tag{4.9}$$

$$\left[\mathbf{A}^{\mathrm{H}}\mathbf{b}\right]_{n_x n_y} = \frac{1}{(k_0(z_h + z_x))^2} \sum_{u=1}^{N_{Laguerre}} \left[w_u \, J_0\left(k_0 \mathbf{R}(\mathbf{x},\mathbf{y})_{\mathbf{n_x n_y}} \sqrt{1 + \left(\frac{\mathbf{x_u}}{\mathbf{k_0(z_h + z_x)}}\right)^{\mathbf{2}}}\right)\right]$$
$$+ \sum_{v=1}^{N_{Legendre}} \left[w_v \, e^{jk_0(z_h - z_x)\cos(x_v)} J_0\left(k_0 \mathbf{R}(\mathbf{x},\mathbf{y})_{\mathbf{n_x n_y}} \sin(\mathbf{x_v})\right) \sin(x_v)\cos(x_v)\right] \tag{4.10}$$

The coefficients w_u, x_u for Laguerre quadrature and w_v, x_v for Legendre quadrature can be calculated from N-element Laguerre and Legendre polynomials. The arguments in Bessel functions J_0 and J_1 (first kind and zero/first order) depends on frequency of examined sound field (k_0) and also on distance $\mathbf{R}(x,y)_{n_x n_y}$ of measurement plane (z_h) from source surface (z_x). Thus, for different calculation frequency and/or for closer or far distance of microphone array from source surface, new values of Bessel functions have had calculated.

Proposed Improved Implementation of SONAH

Presented new implementation of SONAH is derived from the basic infinite integral equations Eq. (2.21) and Eq. (2.22) with respect to the original idea of the SONAH algorithm, where the limited number of the elementary waves is considered. The original integrals can be represented in polar coordinates and then transformed to the finite sum of the elementary waves. The optimal set of elementary waves used for SONAH calculation (number of waves, maximal wave-number) can be determined from frequency range of used microphone array and its configuration.

$$\left[\mathbf{A}^{\mathrm{H}}\mathbf{A}\right]_{n_x n_y} = \frac{1}{2\pi} \sum_{u=1}^{N_k} \left(k_u \cdot \left|e^{jz_h\sqrt{k_0^2 - k_u^2}}\right|^2 \cdot J_0\left(k_u \mathbf{R}(x,y)_{n_x n_y}\right) \cdot \Delta k\right) \tag{4.11}$$

$$\left[\mathbf{A}^{\mathrm{H}}\mathbf{b}\right]_{n_x n_y} = \frac{1}{2\pi} \sum_{u=1}^{N_k} \left(k_u \cdot \left|e^{jz_h\sqrt{k_0^2 - k_u^2}}\right|^2 \cdot J_0\left(k_u \mathbf{R}(x,y)_{n_x n_y}\right) \cdot e^{-j(z_h - z_x)\sqrt{k_0^2 - k_u^2}} \cdot \Delta k\right) \tag{4.12}$$

Number of elementary waves N_k used for calculation can be determined from maximal measured frequency and corresponds to the spatial resolution - spacing between microphones in the array.

$$k_u = u \cdot \Delta k = u \cdot \frac{8\pi}{\Delta x \cdot (N_k - 1)} \tag{4.13}$$

The equation Eq. (4.13) defines wavenumber range (discrete values) of elementary waves used for SONAH calculation $k_1 \ldots k_u$, where $u = 1, 2 \ldots N_k$, and k_1 is the first elementary wave with lowest wavenumber, k_u is the elementary wave with highest wavenumber and x is spacing between microphones. This simplification has one useful advantage,

Table 4.1: Calculation time of one frequency component with old and improved SONAH algorithm for two array configurations

Array configuration	SONAH implementation - calculation time [s]	
	Old implementation	Proposed improved implementation
8x8	1.57	0.06
16x16	6.18	1.08

which can speed up NAH calculation (sound field prediction) in many measurement set-up cases, of only one-time calculation of all Bessel functions for selected measurement set-up - spacing between microphones and stand off distance of microphone array from sound source surface. This means that the first-time calculated Bessel functions can be used for any other frequency components of future NAH calculation with the same set-up.

Comparison of Computational Cost

Test of computational cost of both implementations of SONAH were performed on Centrino based computer station with Pentium M 1.7GHz processor with 1 GB of internal RAM. Both algorithms were implemented in MathWorks Matlab v.6.5 R13 and calculation of pressure prediction error and speed test was performed.

Two different measurement setups are considered for this test - one large measurement microphone array with 16x16 microphones and small one with 8x8 microphones. The calculation times and errors of pressure prediction for both cases and both implementation of SONAH are compared and evaluated.

The calculation time of new proposed implementation of SONAH is more than 20 times faster for small array and 5 times faster for large array than old implementation with numerical integration. The main reduction of computation cost of new algorithm is in one-time calculation of Bessel functions, while old implementation has to calculate all Bessel functions independently (dependent variables in the function parameters). In Fig. 4.10, there are presented the errors of pressure prediction of both implementations in usual frequency range for smaller and larger microphone array. In this test case SONAH I. means old implementation and SONAH II. corresponds to the proposed new implementation of SONAH algorithm. The both implementations are set for the best performance and the lowest prediction error.

From the above result it is evident that for speed up SONAH calculation, the new computer implementation has been successfully evaluated with very good results. The reduction of computation cost in compare with recent implementation with numerical integration is more than 5 times and the pressure prediction error in near-field is in the same level as with recent version.
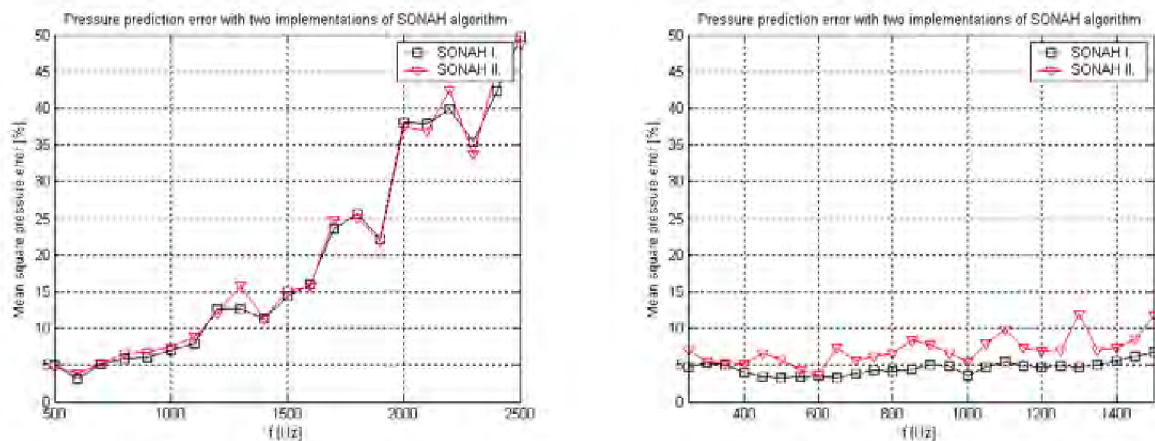
Figure 4.10: Prediction error of calculated pressure in near-field with two implementations of SONAH algorithm for two array configurations - 8x8 microphones (left) and 16x16 microphones (right).

4.3.4   Novel Method for Determination of Regularization Parameter

In this section, two different NAH algorithms are used together to obtain correct value of the regularization parameter for any near-field acoustic holography algorithm. The main idea of the novel method is in comparison of results of pressure prediction of two different acoustic holography algorithms. If the selected algorithms are using different calculation procedure for pressure prediction and involves different procedure for regularization then different influence of regularization parameter to prediction accuracy could be expected. From this pre-requisition we can assume if proper amount of regularization is applied to both algorithms the highest accuracy of pressure prediction could be achieved and difference between pressure prediction could be minimal. If the regularization parameter has not been selected ideally, then difference between predictions obtained with both algorithms will be larger.

For this purpose we can combine results (predicted pressure values) from two selected algorithms (SONAH and classical NAH), while using same amount of regularization for them. In SONAH algorithm, the regularization parameter θ, can be expressed in signal-to-noise ration (SNR) notation in Eq. (4.14).

$$\theta = 10^{-\frac{SNR}{10}} \tag{4.14}$$

In other words, this equation defines the value of the regularization parameter θ, for considered and expected SNR of input measured pressure data for SONAH.

The similar equation can be used for determination of regularization parameter for Wiener filter in classical NAH algorithm, while

$$\varepsilon = \sqrt{\theta} = 10^{-\frac{SNR-35}{20}}. \tag{4.15}$$

The both algorithms use same input pressure data measured with microphone array with non-ideal transducers and some amount of noise in the measurement path, so there could be the same real signal-to-noise ratio. For determination of true SNR in input

data, resulting pressure prediction in near-field of sound source of both algorithms can be compared. The difference between these values is defined in Eq. (4.16), by an error norm between the two algorithm results in percent.

$$DIF = \sqrt{\frac{\sum\limits_{i} \left| p_i^{ClassicalNAH} - p_i^{SONAH} \right|}{\sum\limits_{j} \left| p_j^{ClassicalNAH} \right|} \cdot 100} \qquad (4.16)$$

Due to different calculation method of both algorithms, the difference between pressure values is minimal when proper amount of regularization is used. This feature can be explained in the procedure of using regularization in both algorithms.

While in SONAH algorithm, the regularization reduces singularities in autocorrelation matrix $A^H A$, where each element corresponds to one elementary plane wave, thus regularization influence all plane waves (propagating and evanescent). On the contrary in classical algorithm, regularization in Wiener filter causes filtering of only elementary waves with higher wave-number only (mostly evanescents). This different application of regularization causes different impact into processing of input noisy data and produces different predicted pressure field near sound source surface, if there is not ideal amount of regularization used. An ideal amount of regularization produces the lowest possible pressure prediction error of all NAH methods.

The proposed method can be run once at the beginning (for one significant frequency component), before total sound field mapping (for all significant frequencies), calculating predicted pressure differences DIF in Eq. (4.16) for small region in the center of predicted plane (approx. 50 % of whole predicted plane/microphone array) for all possible SNR assumed in measured data. While minimal value of DIF corresponds to the signal-to-noise ratio in the input data and with using Eq. (4.14), the right value of regularization parameter can be successfully adjusted. After right amount of regularization has been found, for all other frequency components, same regularization parameter can be used.

Evaluation of Novel Regularization Method

All results of new proposed method for determination of regularization parameter has been obtained by simulated measurement set-up. Classical William's setup described at the beginning of this chapter with vibrating steel panel in infinite baffle was used. In this case the dimensions of the plate were 0.35 m x 0.35 m and a thickness of 3 mm. The plate was driven by a harmonic point force of strength 1 N at the position 0.05 m x 0.05 m. The microphone array had 8x8 microphones with 0.05 m microphone spacing. The error norm used for evaluation of the performance of the SONAH algorithm is the total mean square difference between the 'true' pressure and values calculated with the SONAH algorithm, normalized with the 'true' mean square values at all points in the examined plane.

For evaluation of proposed method, the set of simulation cases with different measured input data were used. The difference between each case is in amount of added transducer amplitude or phase mismatch, which defines the real data signal-to-noise ratio. The pressure prediction error of SONAH algorithm and pressure prediction difference between SONAH and classical NAH has been calculated ten times for each value of transducer mismatch represented in added white noise to true measured pressures. Each figure
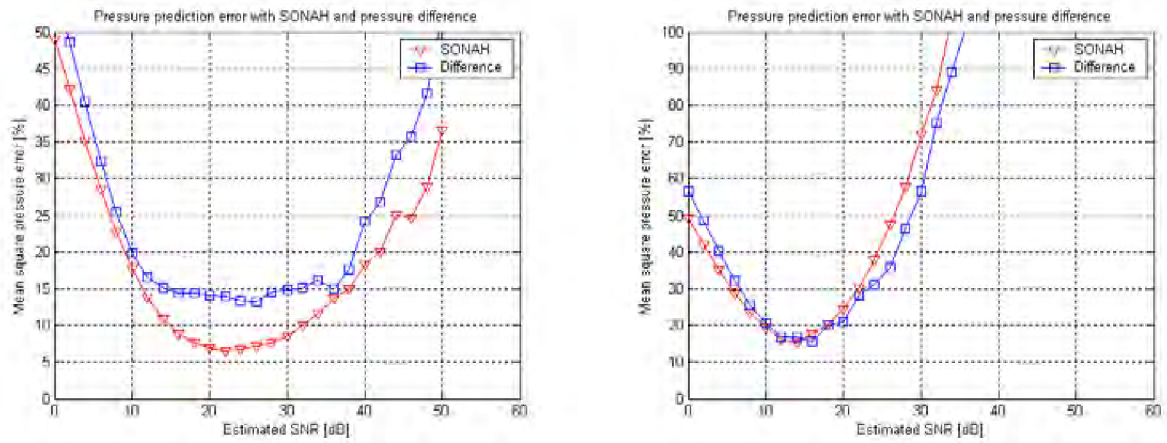
Figure 4.11: Pressure prediction error with the SONAH and pressure difference between two algorithms for $f = 500$ Hz and added amplitude mismatch 0.1 dB (left) and 1 dB (right).
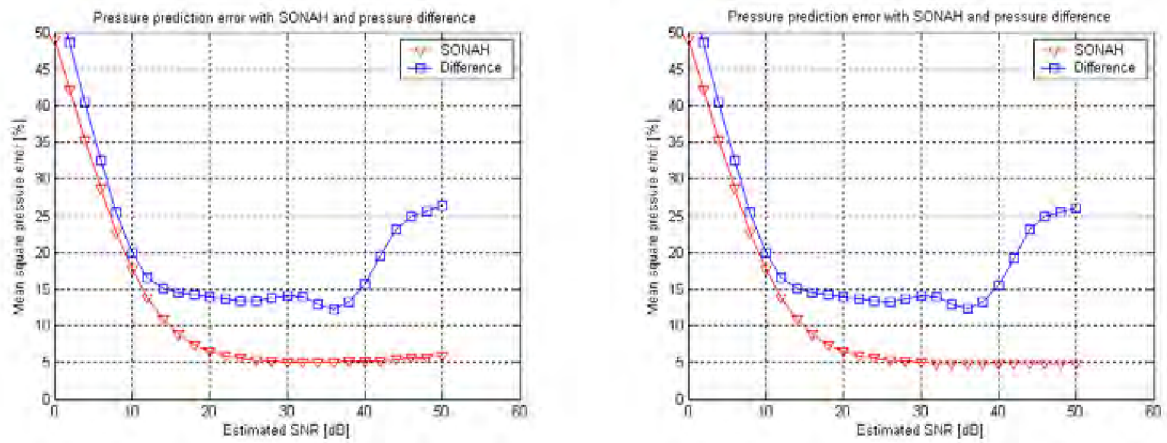
Figure 4.12: Pressure prediction error with SONAH and pressure difference between two algorithms for f = 500 Hz and added amplitude mismatch 0.01 dB (left) and without added mismatch (right).

contains prediction error of pressure calculated with SONAH algorithm at a distance of 10 mm far from sound source surface (red curve with triangles) and an error norm of the difference between predicted pressure data calculated with SONAH and classical NAH algorithm (blue curve with squares). On the x-axis of the figure, there is selected (estimated) SNR for input pressure data and corresponding regularization parameter for SONAH algorithm is set. In Fig. 4.11, there is more added transducer amplitude mismatch, so higher amount of regularization is needed and low value of SNR in input data is determined.

In Fig. 4.12, low and none transducer mismatch is modeled resulting in lower regularization needed and higher SNR determined.

In next Table 4.2, summary of pressure prediction errors for ideal, determined and no regularization in SONAH algorithm is presented.

Table 4.2: Pressure prediction errors with the SONAH algorithm and with different amount of regularization.

Added amplitude mismatch [dB]	Prediction error of pressure field calculated with SONAH [%]			
	Zero regularization	Ideal regularization	Determined regularization	Added error
0	5.0	4.9	4.9	0.0
0.01	6.2	5.0	5.1	0.1
0.02	8.7	5.2	5.5	0.3
0.05	19.4	5.8	5.8	0.0
0.1	32.0	6.6	6.6	0.0
0.2	64.8	8.1	8.2	0.1
0.5	148	11.3	11.6	0.3
1.0	303	15.4	17.6	2.2

As shown in Table 4.2, the added error caused by non-ideal determination of regularization parameter is very low, thus validation of proposed method has been done. In compare with huge prediction errors with zero regularization, proposed method estimates regularization very close to ideal and reduces prediction error successfully. These results have been also presented at the conference [22].

4.4 Double layer array NAH

In conventional planar acoustic holography sources on the "wrong" side of the measurement plane (including image sources due to reflections) contaminate the sound pressure in the measurement plane and give rise to errors. By contrast, the double layer technique can, at least in principle, separate the two contributions from each other [9].

Basic planar acoustic holography theory expects that all sound sources are only on one side of the hologram (measurement array) and there are no other sources. If there is a situation with other sources presented on the other side (mostly behind the hologram), the reconstruction of sound field near examined sources are very difficult and creating huge errors. The other source on the opposite side causes errors in measurement of basic acoustical quantity (acoustic pressure) at the microphone positions. The second source (behind the hologram) can be introduced as mirror image of this source on the same size as examined source. The result of this configuration leads in most cases to underestimation of original sound field in examined plane. In the literature from last decade one research team from Heifei University of Technology in China introduced the possibility to separate sound fields coming from different sides of the measurement (hologram) plane by using double holographic planes - measurement with two layers of acoustic sensors (microphones) [10, 9]. The calculation procedure with measurement in two parallel planes has been also introduced by Brüel & Kjær in 2006 (in the literature in 2008) but they have used Dual layer SONAH algorithm (extension of single layer version [18]) as the processing method for prediction of sound field near the source. This algorithm will be shortly mentioned in the end of this chapter.

The procedure introduced with Chinese research team in 2003 was based on classical acoustic holography method based on transformation into wave-number domain but nobody referenced it in next years. In this thesis the comprehensive research focused on this method has been carried out and initial problems and disadvantages of the originally presented method have been minimized by corrections and further improvements.

The main idea of measurement with two parallel planes in the environment where there are sources on both sides of the measurement planes is described in Fig. 4.13.

This arrangement introduced four parallel planes where there are two of them called "source planes" and the rest are "hologram (measurement) planes" placed in parallel between the source planes.

The complex sound pressure measured at any point in the first hologram plane 1 $p_1(x_1, y_1, z)$ is the sum of the complex pressure $p_{1A}(x_1, y_1, z)$ caused by sound source located and represented by source plane A and the complex pressure $p_{1B}(x_1, y_1, z)$ caused by sound source located and represented by source plane B. The mathematical formulation of this statement is in Eq. (4.17).

$$p_1(x_1, y_1, z) = p_{1A}(x_1, y_1, z) + p_{1B}(x_1, y_1, z) \tag{4.17}$$

Similarly, the complex pressure at any point on hologram plane 2 $p_2(x_2, y_2, z + d)$ is also the sum of the complex pressures caused by the sources on both source planes ($p_{2A}(x_2, y_2, z + d)$ by the source A, $p_{2B}(x_2, y_2, z + d)$ by the source B) as expressed in Eq. (4.18).

$$p_2(x_2, y_2, z + d) = p_{2A}(x_2, y_2, z + d) + p_{2B}(x_2, y_2, z + d) \tag{4.18}$$
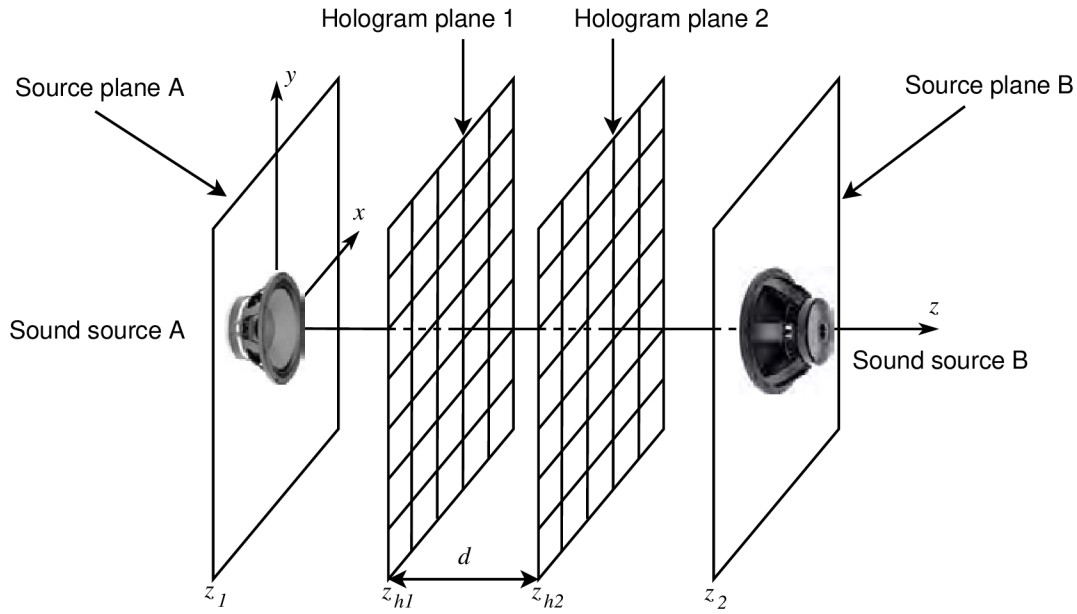
Figure 4.13: Composition of sources and planes in double layer holography [9].

If we consider only one source present (on source plane A) the transfer function of the wave-number spectrum of the complex pressure between hologram planes 1 and 2 can be expressed in Eq. 4.19, where the exponential term is well known direct propagator (Green's function) 2.7.

$$P_{2A}(k_x, k_y, z + d) = P_{1A}(k_x, k_y, z)e^{jk_z d} \qquad (4.19)$$

where $P_{1A}(k_x, k_y, z)$ is a 2D Fourier transform of the complex pressure
                                     $p_{1A}(x_1, y_1, z)$,

       $P_{2A}(k_x, k_y, z + d)$ is a 2D Fourier transform of the complex pressure
                                     $p_{2A}(x_2, y_2, z + d)$,

       k_z is wave-number in z direction, $k_z = \sqrt{k^2 - (k_x^2 + k_y^2)}$.

Similarly, for the sound source on source plane B, the transfer function can be expressed in Eq. (4.20).

$$P_{1B}(k_x, k_y, z) = P_{2B}(k_x, k_y, z + d)e^{jk_z d} \qquad (4.20)$$

If we now transform Eq. 4.17 and Eq. 4.18 by 2D Fourier transform into wave-number domain, the resulting system of equations can be written in Eq. (4.23) and Eq. (4.24) [9].

$$P_1(k_x, k_y, z) = P_{1A}(k_x, k_y, z) + P_{1B}(k_x, k_y, z) \qquad (4.21)$$

$$P_2(k_x, k_y, z + d) = P_{2A}(k_x, k_y, z + d) + P_{2B}(k_x, k_y, z + d) \qquad (4.22)$$

After substituting Eq. (4.19) and Eq. (4.20) into Eq. (4.24) and Eq. (4.23) the equation pair can be rewritten as follows.

$$P_1(k_x, k_y, z) = P_{1A}(k_x, k_y, z) + P_{2B}(k_x, k_y, z)e^{jk_z d} \qquad (4.23)$$

$$P_2(k_x, k_y, z + d) = P_{1A}(k_x, k_y, z + d)e^{jk_z d} + P_{2B}(k_x, k_y, z + d) \qquad (4.24)$$

By solving this system of equations for $P_{1A}(k_x, k_y, z)$, the separation of sound fields coming from different sides of the hologram plane can be expressed in Eq. (4.25) [9]. This equation expects two measurement layers with microphones assembled in matrix. Acoustic quantity is measured in both layers and the separation of incoming sound waves from opposite directions can be achieved.

$$P_{1A}(k_x, k_y) = \frac{P_1(k_x, k_y) - P_2(k_x, k_y)e^{jk_z d}}{1 - e^{j2k_z d}} \qquad (4.25)$$

This equation is generally ill-posed due to the expression in the denominator. For the wave-number components which lies on the radiation circle or they are very near, k_z is zero (or close to) and denominator is singular. After discrete 2D Fourier transform of complex sound pressure field from spatial domain into wave-number domain the discrete points in the 2D wave-number domain that lie closely to the radiation circle are affected with above Eq. (4.25) and the resulting pressure spectrum of sound field generated by the source in source plane A $P_{1A}(k_x, k_y)$ in these discrete points goes to infinity. In the spatial domain this trouble leads to huge reconstruction errors on some frequencies in considered frequency band. This can be also explained as aliasing effect in wave-number domain. The simulation results of the original implementation of above Eq. 4.25 is shown in Fig. 4.14 where mean square error of pressure prediction closer to the source surface has been calculated. For this test case the simulation setup was the same as described in chapter 4.2.2.
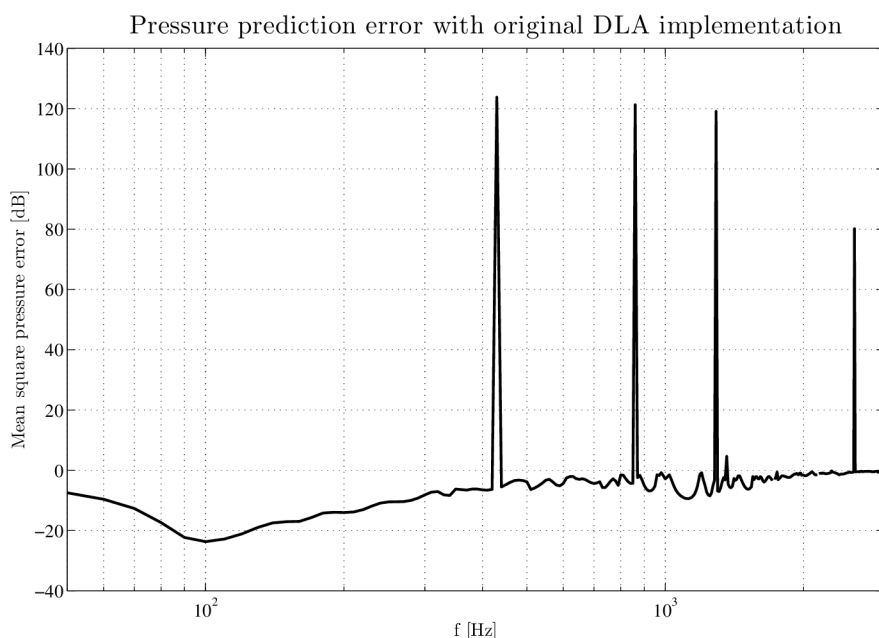
Figure 4.14: Mean square pressure prediction error with original double layer holography implementation.

The only possibility of to avoid the difficulty connected with the k-space aliasing is to smoothen the transformation function (separation term) $\frac{1}{1-e^{i2k_z d}}$ at discrete points in wave-number domain. The solution can be simplified for only smoothen k_z. Similar problem has been described in literature [47] where smoothing (averaging) of forward velocity propagator (modified Green's function) has been necessary to avoid the singularity in the propagator in Eq. (4.26).

$$G_{pv}(k_x, k_y, z+d) = \frac{e^{jk_z d}}{k_z} \qquad (4.26)$$

The solution of the averaging is the integration of G_{pv} in small region (square box) around the discrete point in the wave-number domain. The averaged value of G_{pv} has been expressed with double integration in cartesian coordinates in Eq. (4.27) [47].

$$\int_{(\Delta k)^2} \int G_{pv}(k_x, k_y, z+d) dk_x dk_y = (\Delta k)^2 \overline{G_{pv}} \qquad (4.27)$$

The above integral can be easily solved in polar coordinates in Eq. (4.28).

$$\overline{G_{pv}} = \frac{1}{\Delta\phi k_0 \Delta k} \int_{\phi_1}^{\phi_1 + \Delta\phi} d\phi \int_{k_0 - \frac{\Delta k}{2}}^{k_0 + \frac{\Delta k}{2}} G_{pv} k_\rho dk_\rho \qquad (4.28)$$

From that theory one can also derive the equation for integration of k_z. In polar coordinates, the integration of the original k_z can be expressed in Eq. (4.29).

$$\overline{k_z} = \frac{1}{3k_0 \Delta k} \int_{k_1}^{k_2} k_z k_\rho dk_\rho \qquad (4.29)$$

where $k_0^2 = (m\Delta k)^2 + (n\Delta k)^2 \approx (k_x)^2 + (k_y)^2,$

$k_1 = k_0 - \frac{\Delta k}{2},$

$k_2 = k_0 + \frac{\Delta k}{2},$ $\qquad\qquad (4.30)$

$k_z = \sqrt{k^2 - (k_x)^2 - (k_y)^2}.$

k_ρ is similar to k_0 but in polar coordinates and Δk is stepping in wave-number domain (e.g. dimension of the microphone array).

After integration and transformation to Cartesian coordinates (in wave-number domain) and with condition of the same k-stepping in x and y coordinates, averaged $\overline{k_z}$ can be expressed in Eq. (4.31).

$$\overline{k_z} = \frac{(k^2 - k_1^2)^{\frac{3}{2}} - (k^2 - k_2^2)^{\frac{3}{2}}}{3k_0 \Delta k}, \qquad (4.31)$$

where k is the wavenumber of analyzed (calculated) sound field.

Preliminary simulation results have indicated that this equation could work quiet good and reconstruction error is reduced at the most problematic frequencies. But if we compare errors in other frequencies of the new regularization method with the original solution without k_z integration, errors raised. We can combine both approaches, pure k_z outside the radiation circle region and integration of k_z inside, and achieve better results
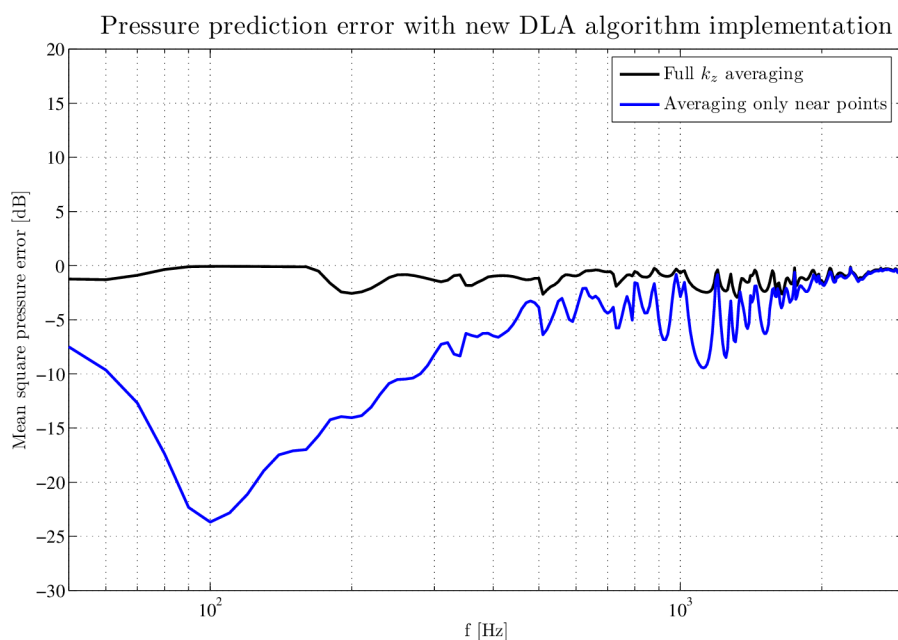
Figure 4.15: Mean square pressure prediction error with double layer holography implementation with averaging of k_z in the whole hologram and near problematic points.

with advantages of both methods. The decision about integration or non-integration of k_z depends on the interaction between radiation circle and discrete points in wave-number domain for the analyzed frequency. The region for k_z integration can be determined with respect to stepping in wave-number domain. The major benefit of the integration can be reached if the treatment is used in the region equals to the discrete point stepping in wave-number domain and it is used on the both sides of the radiation circle. Pressure prediction accuracy with new implementation of double layer technique with averaging of k_z in the whole hologram and only for discrete points near radiation circle is in Fig. 4.16. From this figure it is evident that averaging of k_z only near radiation circle gives better reconstruction (prediction) accuracy.

4.4.1   Improvements in DLA Technique

Some possible improvements of the original algorithm for sound field separation in wavenumber domain could be used in connection with double layer processing and they are presented in this chapter. The methods are derived from single layer calculations.

DLA NAH with Simple k-space Filter

The filtration of evanescent waves in k-space should be also assumed in case of double layer array measurements. The double number of microphones involves higher noise in the measurement and also numerical errors in processing procedure. The equation for the separation of front and back sound field supplemented with partial filtering of evanescent waves of the second sound source (unwanted background noise) in wavenumber domain is presented in Eq. (4.32).

$$
P_{zh}(k_{\mathrm{x}}, k_y) = \frac{P_{zh1}(k_{\mathrm{x}}, k_y) - P_{zh2}(k_{\mathrm{x}}, k_y) e^{j\overline{k_z}D} \cdot K_f(k_{\mathrm{x}}, k_y)}{\left(1 - e^{j2\overline{k_z}D}\right) \cdot K_f(k_{\mathrm{x}}, k_y)} \tag{4.32}
$$

where K_f is well known k-space filter, described in detail in chapter 2.1.3.

The filtration in k-space used in Eq. (4.32) minimizes evanescent waves coming from disturbing sound source behind the double layer microphone array. One can assume that the other source is much far away than the examined source, so the disturbing source affects mostly the propagating part of the wave spectra of the source of interest and the filtration doesn't corrupt the important part of the acoustic field at microphone positions.

Iterative DLA NAH with Recursive Wiener Filtering

To obtain the similar reconstruction error, as with single layer measurement technique, the recursive iterative method can be used too [3]. The Wiener filtration is applied to the resulting sound field coming only from the first (examined) source after sound field separation in Eq. (4.32). The procedure is similar to that one used in single layer configuration in chapter 2.1.4.

Adaptive Enlargement of Hologram Aperture in DLA

In double layer array processing, there could be also used error reduction procedure which enlarges measurement hologram aperture by zero padding. There were few simulation studies and the hologram has been enhanced to twice and four times the original dimensions. Due to the windowing before discrete Fourier transformation, the both measurement planes must be enlarged.

The advanced method is adaptive enlargement as described in chapter 4.3.2, which uses iterative procedure with direct and inverse transformation (from spatial to wavenumber domain) of filtered wavenumber spectrum in k-space. For double layer holography the iterative procedure can be written according to original derivation in Eq (4.33).

$$
p_{zh_{1,2}}^{n(4Mx4N)} = F_{x,y}^{-1} \left[F_{x,y} \left[p_{zh_{1,2}}^{n-1(4Mx4N)} \right] K_f \right] \Leftarrow p_{zh_{1,2}}^{orig(MxN)} \tag{4.33}
$$

Restored pressure data in spatial domain can then be fully used into transformation to k-space, where the kernel of the double layer NAH calculation is applied.
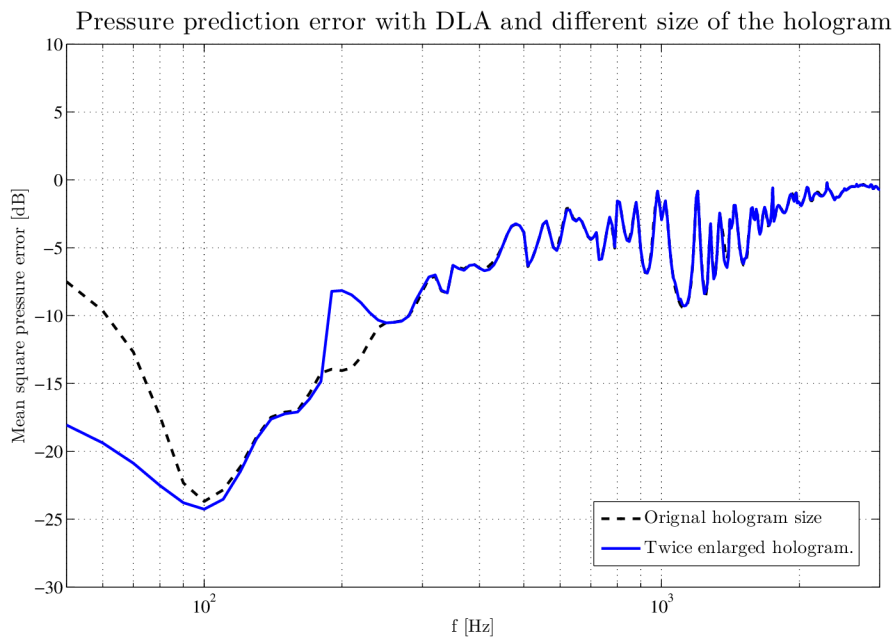
Figure 4.16: Mean square pressure prediction error with double layer holography with and without enlarged the original hologram with zero padding.

4.4.2   Simulation Results with Double Layer Technique

In the first test case there is no noise coming from the "wrong" side of the measurement plane. There is no reason to expect that the double layer method should perform better than the single layer method under such conditions, and this is also apparent from the results shown in Fig. 4.17.
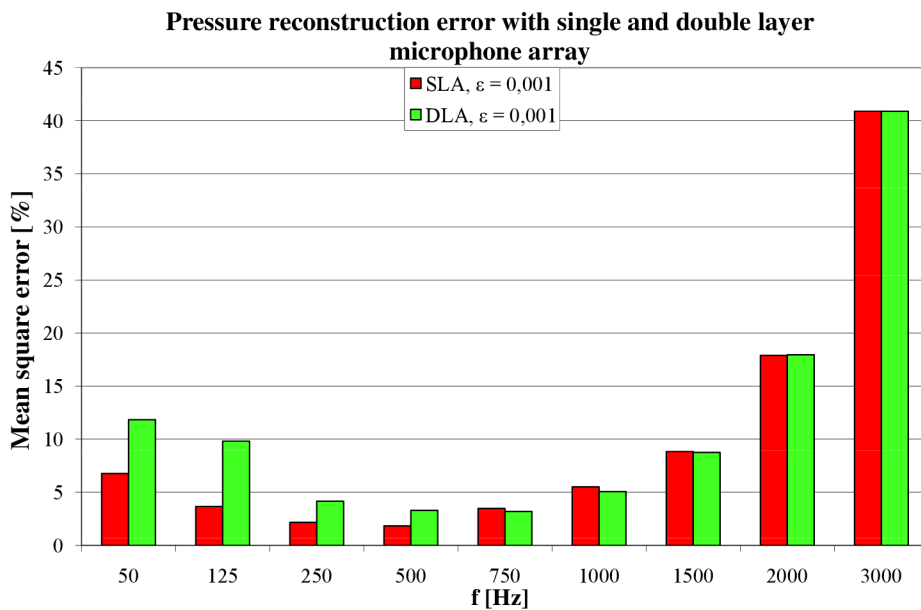
Figure 4.17: Error in pressure reconstruction under ideal conditions, regularization in Wiener filter: $\varepsilon = 0.001$.

In the second test case the measurement is disturbed by noise from the other side of the measurement plane. The second source is similar to the primary source, but the point force driving the secondary panel is ten times larger than the primary force and acting at another position. Thus the disturbing source is stronger than the primary source, but much further away from the measurement plane(s); see Fig. 4.6. Not surprisingly the double layer method performs significantly better than the single layer method in this case, as can be seen from Fig. 4.18. However, the double layer method is also disturbed by the extraneous noise and the general error level is increased.
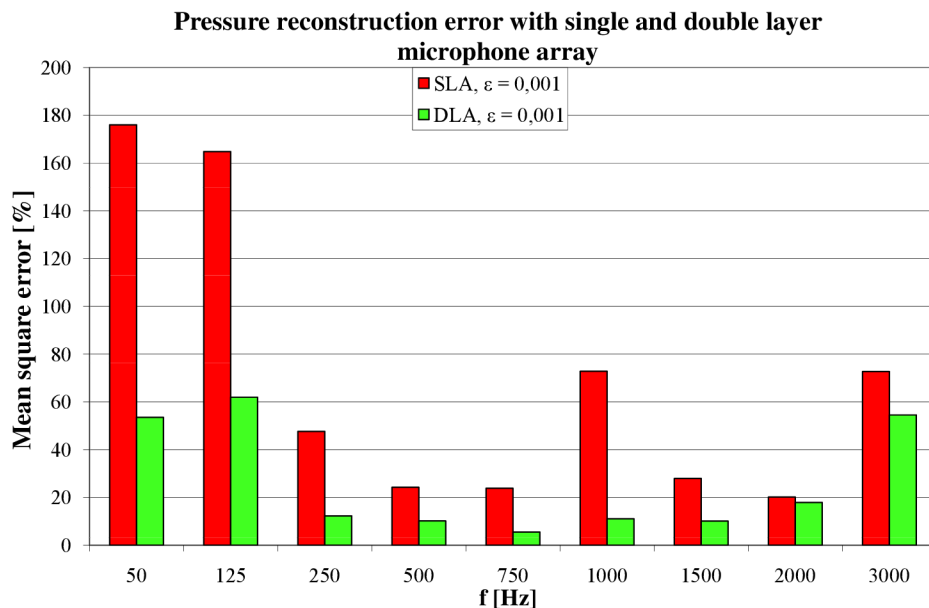
Figure 4.18: Error in pressure reconstruction with disturbing background noise from the wrong side of the array, regularization in Wiener filter $\varepsilon = 0.001$.

In the previous simulations ideal transducers were assumed. However, in measurements with a real transducer array one must allow for a certain amount of amplitude and phase mismatch. This can be simulated by adding random amplitude and phase errors to the "true" pressure at the microphone positions [37, ?]. Figure 4.19 corresponds to Fig. 4.17 (no disturbing background noise), but has been determined by averaging over many random sets of typical amplitude and phase errors ($\pm$ 0.5 dB and $\pm$ 1°). It is apparent that transducer mismatch causes enormous errors unless the regularization parameter in the Wiener filter is increased. With appropriate regularization the reconstruction error drops to acceptable values.

Fig. 4.20 corresponds to Fig. 4.18 (the measurement is disturbed by noise from the "wrong" side of the array), but many random sets of phase and amplitude errors have been added. The same high value of the regularization parameter as in the case without background noise has been used. Such a high value of the regularization parameter will reduce the accuracy under ideal conditions, but clearly improves the performance if the transducers are not properly matched. The advantage of the double layer method can be seen.
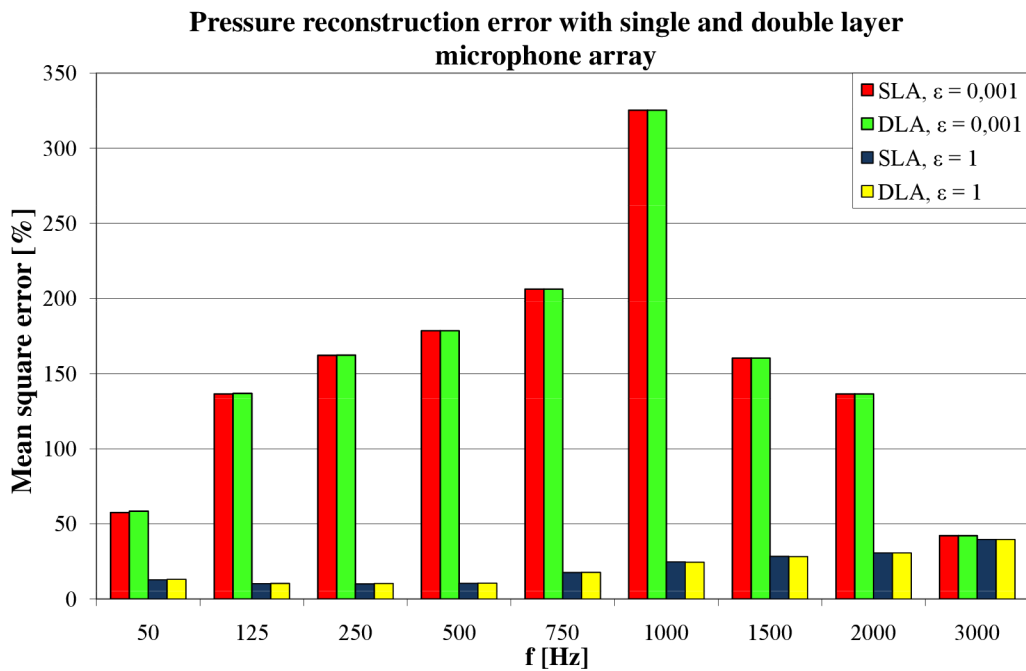
Figure 4.19: Average error of pressure reconstruction without background noise, amplitude mismatch $\pm$ 0.5 dB and phase mismatch $\pm$ 1°; regularization in Wiener filter $\varepsilon = 0.001$ and $\varepsilon = 1$.
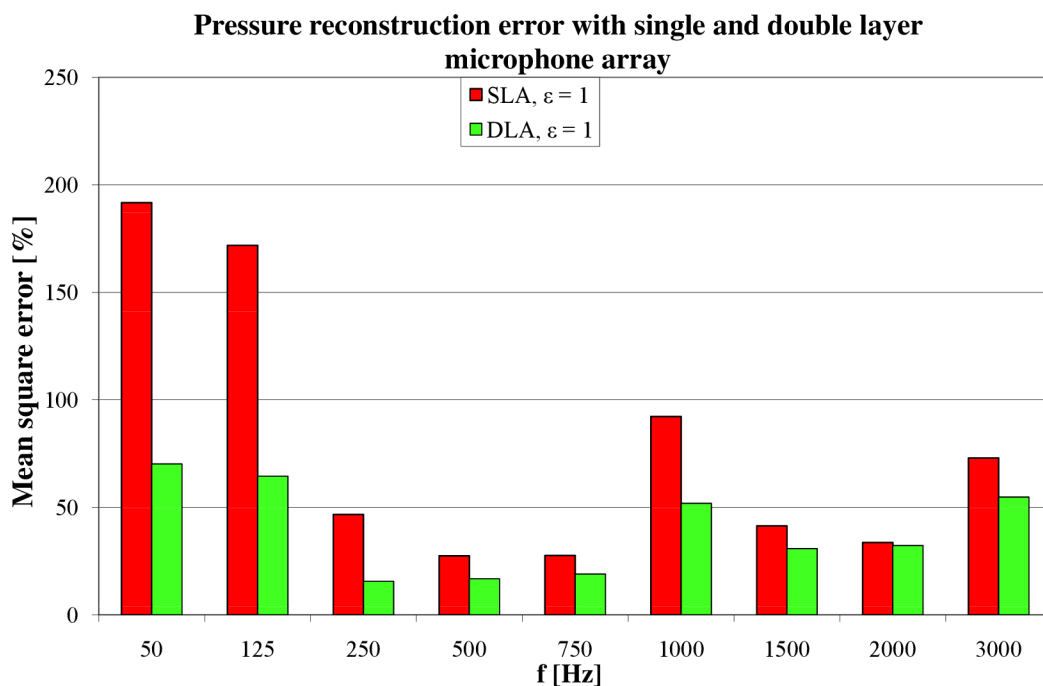
Figure 4.20: Average error of pressure reconstruction with disturbing background noise from the wrong side of the array, amplitude mismatch $\pm$ 0.5 dB, phase mismatch $\pm$ 1°; regularization in Wiener filter $\varepsilon = 1$.

Simulation Conclusion in Simple Case

The effectiveness in error reduction with double layer array processing, when there are sources on both sides of the microphone array is evident from the simulation results. There
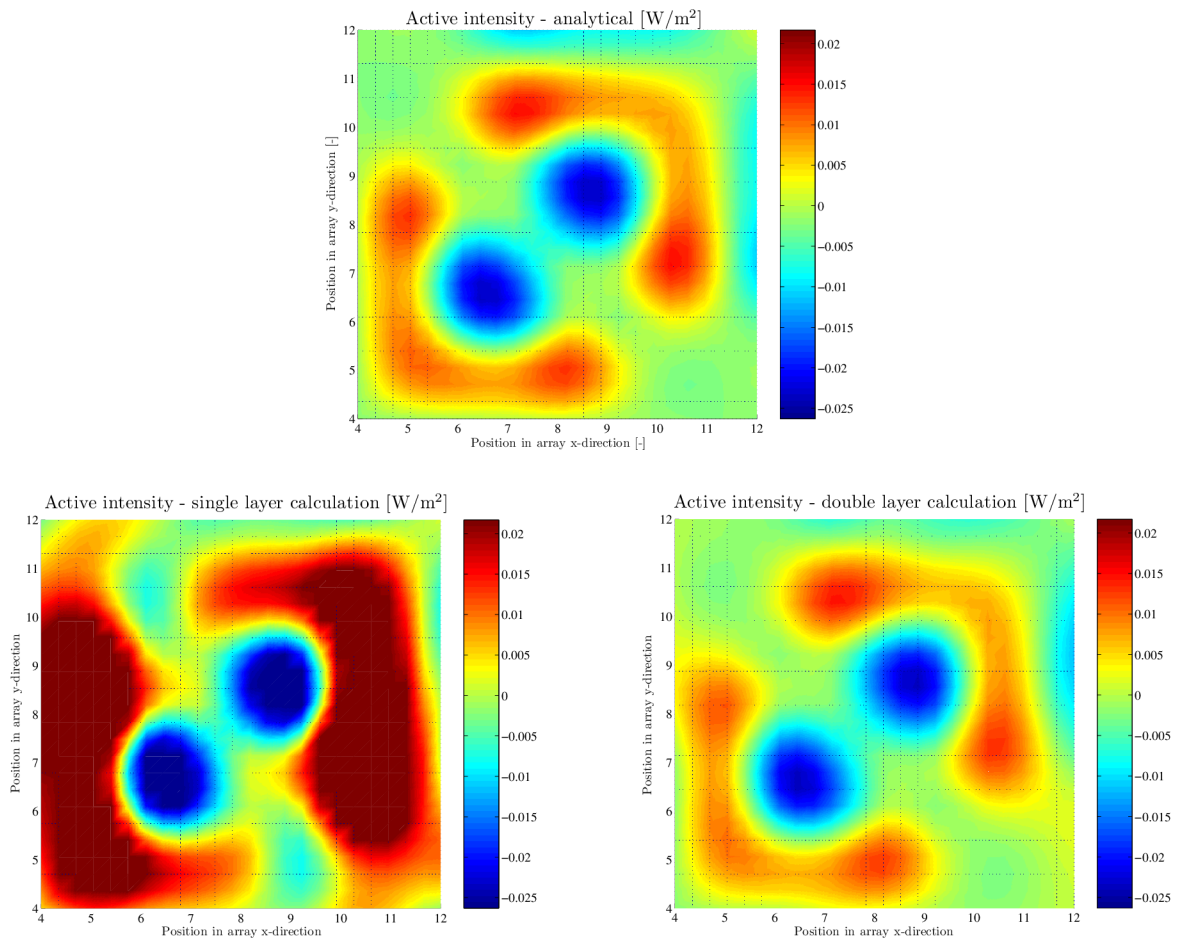
Figure 4.21: Reconstructed active intensity directly above the vibrating plate (in central part of the microphone array) for frequency 1 kHz; upper - analytical solution; bottom left - single layer reconstruction; bottom right - double layer reconstruction with disturbing background noise from the wrong side of the array, regularization in Wiener filter $\varepsilon = 0.001$.

are some problems in low frequency range caused by non-accurate phase angle detection in double layer, and thus producing larger reconstruction error. On the opposite side of the frequency range, the reconstruction error arises due to the certain type of filtration in wavenumber domain. In practice, it is not possible to obtain ideal conditions without background noise and transducers mismatch. This can be only reduced by other activities, but probably more expensive than using double layers.

4.5 Entering Intensity Measurement

4.5.1 Main Concept

Most of the recent NAH algorithms progressively developed in last three decades could be used in such conditions which are very close to free-field. Thus, no other disturbing sound sources than identified source under microphone array are present. In real measurement conditions, unwanted sound sources located behind the array are usually present and they are generated by real sources (vibrating panels) and reflections from the walls opposite to the source surface under examination. All these disturbances (not free-field conditions) can be found in cabins of the automotive vehicles, aircrafts, small rooms etc. This means it is necessary to handle all these conditions and extract only sound field components which are related to the examined sound source. These components can be expressed with one sound field quantity, as entering intensity - sound intensity of the source (vibrating panels) in front of the measurement array [21]. The disturbing sound field coming from behind, defined as incoming filed, is scattered on the examined surface with defined acoustic surface absorption or admittance and propagated to the array - scattered field. Both of these sound field components coming from there examined source direction (entering and scattered field) are present at measurement positions and can be entitled - outgoing field expressed as sound intensity or sound pressure. Total sound field present at measurement point contains both incoming and outgoing sound field components. All these definitions can be written mathematically with Eq. (4.34) to Eq. (4.38) with the pressure as the general quantity [21].

$$p_{measured}(z) = p_i(z) + p_o(z) \tag{4.34}$$

$$p_i(z) = p_{inc}(z_0)e^{jk(z-z0)} \tag{4.35}$$

$$p_o(z) = p_{ent}(z) + p_{scatt}(z) \tag{4.36}$$

$$p_{ent}(z) = \frac{\rho c u(z_0)}{1+a}e^{-jk(z-z0)} \tag{4.37}$$

$$p_{scatt}(z) = \frac{1-a}{1+a}p_{inc}(z_0)e^{-jk(z-z0)} \tag{4.38}$$

From above equations it is evident that determination between incoming (p_i) and outgoing (p_o) sound field is required and the NAH calculation algorithm should determine them. To calculate entering intensity field (p_{ent}), consecutively panel velocity (u_{z0}), knowledge of surface properties (acoustic surface admittance a) are also necessary. To fulfil these prerequisites, the procedure leads to two-step calculation method. In the first step, determination of the surface parameters has been carried out while no sound field is generated by the source under test (no vibrations from the panel). The incoming sound field is generated by artificial sound sources (omnisources) during real measurements and for simulation of the algorithms incoming plane wave from behind of the measurement array could be modeled. In the second step, calculation of entering intensity (EI) generated by vibrating panel under test could be performed, based on knowledge of acoustic

parameters of the panel surface obtained in previous step. With this procedure, the disturbing sound field from behind of the array can be successfully extracted and correct calculation of only entering sound field can be performed.

Originally this procedure has been developed for measurement with double layer SONAH algorithm [21], but in the next chapter 4.5.2 extension of this principle into classical NAH algorithm with spatial transformation has been proposed.

4.5.2 Implementation of EI Concept in Classical NAH

This implementation of Entering Intensity calculation is based on classical NAH calculation with spatial transformation and with enlarging the hologram aperture and spatial filtering to reduce edge effects on the prediction surface. This method is not exactly "patch" method, but with used improvements can compete with true patch methods (e.g. SONAH, HELS). The complication with prediction of small part of sound field near sound source surface much larger than array with strong energy far from the array can still arise, but its influence will be reduced.

The original method without enlarging hologram aperture can't be used with patch-to-patch measurements due to huge reconstruction errors on the edges of the prediction plane caused by windowing in spatial domain. With the expansion of the hologram plane aperture, the damaged pressure information can be restored with iterative procedure involving low filtration of evanescent waves (in the k-space) in the band closed to the maximal spatial frequency of used microphone array. This iterative procedure has been already described in chapter 4.4.1. The basic kernel procedure for double layer processing in wavenumber domain has been described previously in Eq. (4.32).

To determine only entering sound field coming from surface under test (measured) the next calculation procedure has to be processed with two steps.

In the first step, determination of surface properties (in virtual source plane) should be calculated. For this purpose, only sound field from behind of the array (disturbing sound field) should be present. Thus examined panel should not vibrate and produce any outgoing sound field. Disturbing sound field from behind of the array could be simulated as incident plane wave or in real word created by artificial sources (loudspeakers).

After successful estimation of incoming and outgoing (in this case only scattered) sound field at first microphone layer based on Eq. (4.32) (DLA general equation), the spatial transformation of these two sound field components back to virtual source has been performed. Incoming sound field evanescent wave components have been attenuated and outgoing evanescent waves have been amplified. For determination of incoming sound field at source surface Eq. (4.6) (recursive Wiener filtration) should be used to avoid huge reconstruction errors caused by strong amplification of very small evanescent components of the sound field. At "virtual" source surface, determination of surface admittance a based on Eq. (4.39) could been done.

$$p_{out}(z_{virtual\_source}) = \frac{1-a}{1+a} p_{in}(z_{virtual\_source}) \qquad (4.39)$$

Surface admittance has been smoothed in the area parallel to the prediction plane area to avoid strong discontinuities in the surface property values.

The second, "measurement", step is using surface property values determined in the first step to estimate entering sound field components from outgoing sound field measured

by microphone array, where separation of incoming and outgoing sound field has been done in Eq. (4.32) (DLA general equation) and scattered field has been determined on knowledge of surface property. The outgoing sound field contains scattered field and entering field as expressed in Eq. (4.40.)

$$p_{out}(z_{virtual\_source}) = \frac{1-a}{1+a} p_{in}(z_{virtual\_source}) + p_{ent}(z_{virtual\_source}) \qquad (4.40)$$

The above equation is idealized due to the fact that no one can calculate entering pressure field on the source surface due to strong amplification of disturbed evanescent wave components. Thus the source surface is called virtual. Entering sound field at calculation points (very close to the surface, but not on the surface) could be determined in Eq. (4.41).

$$p_{ent}(z_0) = F_{x,y}^{-1} \left[F_{x,y} \left[p_{out}(z) \right] K_f G_p^{-1} - \frac{1-a}{1+a} F_{x,y} \left[p_{in}(z) \right] G_p \right] \qquad (4.41)$$

Calculation of the first term of Eq. (4.41) should be also done iteratively, similarly to Eq. (4.6) using Wiener filter to reduce reconstruction errors.

4.5.3 Simulation Results with Double Layer Technique on 3D Model

Evaluation of the double layer NAH algorithm has been made on 3D model of curved surface designed in COMSOL with assigned sound source properties, definition of microphone position in 3D space and calculation points near source surface. The model parameters are space coordinates of field points and acoustic variables as sound pressure and normal velocity, or sound intensity, which is used as input data for all algorithms (pressure data at microphone positions in this case) and for comparison of results (sound field near source).

3D Model of Curved Surface

The small simple 3D model with field points of measured pressure and pressure field at microphone positions, when one part of the surface below the array acting as vibrating plate with calculated surface velocity are shown in Fig. 4.22 and its cross sections in Fig. 4.23.
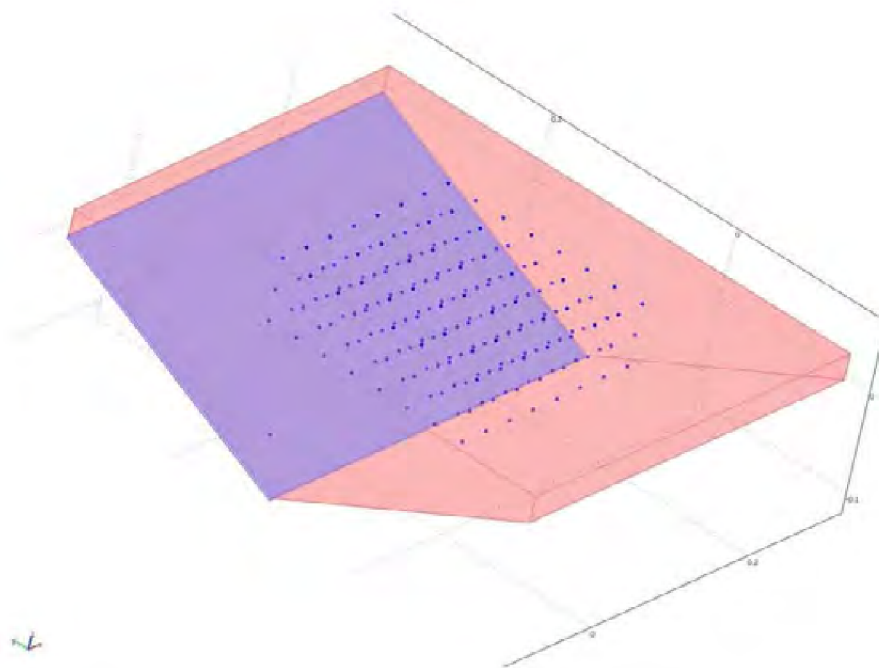
Figure 4.22: 3D model of curved surface designed in COMSOL, free field conditions behind the array or incoming plane wave from behind, blue surface - vibrating surface.

For evaluation of the algorithms when the background sound field is present, modified setup of 3D model has been used. The background sound field is simplified and is modeled as an incoming plane waves coming from behind of the array. This setup reflect more realistic measurement conditions in enclosed spaces.

The microphone array used in this setup has 8x8 microphones with 30 mm microphone spacing and 30 mm between layers. The prediction plane is 30 mm far from the front layer and the distance between the first layer and the source surface vary between 25 mm and 90 mm (in the area between array and surface).

x-y cross section (side view)   x-z cross section (top view)
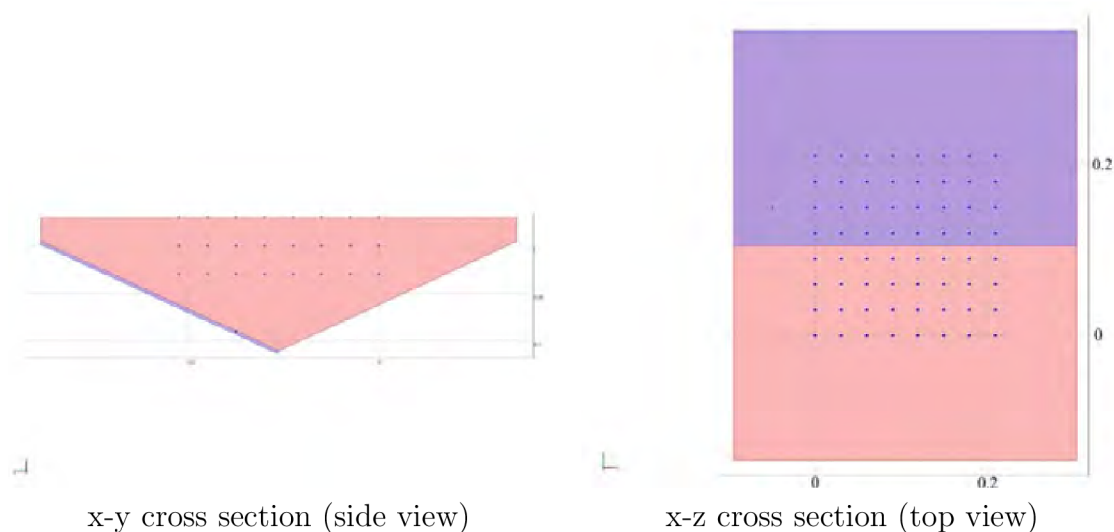
Figure 4.23: Cross sections of 3D model, measurement points (microphone positions) - two upper layers, calculation points (bottom layer).

Determination of Field Pressures and True Values in 3D Model

Calculation of field pressure, velocity and intensity values has been carried out in COM-SOL environment, where the definition of appropriate surface parameters and excitation of the panels can be set. Also plane wave excitation from behind of the microphone array can be modeled and used in calculation.

The exact sound field values (pressure, velocity, intensity) at calculation points and field point pressures have been obtained by finite element simulation of 3D finite element model with added artificial sound source defined as a vibrating steel plate with thickness of 3 mm excited with point force near the bottom corner of the model (dark red area in Fig. 4.24).

Whole FE model consists of the acoustic model of the airspace above the real surface, where one half of the surface is modeled as thin vibrating panel with point force excitation (coupled 3D structural model). The 3D acoustic model has approx. 54 000 finite elements for frequencies up to 5500 Hz, while the largest element size is 1/4 of the shortest wavelength. Finite element mesh of the acoustic model is in Fig. 4.26.

The exactly calculated sound field values have been used as a reference for comparison and evaluation of the prediction accuracy of the algorithm. As the input for determination of surface properties, sound pressure field in 3D model with only plane wave from background has been used (sound intensity distribution in Fig. 4.27). Entering sound field generated by vibrating plate is in Fig. 4.28 and total sound field in Fig. 4.29.

All sound field distributions (incoming, entering, total) have been calculated for the useful frequency range of the microphone array, which is in this case up to 5 500 Hz. Sound intensity field in the 3D model for few typical frequencies is in Fig. 4.30 and in Fig. 4.31.

Error Norms for 3D Simulation

For determination of accuracy of double layer algorithm when using complex 3D model, the prediction of acoustic particle velocity and sound intensity field has been calculated.
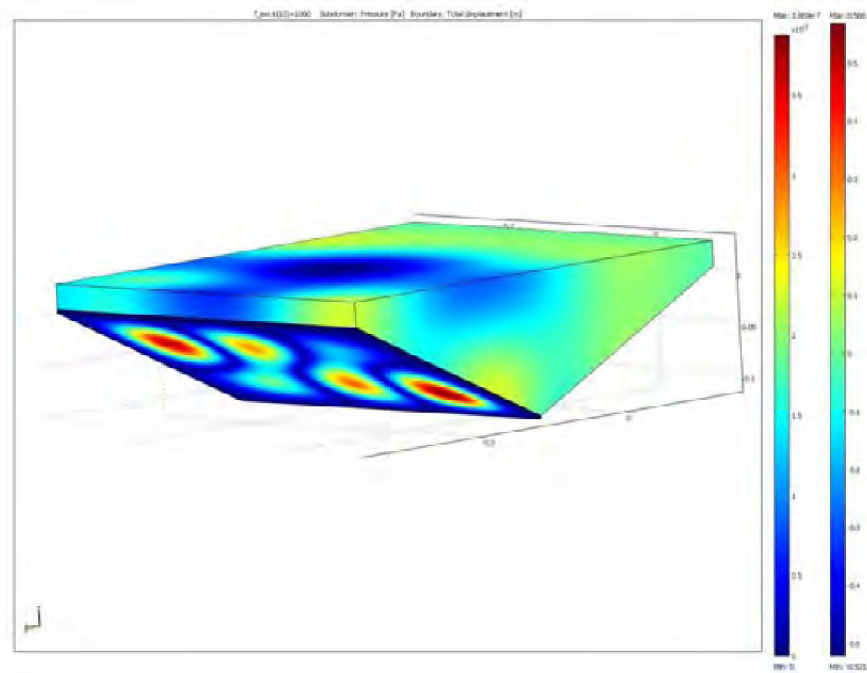
Figure 4.24: Pressure field distribution in 3D model calculated with COMSOL for point force excitation with frequency of 1 kHz, background free field conditions.
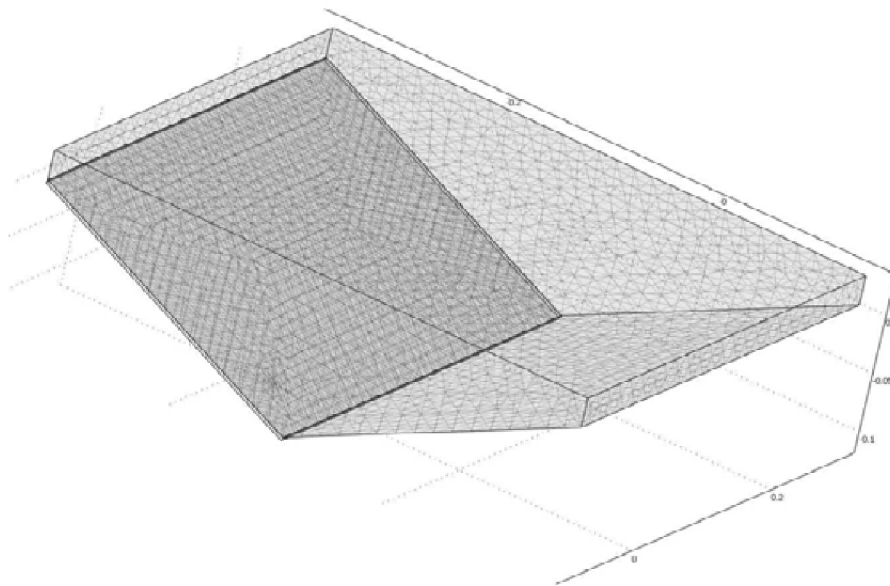
Figure 4.25: COMSOL acoustic volume mesh of the 3D model contains 54 000 finite elements.

New error norms are based on that originally presented in the section 4.2.3. The error norm for the predicted velocity values at defined calculated points near source surface is defined in Eq. (4.42).

Panel surface mesh   Panel surfacedisplacement
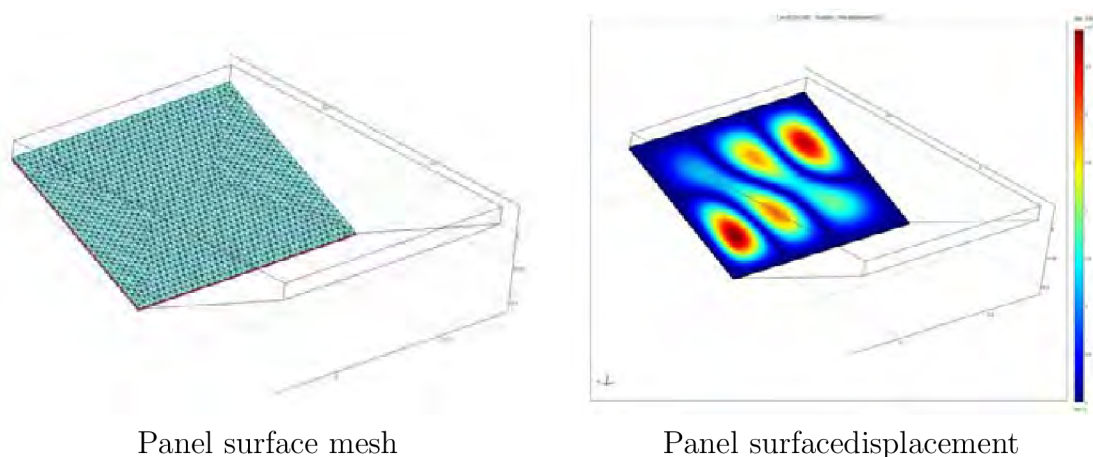
Figure 4.26: COMSOL structural volume mesh of the vibrating panel contains 8000 finite elements (left) and a displacement of the panel for point force excitation with frequency of 1 kHz (right).
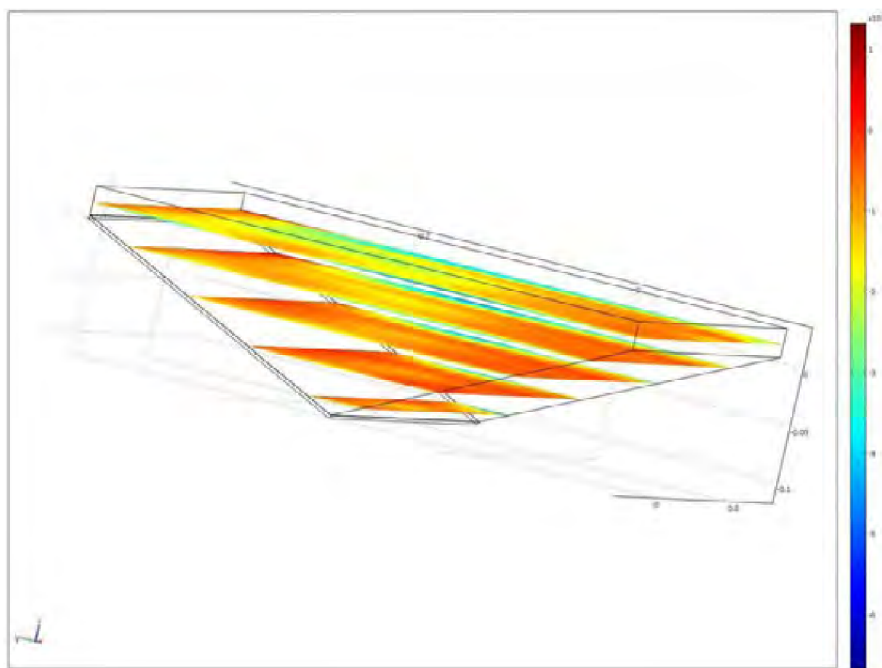
Figure 4.27: Sound intensity field distribution in 3D model with plane wave coming from background and no panel vibrations.

$$MSE_v = \sqrt{\frac{\sum_i \left| v_i^{true} - v_i \right|^2}{\sum_j \left| v_j^{true} \right|^2}} \cdot 100\% \qquad (4.42)$$

The sound intensity error norm is in the similar form, but only active intensity is compared, as described in Eq. (4.43).

$$I_{z0\_activ} = re(p_{z0})re(v_{z0}) + im(p_{z0})im(v_{z0}) \qquad (4.43)$$
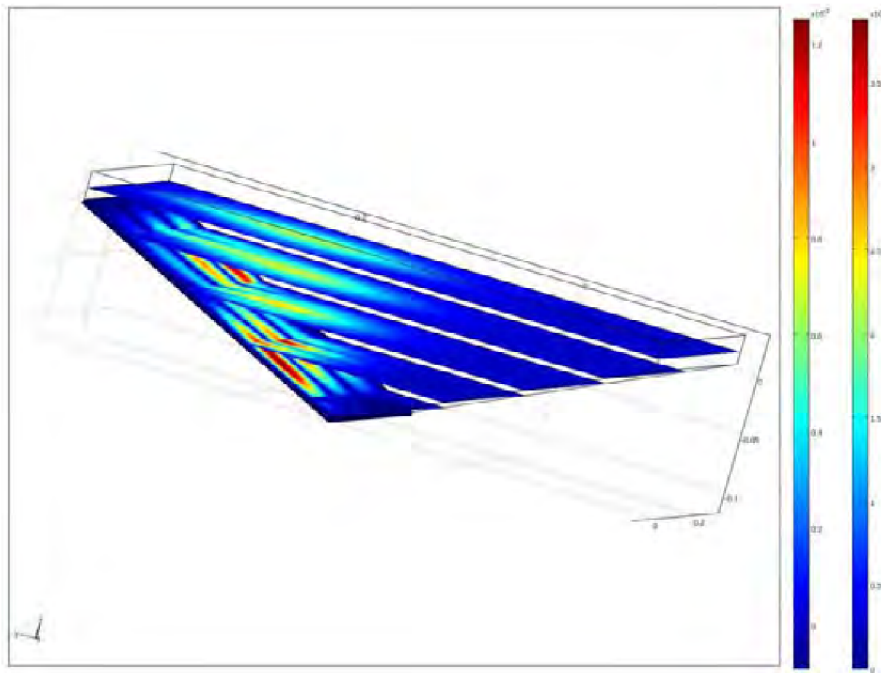
Figure 4.28: Sound intensity field distribution for panel point force excitation (left inclined panel) with right inclined panel with defined surface impedance, frequency of 1 kHz.
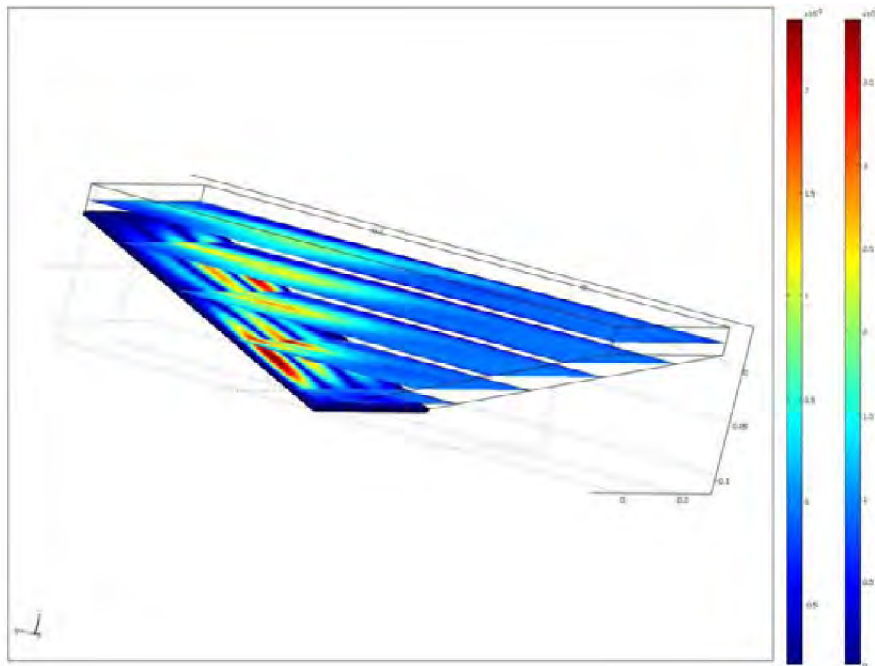
Figure 4.29: Sound intensity field distribution for combined panel point force excitation (left inclined panel) and plane wave coming from top, frequency of 1 kHz.

The error norm for active intensity is in the form expressed in Eq. (4.44).

500 Hz   1 kHz
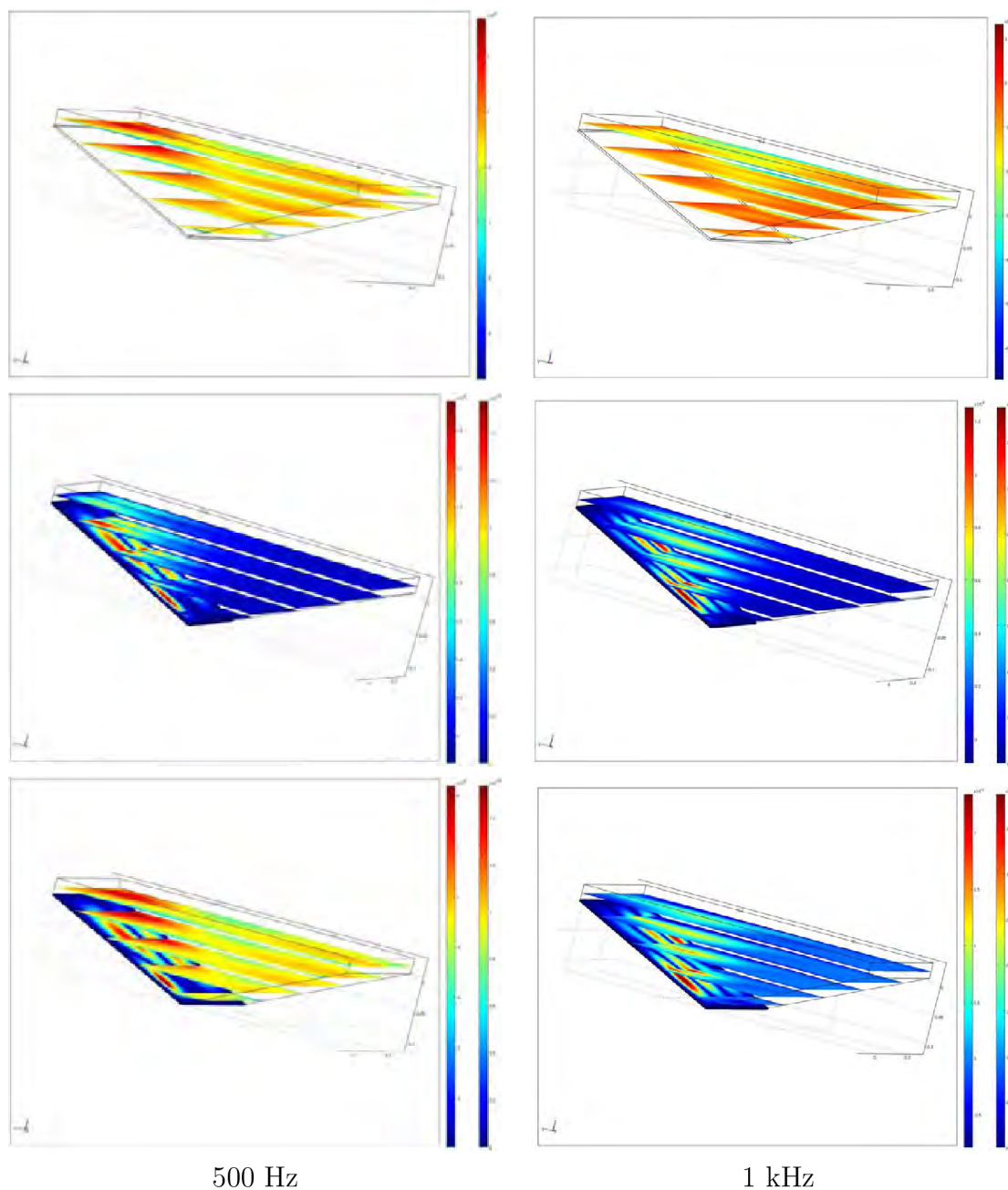
Figure 4.30: Sound intensity field distribution for incoming sound field (top), entering sound field (middle) and total sound field (bottom), frequency of 500 Hz and 1 kHz.

$$MSE_I = \sqrt{\frac{\sum\limits_{i} \left| I_{z\_i}^{true} - I_{z\_i} \right|^2}{\sum\limits_{j} \left| I_{z\_j}^{true} \right|^2}} \cdot 100\% \qquad (4.44)$$

The calculating points (where acoustic quantities are predicted) is selected in the plane very near curved surface which is required for algorithms with spatial transformations where the prediction point should be in parallel plane to the measurement planes. There could be another procedure to obtain predicted data in another parallel plane

500 Hz   1 kHz
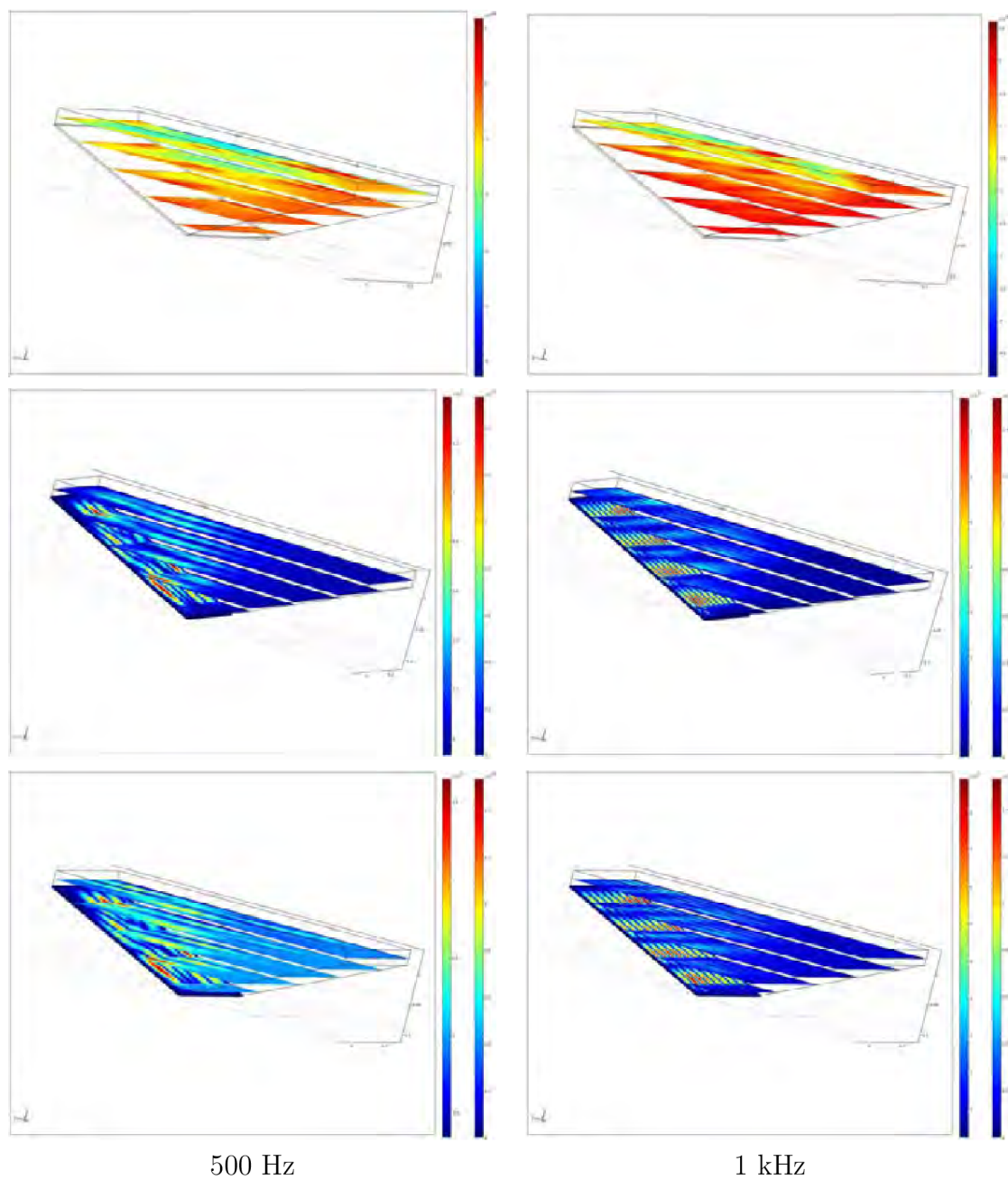
Figure 4.31: Sound intensity field distribution for incoming sound field (top), entering sound field (middle) and total sound field (bottom), frequency 2.5 kHz and 5 kHz.

(closer to the corner of the vibrating plate), but it will cause additional computation for classical NAH which will probably increase the reconstruction error for this algorithm and the description of this treatment and its evaluation will extend this investigation unacceptably.

Results for Free-field Conditions in 3D Model

With double layer NAH algorithm implemented as described in chapter 4.5.2 the prediction of active entering intensity field near source surface modeled as vibrating panel enclosed with 3D triangular shaped area has been calculated. In this first test case only vibrating panel in 3D model generates sound field at microphone positions. The surface properties have been set manually, but these values are not important in this case. Only entering sound field is present in the outgoing sound field and total sound field is only outgoing. Thus, no scattering on the source surface happened. The prediction accuracy represented in MSE is in Fig. 4.32 and entering intensity field maps for certain frequencies in the examined frequency range for calculation based on admittance is in Fig. 4.33. The 3D model has one bottom tilted surface (vibrating panel) totally absorbing and another surface (soft wall) with acoustic impedance of $0.2\rho c$.

Figure 4.32: EI prediction accuracy with double layer holography (DLA-NAH) based on transformation to wavenumber domain, free field conditions.

The results in free field conditions where only examined panel is vibrating show that entering intensity prediction can be achieved with quite good accuracy (indicated EI accuracy in percent is calculated in the whole prediction plane, thus 100 % is not representing totally un-accurate prediction) and resulting entering intensity field maps corresponds to the maps obtained with direct calculation in COMSOL environment.

Results with Background Disturbing Sound Source

The second test case with double layer acoustic holography algorithm based on transformation into k-space. The simulated measurement setup in this case contains vibrating panel in 3D model which generates sound field at microphone positions and background incoming plane wave is disturbing the input measurement data. The surface properties of the vibrating panel have been set as an input parameter for double layer NAH calculation. There values have been used to correctly calculate scattered sound fields. The active intensity prediction accuracy in closer distance to the panel surface is expressed in Fig. 4.34

Figure 4.33: Predicted active sound intensity field maps with double layer NAH (known true values - odd column, calculated with DLA-NAH - even column), free field conditions.

and appropriate sound field maps for frequencies in the range of used microphone array is in Fig. 4.35.

From the results where background disturbing field (modeled as incoming plane wave) is influencing the measured pressure field, prediction accuracy is lower in compare with free field conditions, as expected. The accuracy indicates that extraction of background sound field is not complete, but from the estimated entering intensity maps close to the vibrating surface it is evident that localization of sound source, consequently the position of high energy radiation (position of the driving force and mechanical response of the panel) from the surface can be determined. The localization is less accurate with higher frequencies. This could be expected due to the filtration of high wavenumber components in the measured sound field spectrum.
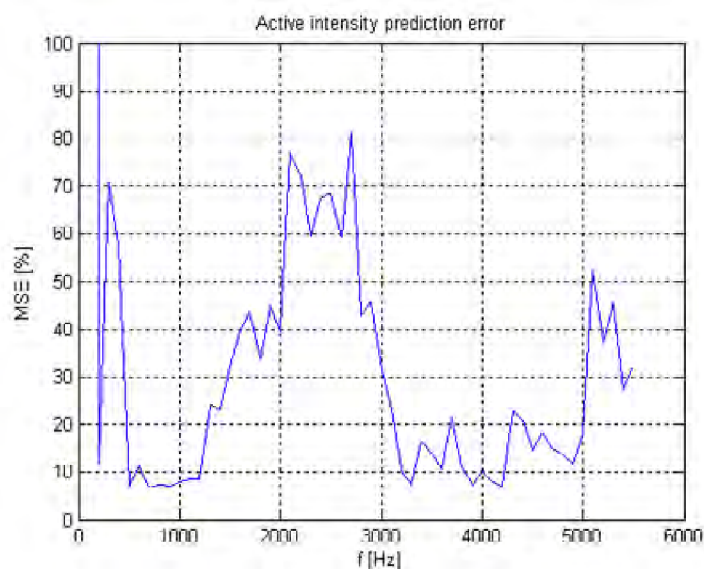
Figure 4.34: EI prediction accuracy with double layer holography (DLA-NAH) based on transformation to wavenumber domain, background disturbing sound field (plane wave) present.
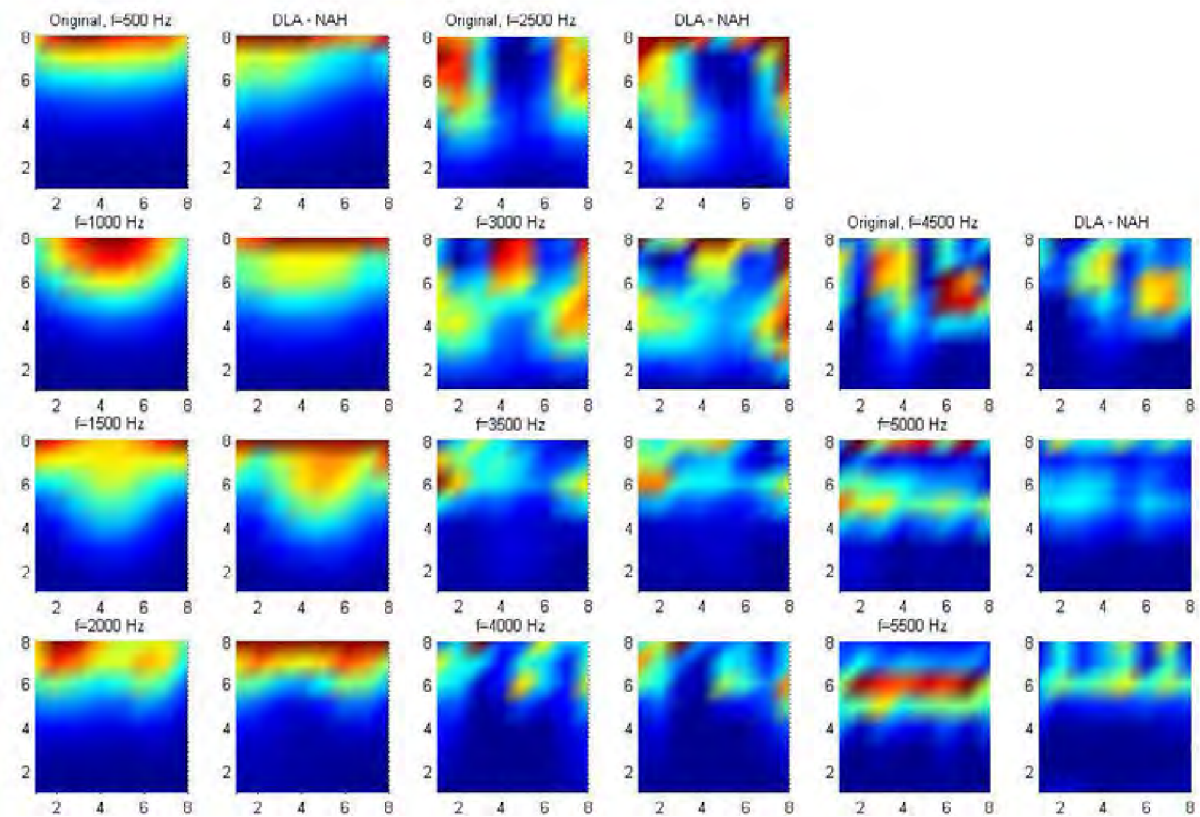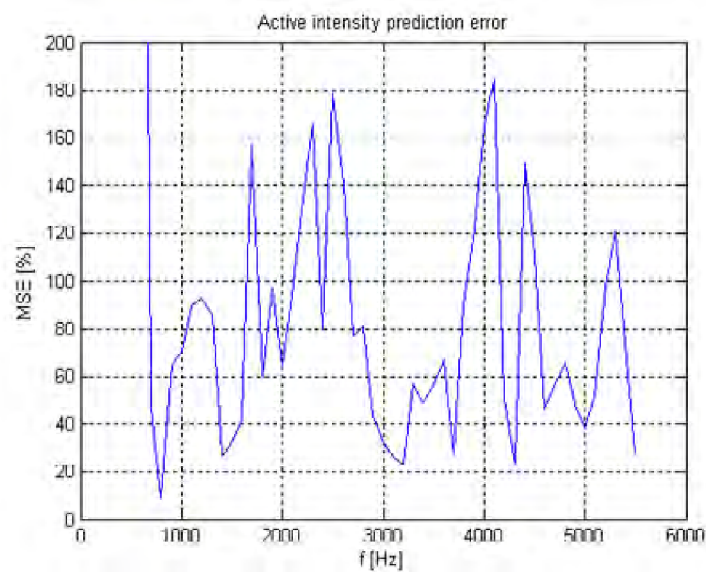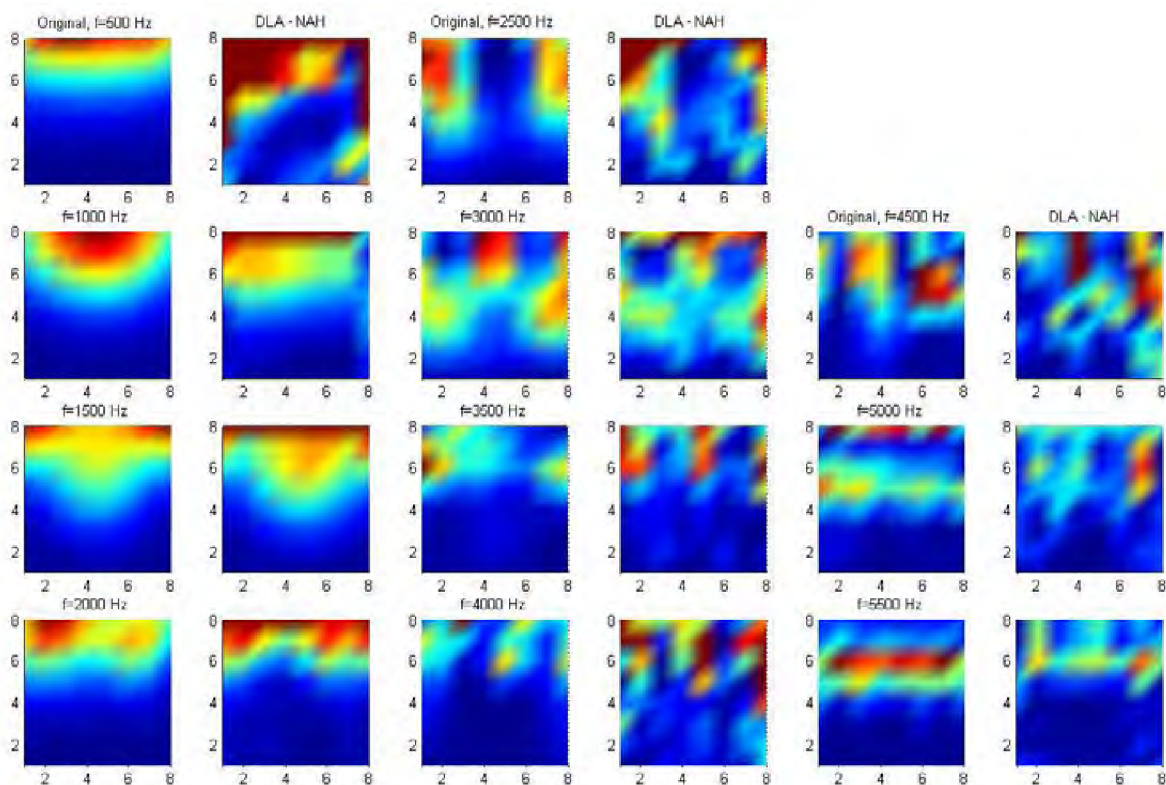

Figure 4.35: Predicted active sound intensity field maps with double layer NAH (known true values - odd column, calculated with DLA-NAH - even column), background disturbing sound field (plane wave) present.

4.6 Methods for Prediction of Sound Fields Based on Patch Measurement

The portions of pressure field measured with microphone array could be combined into one large area hologram basically, in the case where the NAH algorithm with spatial transformation is used, by two approaches. The procedures are different in the domain, where the patches are got together. The patches could be assembled in spatial domain, after the holography calculation (backward transformation), where the resulting sound maps are present. The other approach can act in wave-number domain, where the patches are re-transformed from the spatial domain. Both procedures will be described in more detail in next paragraphs. This chapter is mainly based on the results which I have published on Inter-noise 2008 congress [23].

Assemble the Patches in Spatial Domain

The first approach combine the portions of predicted pressures (patches) in spatial domain, where one portion of predicted near-field pressure data is appended with neighbour portion to cover whole examined area above vibrating surface under test. In this case the NAH calculation is separate for each patch, and the combination of the patches has been done when all the reconstructed (predicted) sound maps are present.

Each patch can be processed separately, thus only resulting sound maps have to be stored. After completion of all NAH calculations, the resulting predicted sound maps (patches) are put together. This procedure involves few degrees of freedom, how the patches could be assembled into large one, depending on the acquisition method of the original sound field values. The patches can be obtained with these attributes:

1. No overlapping areas (exact match of all patches),

2. Small overlap on the edges (patches slightly shifted),

3. Row/column overlapping (intentional).

The first case, where the patches are precisely acquired and connected without any overlaps or gaps, there can be the predicted patches (after NAH calculation) put exactly together without no overlapping in the resulting sound map, but the edge effects on each predicted patch can not be eliminated by any averaging method. This procedure for assembling four patches can be expressed in Eq. (4.45).

$$p_{zx}^{(4Mx4N)} = \begin{vmatrix} p_{zx1,1}^{(MxN)} & p_{zx1,2}^{(MxN)} \\ p_{zx2,1}^{(MxN)} & p_{zx2,2}^{(MxN)} \end{vmatrix} \tag{4.45}$$

Also the physical measurement of such precise patches is very complicated due to the precise positioning of the microphone array. Probably in real measurement conditions it won't be the common method. The second case is more realistic, due to the fact that the positioning of the array won't be so accurate, few millimeters deviation is common in real measurements. The resulting sound field values on the edges will be the approximation

of the edge values calculated from both neighbour patches, as expressed in Eq. (4.46).

$$p_{zx}^{(4Mx4N)} =$$

$$
\begin{bmatrix}
p_{zx1,1}^{(M-1)x(N-1)} & \dfrac{p_{zx1,1}^{(M-1)xN(\max)}+p_{zx1,2}^{(M-1)xN(1)}}{2} & p_{zx1,2}^{(M-1)x(N-1)} \\[2ex]
\dfrac{p_{zx1,1}^{M(\max)x(N-1)}+p_{zx1,1}^{M(1)x(N-1)}}{2} & \dfrac{p_{zx1,1}^{M(\max)xN(\max)}+p_{zx1,2}^{M(\max)xN(1)}+p_{zx2,1}^{M(1)xN(\max)}+p_{zx2,2}^{M(1)xN(1)}}{2} & \begin{matrix} p_{zx1,2}^{M(\max)x(N-1)} \\ p_{zx2,2}^{M(1)x(N-1)} \end{matrix} \\[2ex]
p_{zx2,1}^{(M-1)x(N-1)} & \dfrac{p_{zx2,1}^{(M-1)xN(\max)}+p_{zx2,2}^{(M-1)xN(1)}}{2} & p_{zx2,2}^{(M-1)x(N-1)}
\end{bmatrix}
$$
(4.46)

The last case should be probably most common method for treatment of such patch measurement. The overlapping of the one or two rows or columns of the matrix, which represents the predicted sound field near source surface, will smooth the solution on the contact points between the patches. Thus, for covering the same area as with the previous two methods, in this case, one more patch should be acquired. Eq. (4.47) represents the combination of the patches with two rows and columns from each patch (edge data) left out.

$$
p_{zx}^{(4Mx4N)} =
\begin{bmatrix}
p_{zx1,1}^{(M-1)x(N-1)} & p_{zx1,2}^{(M-1)x(N-2)} & p_{zx1,3}^{(M-1)x(N-1)} \\[1ex]
p_{zx2,1}^{(M-2)x(N-1)} & p_{zx2,2}^{(M-2)x(N-2)} & p_{zx2,3}^{(M-2)x(N-1)} \\[1ex]
p_{zx3,1}^{(M-1)x(N-1)} & p_{zx3,2}^{(M-1)x(N-2)} & p_{zx3,3}^{(M-1)x(N-1)}
\end{bmatrix}
$$
(4.47)

Combination of Patches in Wavenumber Domain

The second approach uses preprocessed data during the holography calculation and combines the pressure image portions in wave-number domain into one large image of measured pressure field. The patches are combined after adaptive aperture enlargement, where field pressure image of the patch has been calculated based on adaptive hologram aperture enlargement. The number of hologram points in wave-number domain is four times higher than in original hologram, thus providing better wave-number resolution. The wave-number patches are then combined on basis of adjustment of added resolution points. The resulting pressure image in wave-number domain contains information from all measured patches, where patches transformed into wave-number domain has been assembled into large one and in iterative procedure, as a part of the NAH algorithm with spatial transformation and adaptive hologram aperture enlargement, restoration of the complete large sound field map could be done. This procedure mathematically describes in Eq. (4.48).

$$
P_{zh}^{n(4Mx4N)} = F_{x,y}\left[F_{x,y}^{-1}\left[P_{zh1}^{n-1(MxN)} K_f \right] + F_{x,y}^{-1}\left[P_{zh2}^{n-2(MxN)} K_f \right] \right.
$$

$$
\left. + F_{x,y}^{-1}\left[P_{zh3}^{n-2(MxN)} K_f \right] + F_{x,y}^{-1}\left[P_{zh3}^{n-2(MxN)} K_f \right] \right]
$$
(4.48)

$$
P_{zh}^{n(4Mx4N)} \Leftarrow P_{zh1}^{orig}, P_{zh2}^{orig}, P_{zh3}^{orig}, P_{zh4}^{orig}
$$

As described above, the presented NAH algorithm is very useful for such combination of patches, because the preprocessing of the algorithm using very similar procedure and can be easily adopted for the assembling of more than one measurement patch.

Comparison of Approaches on Simulated Measurements

The results of the prediction (reconstruction) of sound field near source based on the measurement at four array positions are presented in this chapter. The visual comparison of the measured sound field at microphone positions (marked z_h), predicted maps (marked z_x calculated) and "true" maps (marked z_x analytical) of all acoustic quantities (pressure, particle velocity, sound intensity) is on the figures. In the spatial domain, the assembly of the patches has been tested on three different procedures. In Fig. 4.36, there is no overlapping of the measured patches used.
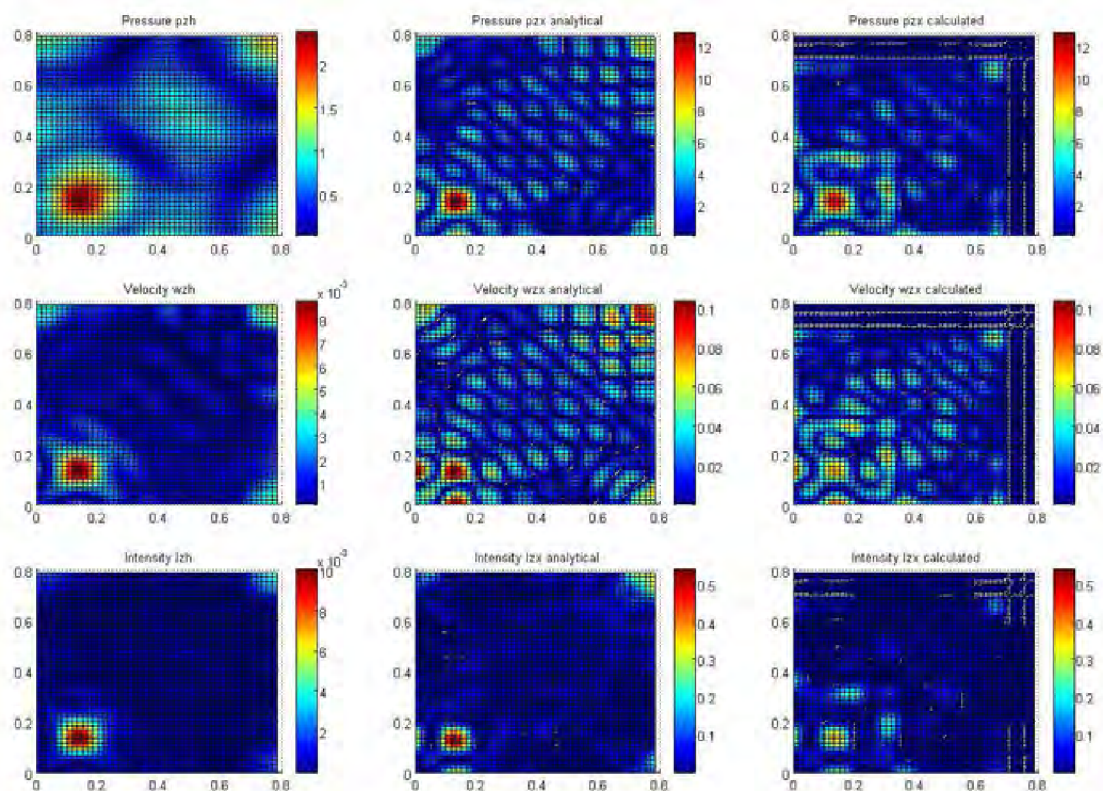
Figure 4.36: Measured, "true" and calculated sound field maps with no overlapping, for the force frequency of 500 Hz and strength 10 N.

On the reconstructed sound map (third column) in Fig. 4.36, there are visible reconstruction errors on the edges of each calculated patch, which can't be minimized with any postprocessing. Fig. 4.37 represents better reconstruction accuracy due to the overlapping two rows/columns at edges of each patch and the reconstruction errors shown in the first case is minimized significantly. The resulting sound map is a bit smaller due to the overlapping of four patches. Thus the predicted sound field on the up and right edge of each subplot is, for the simplicity, set to zero.
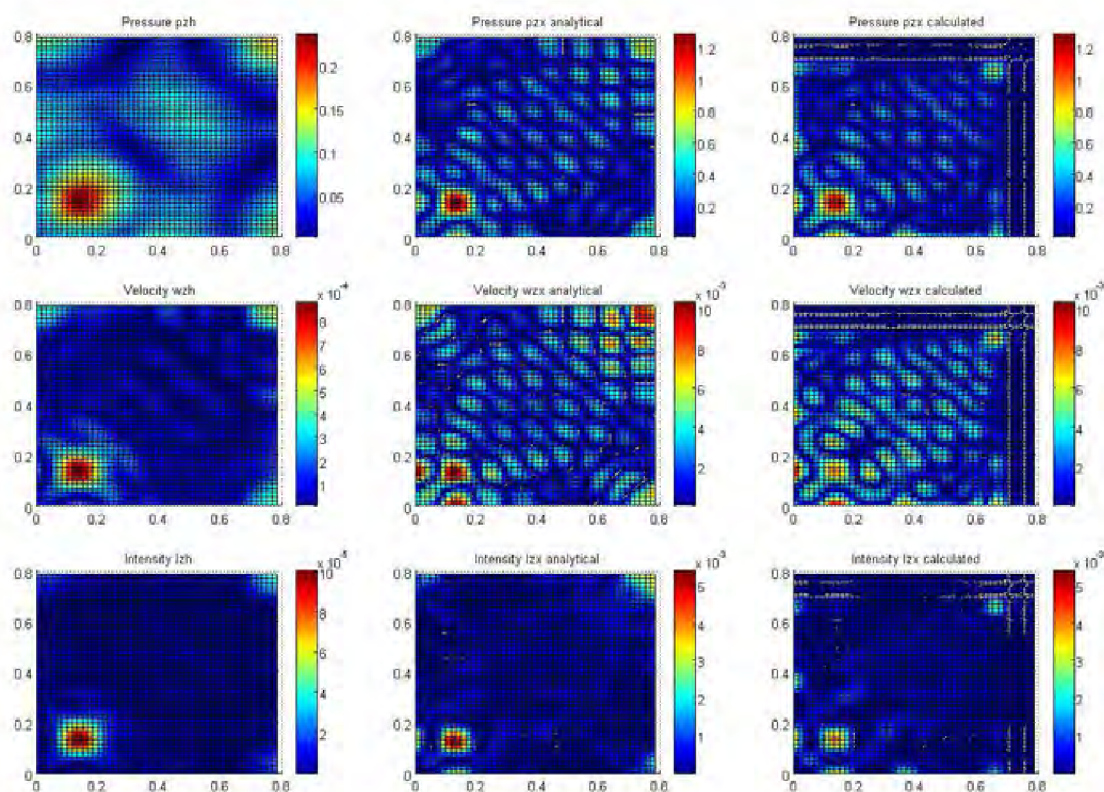
Figure 4.37: Measured, "true" and calculated sound field maps with overlapping of one edge row/column, for the force frequency of 500 Hz and strength 10 N.

The last figure in this chapter, Fig. 4.38, shows the reconstructed sound field in case when one measurement array (contains 16x16 microphones) cover all area under test. This test case has been selected for better comparison of the prediction accuracy of different methods for patch assembly. This method has the best possible accuracy in this case and no interior edge effects are present.

The overall comparison of the prediction accuracy in usual frequency range is in Fig. 4.39, where each line represents different patch assembly. It is evident that if the assembly is without overlapping (green curve), the prediction accuracy is very low in compare with overlapping (black curve) and finally the large array (blue curve) has the best accuracy.

Patch Assembling in Wavenumber Domain

In wave-number domain, the procedure involves iterative combination of all patches into large one. Thus, the resulting sound maps without (Fig. 4.40) and with (Fig. 4.41) adaptive enlargement of hologram aperture have better reconstruction accuracy than assembling in spatial domain in center of the hologram.

The procedure with adaptive enlargement of the hologram eliminates effects on the edges of the final large hologram. The enlargement is four times the original hologram and it in iterative procedure filters the wave-number spectrum while maintaining original spatial pressure values unchanged. The edge effect is clearly evident in Fig. 4.40, where
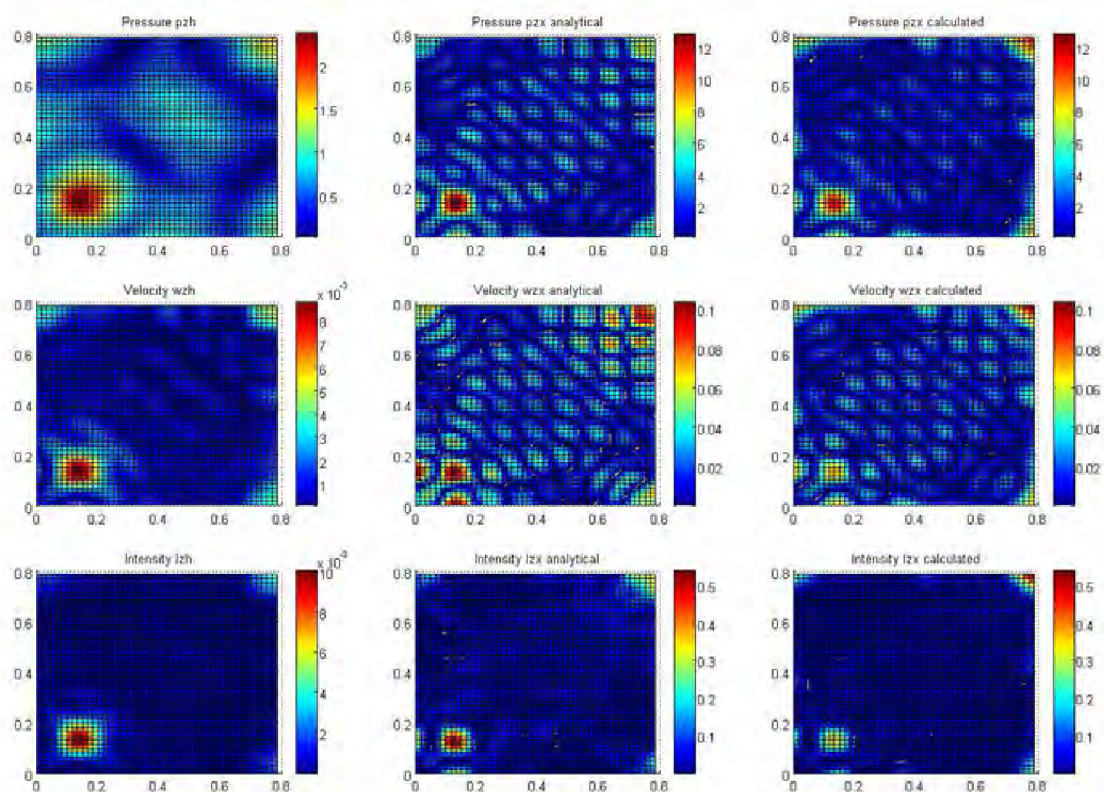
Figure 4.38: Measured, "true" and calculated sound field maps obtained by large array (16x16 microphones), for the force frequency of 500 Hz and strength 10 N.

there is no enlargement and the non smooth wave-number spectrum produces very high errors on the edges in spatial domain after backward sound field calculation (prediction).

Also the overall comparison of the prediction accuracy in usual frequency range is in Fig. 4.42 for assembly of four patches in wave-number domain with adaptive enlargement of the hologram (black curve) and with the large array (blue curve), which covers the whole measurement area. In Fig. 4.42 it is evident that the assembly method in wave-number domain produces very low added error in the selected frequency range.

The proposed patch assembly methods in both domains produces acceptable amount of added error into resulting (predicted) sound field near source surface. In spatial domain, the overlapping of the measured patches is necessary due to the presence of unwanted edge effects inside the resulting holograms in case when no overlapping is used. In wave-number domain, the assembly method works with very low added error to the situation where very large array (four times larger = four times more microphones) is used. In this case, the importance of adaptive hologram enlargement is evident, where also this method eliminates edge effects of resulting sound maps. In the spatial domain, there could be also other patch algorithms used, for example SONAH, which is described in chapter 2.1.5.
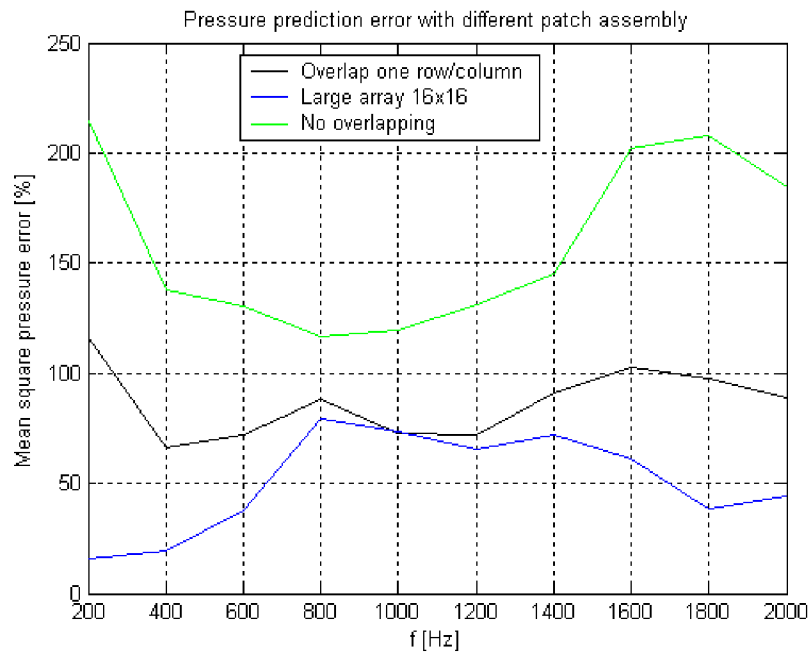
Figure 4.39: Pressure prediction accuracy obtained with different assembly methods.
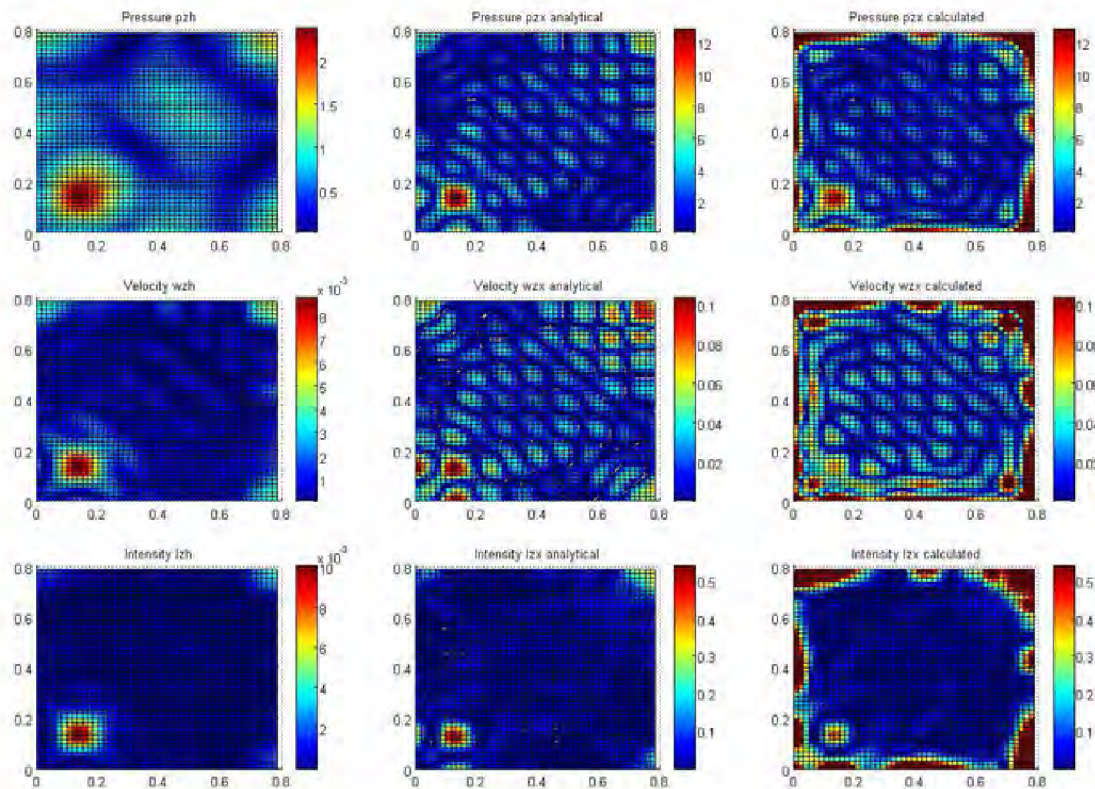
Figure 4.40: Measured, "true" and calculated sound field maps with assembly of patches in wave-number domain, no adaptive enlargement of the hologram, the force frequency is 500 Hz and strength 10 N.
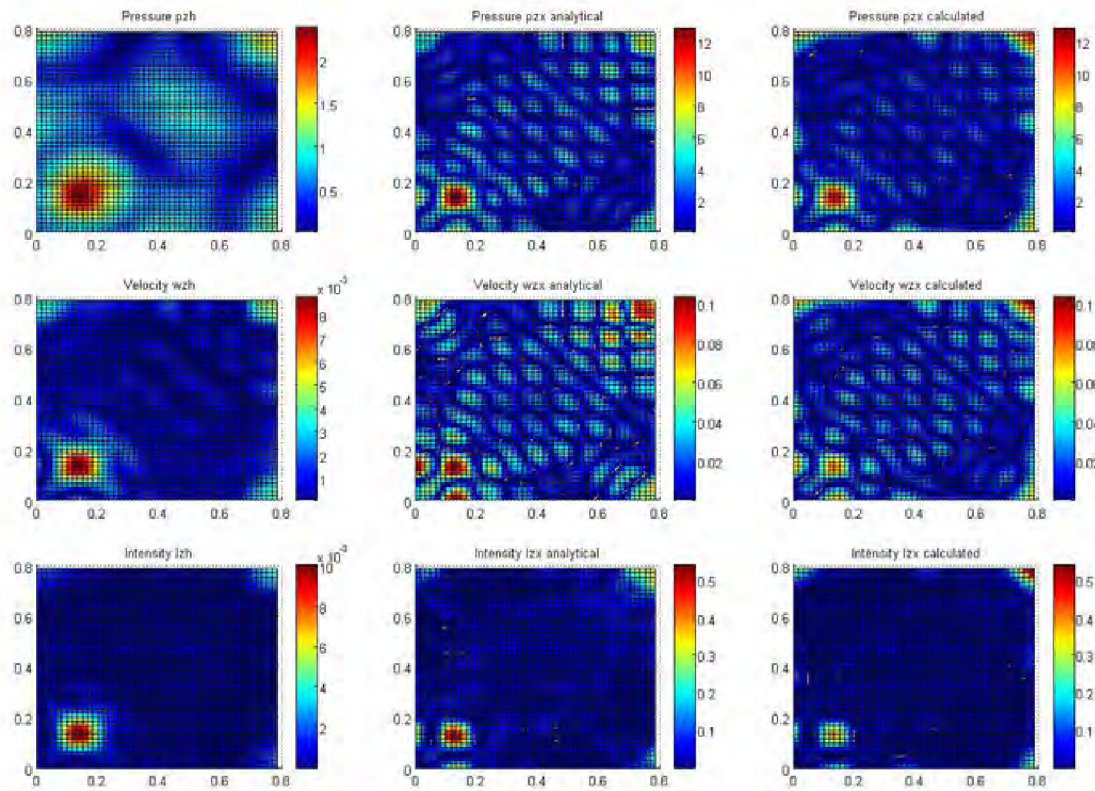
Figure 4.41: Measured, "true" and calculated sound field maps with assembly of patches in wave-number domain, with four times adaptive enlargement of the hologram, the force frequency is 500 Hz and strength 10 N.
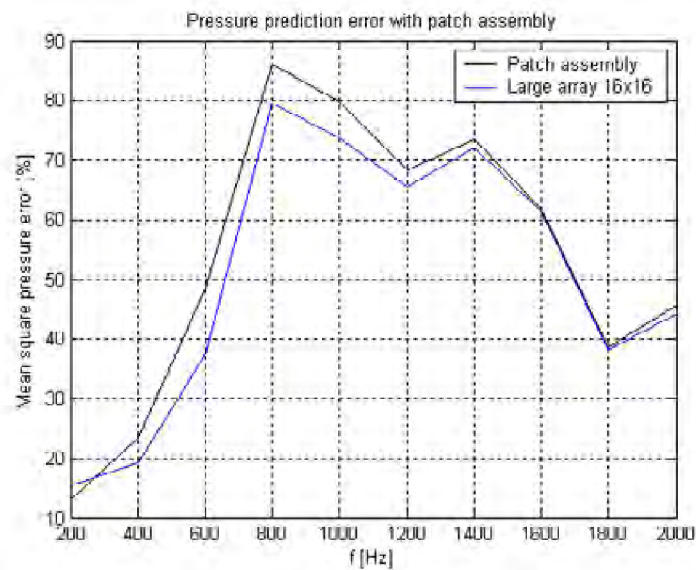
Figure 4.42: Pressure prediction accuracy obtained with assembly of patches in wavenumber domain.

Measurement System for Acoustic Holography

<div style="text-align: right;">

5

</div>

The important part of each acoustic holography method is also the procedure of measurement of sound field information near the examined vibrating object. These information act as and input data for the holography algorithm and their quality is crucial for successful prediction (or reconstruction) of sound field close to the source surface (the most usual case of prediction). The commonly used sensors and measurement system have been described in the first chapter on page 20, but in most cases the whole measurement systems with such sensors (precision array microphones, $p - u$ probes, $p - p$ probes) are very expensive thus limit the applicability of such systems in practice. Design and real construction of cheap measurement system which can satisfy the requirements of the acoustic holography methods has been also one of the goals of this thesis and some results are described in next paragraphs.

5.1 Design of Hardware for NAH Processing

The main reason for design and hardware construction of novel measurement hardware is to lower the expenses for purchase such system while maintaining the important parameters of the system which is required for the data processing algorithms.

5.1.1 Smart Microphones for Use in Array Processing

The acoustic sensors for measurement of sound field for processing with NAH are mostly precision array microphones with ideal or close to ideal frequency response and long-term stability. Equivalent to quality is also the price of such sensors. But in acoustic holography we have to measure at many discrete points, thus require high number of the sensors.

Smart Microphone for Linear Array

For the reason mentioned in previous paragraph designers try to improve common microphones to satisfy the requirements of NAH method. One of the possibility how to improve the characteristics of the sensors and also inexpensive is software correction of, for example, measured data with frequency response of the microphone obtained during calibration. After calibration procedure of cheap microphone, the information about frequency characteristics can be stored in computer and later used for correction of data. Another more inventiveness possibility is to store the frequency response of directly in the memory included in the sensor as TEDS (Transducer Electronic Data Sheet). Design of such sensor can be inspired with international standard IEEE 1451.4 [1] which defines

the mixed signal interface for connection of smart sensors with included digitally stored information. These information have been used to build cheap smart microphone.

Designed smart microphone includes cheap electret capsule VM4530 as an acoustic transducer, built-in preamplifier MAX4175 [54] with gain of 25 and nonvolatile EEPROM memory DS2433 [53] with 4kbits of storage space and with 1-wire connection protocol. Electrical scheme of such smart sensor is in Fig. 5.1.
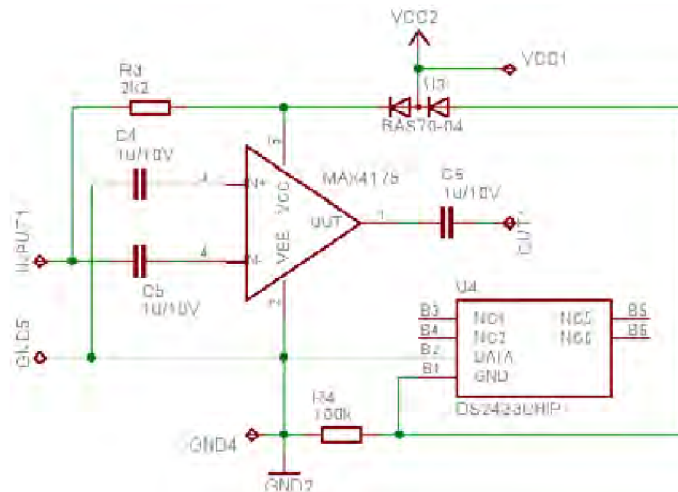
Figure 5.1: Schematic diagram of designed smart microphone with built-in preamplifier and TEDS memory.

The mechanical construction of the microphone with metal case is in Fig. 5.2.

Figure 5.2: Mechanical construction of designed smart microphone.

In the TEDS memory there is stored frequency response of the electret capsule (including response of preamplifier) in applicable frequency range (50 Hz to 2 kHz). This information can be downloaded from the sensor during initialization of the measurement system. The typical amplitude frequency characteristic of one constructed smart microphone is in Fig. 5.3. It can be seen that characteristic is quite flat especially in frequency range of main interest (between 100 Hz and 1 kHz).

This smart microphone has been designed for using in linear microphone array with scanning, step-by-step, measurement technique.
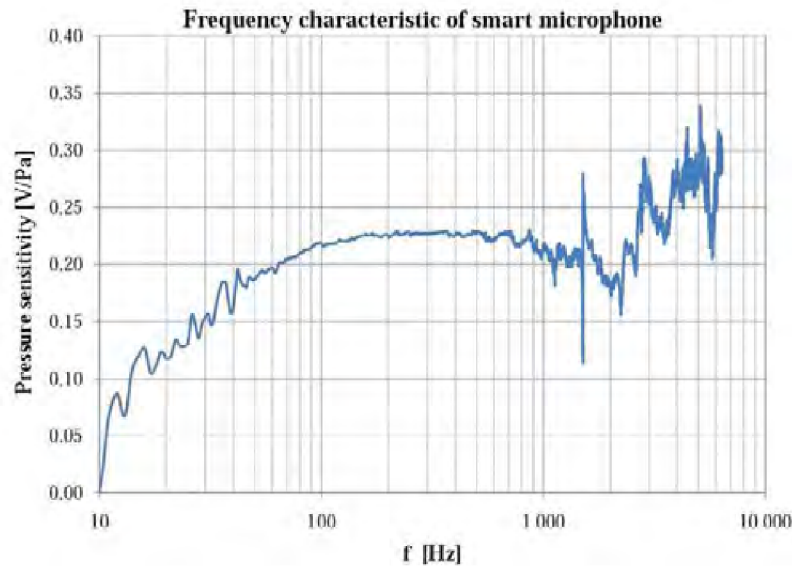
Figure 5.3: Frequency characteristic of designed smart microphone (electret capsule VM4530 and preamplifier MAX4175).

Smart Microphone for Matrix Array

Further development of MEMS sensors opens new possibilities of using such sensors. In the market there are about five main producers of MEMS capacitive microphones mostly supplying cell phone manufacturers. The parameters of such microphone is worse in compare with classical large scale capacitive microphone, but for its dimensions, price and easier connectivity in some cases, it can be used for array measurement. Using of MEMS microphone always involves software correction of measured data with frequency response of the microphone obtained during calibration. Construction of an array for acoustic holography processing with MEMS microphones has been published in last years [5].

Recently, microphone manufacturers are starting to offer MEMS microphones with digital interface with improved parameters and easier connection to the processing system. One representative of such microphone is type SPM0405HD manufactured by Knowles Acoustics [56]. It is capacitive transducer with built-in preamplifier and sigma modulator. The output of the smart sensor is 1-bit data stream and corresponding pressure value has to be calculated with numerical decimation and filtration. One of the simple possibility is using CIC filter (Cascaded Integrator-Comb Filter) as decimator converting 1-bit data stream into 16-bit data [8]. The implementation of the CIC decimation filter is very easy and can be directly implemented into FPGA for fast processing of many input channels. The construction of this microphone also simplifies the connection of the microphone to the processing system when measured data from two microphones can be sent simultaneously on the same physical line. It can be achieved with transmission of the data from one microphone in positive level of clock signal and another one during with negative level of clock signal. The connection of both microphones to the processing system with one transmission line is presented in Fig. 5.4.
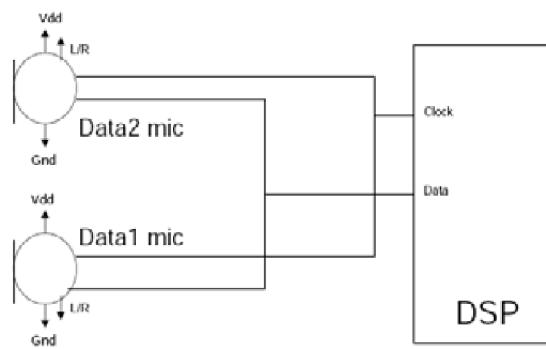
Figure 5.4: Connection of two digital MEMS microphones to the DSP [56].

5.1.2   Linear Scanning Measurement System

Within the scope of this thesis, the linear scanning system with smart microphones has been designed and constructed. The measurement array has 16 microphones in one column and can cover the distance of approx. 1 m. The spacing between microphones is 5 cm and movement of the array is provided with stepper motor controlled from the PXI system.The picture of whole system is in Fig. 5.5.

Figure 5.5: Measurement system with linear microphone array and smart microphones.

The electric signals from the microphones is converted with two devices of 8-channel A/D converter ADS1278 with simultaneous sampling [52] and acquired in digital form with PXI system from National Instruments with FPGA card (NI-RIO 7811R [55]) for fast sampling rate. The system can handle 16 channels with resolution of 24 bits and sampling rate of 52 kHz. The processing algorithm is programmed in LabVIEW environment and compiled into FPGA device. Measurement with this system requires using of reference microphone which is connected to the A/D conversion card into PXI. The correlation between reference sensor and array microphones is calculated during the measurement in computer.

5.1.3   Matrix Array Measurement System

Also matrix measurement system has been designed and constructed as a result of this research. The matrix array contains 64 digital MEMS microphones from Knowles Acoustic in 8x8 configuration with equal spacing of 3 cm in both directions. The microphone array is connected directly to FPGA card in PXI system from National Instruments. Decimation and filtration of all digital signals are processed in real time, thus visualization of measured and potentially also predicted sound field can be done in real time. The measurement system with PXI chasis and constructed matrix microphone array with digital microphones is in Fig. 5.6. The acquisition of digital 1-bit data stream is simultaneous for all microphones, thus no reference sensor is needed.

Figure 5.6: Measurement system with matrix microphone array and digital MEMS microphones.

Experimental Vibration Analysis with NAH method

<div style="text-align: right">

6

</div>

The experimental verification of using acoustic holography for vibration analysis has been done on laboratory model of vibrating object which is used for examination of natural frequencies of the vibrating body. The model is used in classes for teaching of conventional modal analysis with contact vibration sensors - accelerometers. The advantage of prepared model of known vibration distribution (positions od nodes and antinodes) is in verified procedures of determination of natural modes and position of the radiating antinodes which can be used for set-up the experimental test case using the microphone array and the acoustic holography method to obtain similar results as with classical measurement. It is also evident that non-contact method can avoid influence of the measurement system (contact sensors) to the vibrating object. The most popular non-contact method for vibration analysis is Laser Doppler Vibrometry (LDV) using laser beam to measure position displacement of the point on the diagnosed surface. This method is very accurate, but the measurement setup is very expensive and time consuming, due to many measurement points. There can be used scanning LDV principle to set-by-step point measurement of the surface displacement or velocity, but this system is also slow and moreover much more expensive than single point LDV.

In compare with LDV the acoustic holography method using array of microphones which measures acoustic pressure generated with vibrating surface of the measured object is faster and provides more complex information about sound field above examined source and could provide these information in real time. Its disadvantage is less accuracy of analysis of surface vibration velocity, so it can precisely visualize the sound field near sources and localization of such source with determination of its parameters (e.g. radiating power).

The measurement system used in this test case, where sound pressure field values were acquired as an input for acoustic holography method, was an old designed linear microphone array with only electret capsules with preamplifier included in the microphone metal case. For all microphones there have been measured their individual frequency response (amplitude and phase) to correct the measured values with stored frequency response function. With the smart microphones with integrated TEDS, where frequency response function can be stored, the correction of measured data can be done in real time. This proposed feature has not been used in this test case.

The description and results of this experimental validation of using acoustic holography for non-contact vibration analysis have been published in conference proceedings [24] and in journal [25].

6.1 Beam Vibrations

As an examined vibrating object, the laboratory model with steel beam has been selected. Beam vibrations depend on the type of boundary conditions (free, simple supported, guide supported, etc), which determine the natural modal frequency. Modal frequencies are also varying on the beam material constants and dimensions. For natural frequencies of the free-guide supported steel beam (rod) one can use Eq. (6.1) [25].

$$f_i = \frac{1}{2\pi} K_i \sqrt{\frac{EI}{m'l^4}} \tag{6.1}$$

where K_i is a type of mounting of the beam or rod [-],
         E   is Young's module [Pa],
         I is a diameter parameter $[m^4]$,
         m' is a unity weight of the beam [kg],
         l is a length of the beam (in this case half the dimension) [m].

Theoretical natural frequencies can be calculated using Eq. (6.1), with selecting appropriate K_i constant for used type of mounting. In our test-case, the steel beam is not supported in general meaning, it is only guided by vibrating center of the shaker. From this precondition it can be determined that the condition of one end of the beam is free and one is guided. But in real conditions, the beam is mounted as free-free due to excitation of vibrations by the shaker in one end of the beam, where there is no other load except the shaker's center mounting (mass of the shaker system) and it causes free boundary condition at this position. The other side has totally free boundary conditions (no load and no support). With above mentioned arguments, the K_i constant can be determined as represented in Eq. (6.2) [25].

$$K_i = \left(i\pi + \frac{\pi}{2}\right)^2 \tag{6.2}$$

where i is a number of mode (natural frequency).
The diameter parameter I can be calculated in Eq. (6.3).

$$I = \frac{b \cdot h^3}{12} \tag{6.3}$$

where b is width of the beam [m],
         h is a thickness of the beam [m].

Calculation of natural frequencies for first few modes has been performed and results are in Table 6.1. Parameters of the beam material were: $\varrho = 7800 \ kg/m^3$, E = 200 GPa, and dimensions l = 0.31 m, b = 0.02 m, h = 4.75 mm.

Natural frequencies has been also verified with classical setup with accelerometers and corrections of the frequencies due to the accelerometer mass loading have been used. The natural frequencies of the few first modes with correction are also in table 6.1. The mass of one accelerometer with 24.3 g has been recalculated to virtually lengthen the beam, while density of beam and accelerometer is approximately the same.

Table 6.1: Theoretical frequencies of the first four natural modes of vibrating steel beam and corrected values for accelerometer mounting mass.

Mode nr.	Theoretical f_i	Corrected f_i
1	255.4	225.3
2	709.3	626.0
3	1390.3	1226.9
4	2298.2	2028.1

6.2 Modal Analysis Setup

Main purpose of this chapter is to present that acoustic holography methods can be used for non-contact modal analysis of guide supported (free excited) steel beam. This type of sound source and the configuration of the test-case have been selected due to its acceptable simplicity and ability to show qualities of presented non-traditional non-contact method for technical diagnostics. The steel beam has been mounted on the shaker and excited in the center to produce vibration and sound field radiation at frequencies corresponding to natural modes of the beam. The radiated sound field near the beam surface has been measured with a linear microphone array with 9 microphones in a column. After acquiring one column position, the linear array moves to the new position and acquire new pressure data. With 15 columns, the measurement process is finished and the data can be used for holography calculation.

There are two disadvantages with this setup connected to using of linear microphone array and scanning principle. One is the condition of stable vibrations and position of the source and the second is necessity of using reference microphone for non-simultaneous sampling of column pressure data. The whole measurement setup is in Fig. 6.1. Fig. 6.1 presents the examined sound source - the steel beam mounted on the shaker in its center, the linear microphone array with positioning system for movement of one column with 9 microphones, a computer for data acquisition and processing, a generator and an oscilloscope to verify right setting of shaker excitation level and frequency.

Linear microphone array is 14 cm far from beam surface and calculated positions are in 1 cm distance. Spacing between microphones is 5 cm, so the maximal frequency of this array is about 3.5 kHz. Lower frequency limit is defined by dimensions of the whole array and over-sampling in wave-number domain. In this case lower limit is about 200 Hz. More decreasing of the low-frequency limit leads to higher reconstruction errors on low frequencies near the limit and also more time-consuming due to higher number of calculated points in the virtual microphone array. To verify modal frequencies of the beam, two accelerometers were mounted on the beam. One accelerometer is mounted in the center (also in shaker center) and another one on the side. Accelerometer signal is connected to the oscilloscope to monitor the beam vibration amplitude and the phase difference between accelerometers which determine modal frequency of the beam. For analyzing non-stable sound sources or sources under movement, it is necessary to use rectangular microphone array with microphones assembled in matrix. This configuration is more effective, but also much more expensive. Detailed view of the linear microphone array with the electret microphones mounted in the case, the steel beam and the shaker is in Fig. 6.2.

Figure 6.1: Measurement setup for modal analysis of guided-supported steel beam with linear microphone array for acoustic holography method.

All pressure values measured with microphones have been loaded to the personal computer with data acquisition card NI-6024E and processed with LabVIEW software package. The core of the algorithms in LabVIEW was exported from Matlab environment. The sampling frequency has been set to 8 kHz, which is enough for whole frequency range of acquired acoustic signals. Signals from microphones are synchronized (phase corrected), especially signals obtained in different columns, where there are no direct information about phase shift between each column measurement performed in different time. For this phase correction, one reference microphone has been used. It is mounted very near to the analyzed sound source and it is placed in the same position while the linear microphone array moves from column to column. Phase difference of the signals measured in two different columns can be calculated from the knowledge of correlation between the array microphone signal and the reference microphone signal as mentioned in the first chapter.

6.3 Modal Analysis Results

Measurement of sound field radiated by the vibrating beam has been done for few natural modes of the steel beam mounted on the shaker and excited on the supposed frequencies. For the processing the measured pressure signal in the hologram plane, two acoustic holography algorithms have been selected. There were selected one algorithm based on transformation into wavenumber domain and one algorithm calculating the backward prediction (closed to the surface) directly in spatial domain. The algorithm with Fourier

Figure 6.2: Linear microphone array in the acoustic near field of vibrating steel beam excited by shaker.

transformation was implemented with zero padding of the original hologram and with filtration of high evanescent waves in wavenumber domain with iterative procedure based on Wiener filter. As a representative of the direct calculating algorithm, the SONAH algorithm has been selected.

Each algorithm has specific setting of input parameters to obtain realistic results. One of the most important parameter to set is already mentioned regularization parameter. In the classical algorithm with recursive enhancement with Wiener filter, the regularization is implemented in Wiener filter transfer function. In the denominator of Wiener filter equation, the implementation of regularization parameter has been already done and reduces strong amplification of evanescent waves on very high frequencies and corresponds to signal-to-noise ratio (SNR). If the expected SNR is 60 dB then regularization parameter is set to 0.001. In the SONAH algorithm, the regularization is implemented in least square solution calculation, where identity matrix is adjusted with small constant to achieve reduction of high evanescent waves and reduce the impact of noise and imperfections in input data. The recalculation from SNR to true regularization parameter was based on Hald's recommendations [19]. Absolute values of acoustic pressure (sound pressure level in dB) obtained in near-field and recalculated closely to the beam surface depend on strength of vibrating force generated by the shaker. For localization of nodes and antinodes there are necessary only relative values between peaks and valleys on sound pressure map. The results from acoustic holography calculation were sound pressure and sound intensity fields near the beam surface. The parameters for acoustic holography calculation for this

case have been set experimentally from previous knowledge about amount of noise in the measurement and imperfections of the transducers (microphones). For the classical algorithm, the regularization parameter was set to 0.1, which corresponds to 20 dB SNR, and also for the SONAH algorithm the regularization was set to very similar SNR value (22 dB).

6.3.1 Results - NAH with Spatial Transformations

In Fig. 6.3, there is a map of sound pressure field for the third natural mode of the beam, which is on frequency 625 Hz. The representation is in dB (sound pressure level), so there is no information about direction of the sound waves.
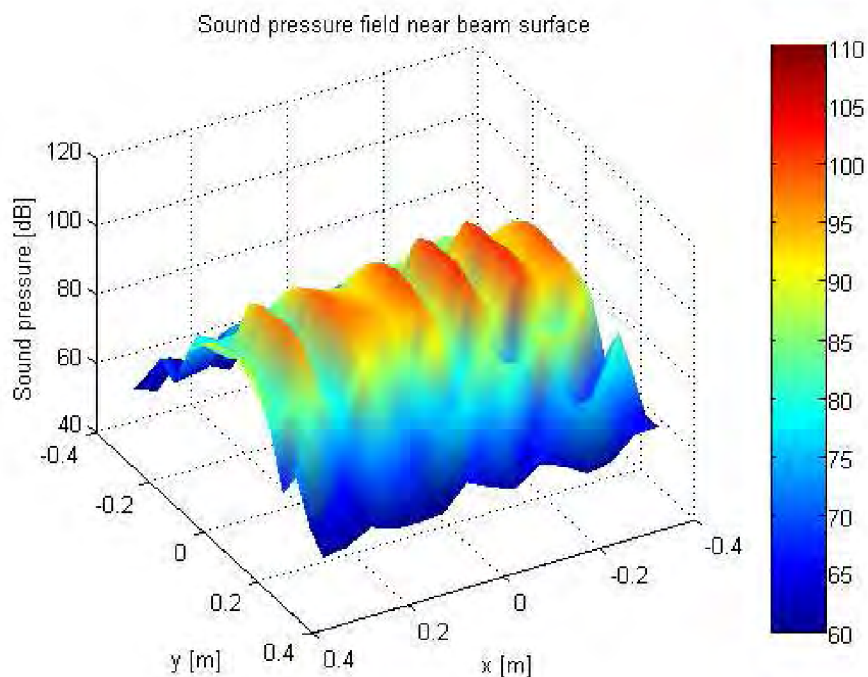

Figure 6.3: Sound pressure field very near (1 cm) from beam surface, vibrating at 625 Hz, classical algorithm.

There can be found only peaks in sound pressure amplitude of all antinodes (with positive or negative phase) together. From the modal theory of the steel beam, the number of antinodes has to be seven and also pressure field near the beam surface has seven peaks (one peak is not so significant, but it is still there - between the second and third).

On the other hand, in Fig. 6.4, there is sound intensity vector field also for third mode and arrows represent the amplitude and directions (phase) of the active intensity vectors. The active intensity is only real part of the sound intensity produced by the beam, and only this part transfer energy to the space.
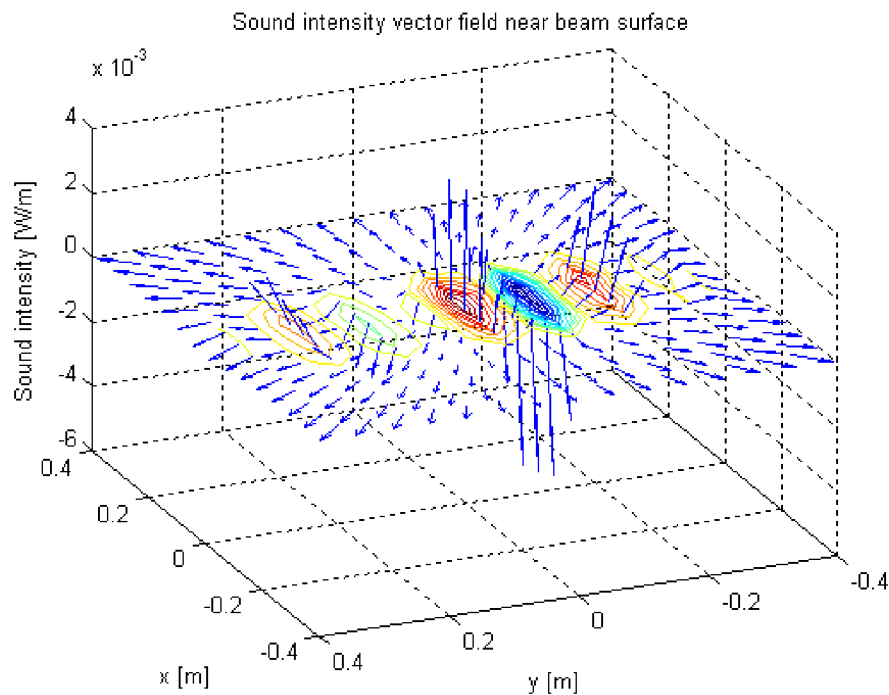
Figure 6.4: Sound intensity vector field very near (1 cm) from beam surface, vibrating at 625 Hz, classical algorithm.

6.3.2 Results - Statistically Optimized NAH

Similar calculation of sound fields very near the beam surface has been performed with SONAH algorithm to verify the results obtained with classical algorithm with spatial transformation. Both, pressure and intensity fields, calculated with the SONAH algorithm with the same test-case provide very similar location of nodes and antinodes, and also the direction of the sound intensity vectors is corresponding to the results with classical algorithm. Sound pressure field (map) very near the beam surface in Fig. 6.5 presents the same distribution of the peaks, which represent nodes and antinodes for the appropriate mode of the vibrations. Absolute values of pressure are corresponding with the values obtained with classical algorithm. With the SONAH calculation larger output (resulting) pressure map can be provided due to avoiding spatial transformations, thus windowing, which reduces useful (and also realistic) area of obtained sound map near vibrating surface.

The third natural mode of the beam has three nodes and four antinodes and it is corresponding to intensity field acquired with the acoustic holography calculation. For better representation, both, the shaker with mounted beam, and sound intensity vector field has been put together, as shown in Fig. 6.7.

Fig. 6.8 is similar to previous one and it represents sound intensity vector field for the second natural mode of the beam, which is on frequency 226 Hz. The number of nodes is four and it is also verified by measurement and acoustic holography calculations.

In the end of the presented results, it is necessary to more describe the theoretical background of used beam setup and mounting to the shaker. All considerations and theoretical calculation has been done for half the beam, because this measurement setup
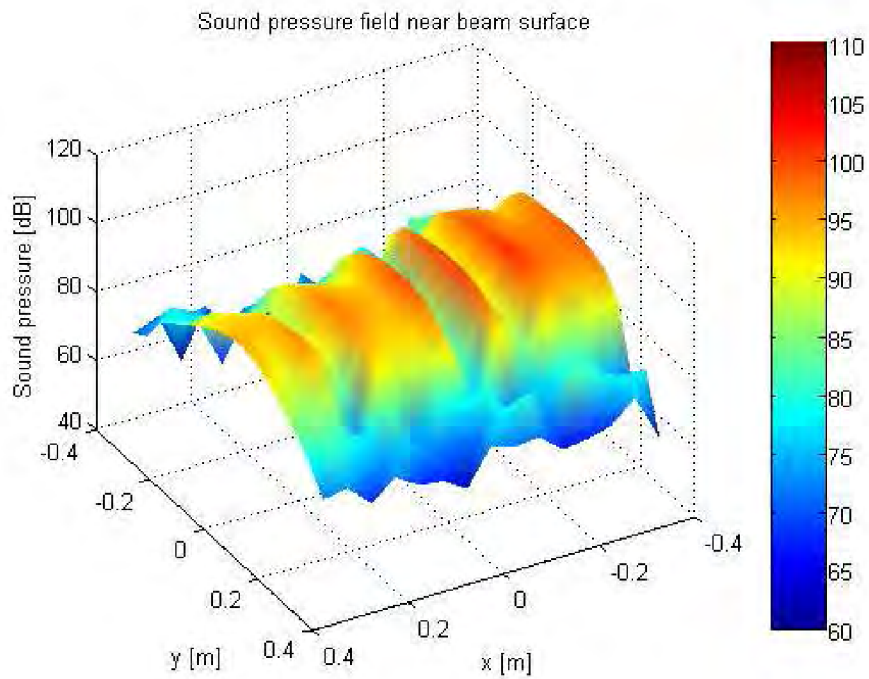
Figure 6.5: Sound pressure field very near (1 cm) from beam surface, vibrating at 625 Hz, SONAH algorithm.
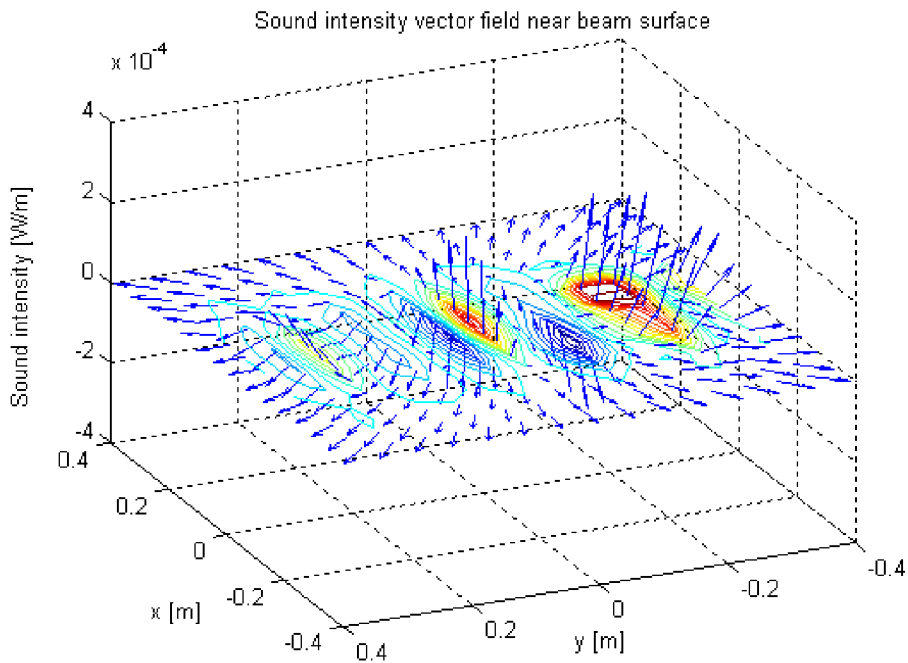

Figure 6.6: Sound intensity vector field very near (1 cm) from beam surface, vibrating at 625 Hz, SONAH algorithm.
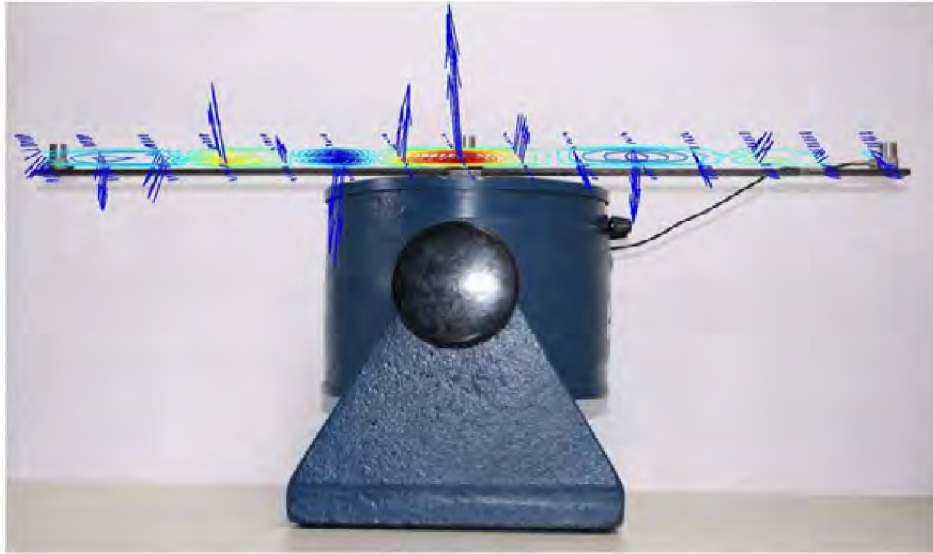
Figure 6.7: Sound intensity vector field above vibrating beam obtained by acoustic holography method, shaker frequency is 625 Hz.
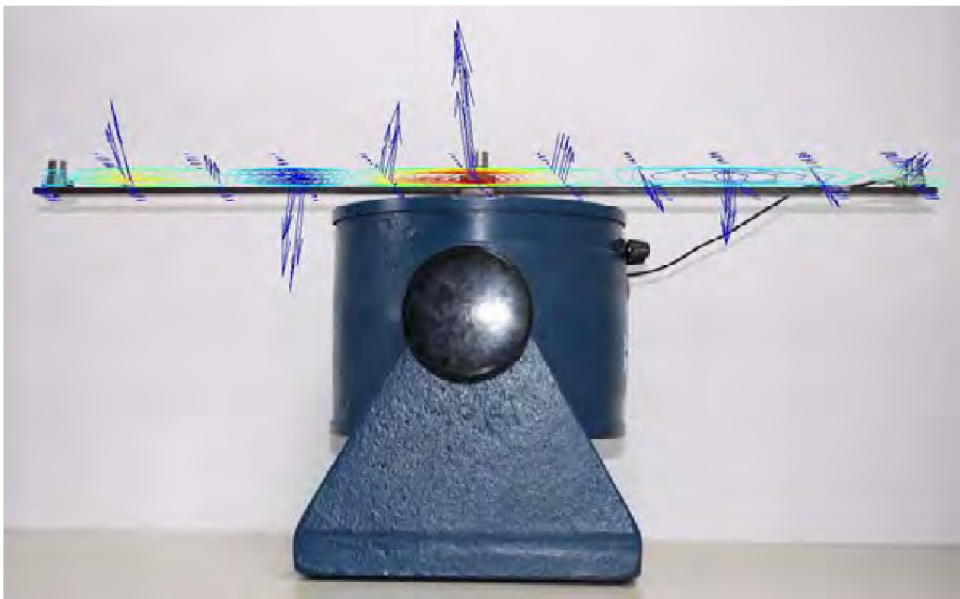
Figure 6.8: Sound intensity vector field above vibrating beam obtained by acoustic holography method, shaker frequency is 226 Hz.

can be described as free-vibrating on the one side and free-guide-supported on the other side (in the center of the shaker). The influence of two virtual beams connected in the center directly above the shaker is neglected, if the symmetry of the beam is ideal (both parts of the beam is same dimensions and with same load applied). Modal analysis of simple free-guide supported steel beam has been preformed with acoustic holography

methods with good results. Localization of nodes and antinodes for two natural modes of the beam has been done. Thus, the acoustic holography can be used for rough vibration analysis of real structures and provides very fast preliminary information for decision of next more complex measurement, where more complicated methods can be used, the LDV for example.

The method with the linear microphone array is suitable for visualization of sound fields produced by constant stable vibrations of non-moving objects. There can be obtained single sound pressure or intensity map time after time only, but no real-time visualization is available. For the on-line real-time visualization of sound fields, the matrix microphone array with optimized algorithms is needed. Application of matrix array to similar modal analysis is planned for future research.

Conclusion and Future Prospects 7

The presented thesis deals with development, optimization and evaluation of near-field acoustic holography algorithms used for vibration analysis. From the huge amount of possible algorithms, the procedures which involve spatial transformation have been selected due to their short computation time with 2D Fourier transformation. After detailed literature study about these holography methods and their improvements, few promising calculation procedures has been selected for further research and application. The tests of each method gives an idea about possible applicability in real measurement condition. The final set of the promising methods contains iterative Wiener filtering, adaptive enlargement of hologram aperture and certainly most simple filtration in k-space. Combination of these methods has been tested on simulations and from evaluation of prediction accuracy the new combined method has been developed.

As a result from this study there has been proposed the new procedure for determination of regularization parameter for NAH algorithms. The regularization significantly influences prediction accuracy of sound field near examined source surface if there is noise in the measurement or if the acoustic sensors are not ideal (amplitude and phase mismatch between sensors). They are not ideal as usual. The method has been successfully evaluated on large set of simulated measurement setups and can estimate signal-to-noise ratio of the input signal in the measured input data. With this information, the setup of subsequent procedures of filtration of unwanted part of the sound spectra (original evanescent waves are affected with the noise and transducer mismatch) is easy and can provide good reconstruction results and accuracy. The procedure involves two different NAH algorithms while each uses different procedure of filtration of the unwanted sound field components. It means that same amount of regularization for both algorithms result in different performance of sound field reconstruction near source surface. If the regularization is ideal (produces lowest prediction error) both algorithms predict same sound field. For this purpose classical NAH algorithm and SONAH algorithm have been used.

To speed up processing with SONAH algorithm which calculates the prediction of sound field directly in spatial domain (involving large matrix multiplication and calculation of Bessel functions) new computer implementation of that algorithm has been developed and later used for determination of proper regularization for NAH. With new implementation, one frequency component is calculated slightly faster than with original implementation, but for other frequencies the calculation is more than 5 times faster. The difference in prediction accuracy between original and new proposed implementation has been also evaluated and is negligible.

The third result of this research was implementation of classical holography algorithm with double layer array measurement and its optimization with similar approaches used in single layer holography to predict sound field near examined source if there is another disturbing source which affects the measured sound field, thus making prediction with single

layer impossible. The procedure separates sound field coming from different sides of the measurement area (measurement planes) and using only partial field for reconstruction. This partial field is related only to examined structure. The algorithm has been optimized for handling noisy data and simulated measurement certify this procedure for separation of sound field and applicability for reconstruction in reverberant fields. This method has been lately extended to measure entering sound field components. It means when the acoustic parameters of the examined source surface is not known, the method tries to estimate these parameters. After successful estimation, separation of sound field can be processed and subsequently calculation of entering sound field (sound energy produced with the examined source).

For large scale measurement, the procedures for combination of each subsequently measured hologram area ("patch") into large one have been also proposed. One procedure combine patches in spatial domain, another one in wavenumber domain. Both methods have been tested on simulated measurement with good results.

Finally, the measurement system for near-field acoustic holography with linear array and with smart, but not expensive, acoustic sensors has been designed and constructed. It uses common electret microphones, built-in preamplifier and electronic memory for storage of TEDS. The system can correct measured values based on information stored in TEDS (for each sensor), thus reduces imperfections of the transducers and amplifiers, as it is strictly required with acoustic holography methods. Also development of matrix microphone array has been successfully preformed. In this case, digital MEMS microphones have been used as a important part of the measurement path. Their main advantages are small size, sufficient sensitivity, digital interface with possibility of sharing one transmission line with two microphones simultaneously.

With similar system with linear array as proposed with this thesis (the older one), the acoustic holography method has been experimentally certified as a possible vibration analysis tool with its main advantages of fast and non-contact measurement. The experimental modal analysis of steel beam mounted on the shaker has been carried out with good results, where positions of nodes and antinodes on the beam surface can be easily determined.

References

[1] 1451.4 IEEE Standard for a smart transducer interface for sensors and actuators — mixed-mode communication protocols and transducer electronic data sheet (TEDS) formats. International standard, IEEE Instrumentation and Measurement Society, New York, USA, 2004.

[2] 20 kHz precision array microphone - Type 4958. Product data, Brüel & Kjær, Nærum, Denmark, 2007.

[3] BAI, M. R. Acoustical source characterization by recursive Wiener filtering. *Journal of the Acoustical Society of America*, vol. 97, no. 5, p. 2957–2663, May 1995.

[4] BAI, M. R. Application of BEM (boundary element method)-based acoustic holography to radiation analysis of sound sources with arbitrarily shaped geometries. *Journal of the Acoustical Society of America*, vol. 92, no. 1, p. 533–549, July 1992.

[5] BÖS, J., KURTZE, L. Design and application of a low-cost microphone array for nearfield acoustical holography. In *Proceedings of the Joint Congress CFA/DAGA'04*, p. 1–2, Strasbourg, France, May 2004.

[6] CHO, Y. T., BOLTON, J. S., HALD, J. Source visualization by using statistically optimized near-field acoustical holography in cylindrical coordinates. *Journal of the Acoustical Society of America*, vol. 118, no. 4, p. 2355–2364, 2005.

[7] Datasheet PU sound probe. Product data, Microflown Technologies, Zevenaar, The Netherlands, 2006.

[8] DONADIO, M. P. CIC filter introduction. Technical report, IEEE, New York, USA, 2000.

[9] FEI, Y., JIAN, C., CHUANXING, B., WEIBING, L., XINZHAO, C. Experimental investigation of sound field separation technique with double holographic planes. *Chinese Journal of Acoustics*, vol. 24, no. 2, p. 111–118, 2005.

[10] FEI, Y., JIAN, C., XINZHAO, C. Sound field separation technique with double holographic planes and its application in the acoustic holography. *Chinese Journal of Acoustics*, vol. 28, no. 5, p. 385–389, 2003.

[11] GOMES, J., JACOBSEN, F., BACH-ANDERSEN, M. Statistically optimised near field acoustic holography and the helmholtz equation least squares method: A comparison. In *Proceedings of the 8th International Conference on Theoretical and Computational Acoustics*, p. 1–10, Heraklion, Crete, Greece, July 2007.

[12] GOMES, J. S. Comparing parameter choice methods for the regularization in the SONAH algorithm. In *Proceedings of EURONOISE 2006*, p. 7–13, Tampere, Finland, 2006.

[13] GOMES, J., HANSEN, P. C. A study on regularization parameter choice in near-field acoustic holography. In *Proceedings of Acoustics'08 Paris Conference*, p. 2875–2880, Paris, France, July 2008.

[14] GOMES, J. S. Double layer microphone array. Master thesis, Department of Physics, University of Southern Denmark, 2005.

[15] GRÄTZ, P. *Vizualizace zvukových polí užitím akustické holografie.* Ph.d. thesis, Brno University of Technology, Brno, April 2003.

[16] GRÄTZ, P. Visualization of sound fields using near-field acoustical holography. *ElectronicsLetters.com - www.electronicsletters.com*, vol. 3, p. 1–12, 2003.

[17] GRÄTZ, P. Iterative near field acoustical holography algorithm. In *Proceedings of the 4th International Carphatian Control Conference ICCC 2003*, p. 10–25, Kosice, Slovakia, 2003.

[18] HALD, J. Planar near-field acoustical holography with arrays smaller than the sound source. In *Proceeding of the 17th ICA Vol. I - Rome 2001*, vol. 1, p. 168–169, 2001.

[19] HALD, J. Patch near-field acoustical holography using a new statistically optimal method. *Brüel & Kjær - Technical Review*, vol. 16, no. 1, p. 40–50, 2005.

[20] HALD, J. Basic theory and properties of statistically optimized near-field acoustical holography. *Journal of the Acoustical Society of America*, vol. 125, no. 4, p. 2105–2120, April 2009.

[21] HALD, J., MORKHOLT, J., HARDY, P., BACH-ANDERSEN, M., KEITH, G. Array based measurement of radiated and absorbed sound intensity components. In *Proceedings of Acoustics'08 Paris Conference*, p. 2899–2904, Paris, France, 2008.

[22] HAVRÁNEK, Z., KLUSÁČEK, S. Identification of regularization parameter for NAH by comparison of results of different NAH calculation methods. In *Proceedings of Inter-noise 2007*, p. 1–9, Istanbul, Turkey, 2007.

[23] HAVRÁNEK, Z., KLUSÁČEK, S. Localization of sound sources in large scale based on multiple patch measurement. In *Proceedings of Inter-noise 2008*, p. 1–11, Shanghai, China, 2008.

[24] HAVRÁNEK, Z. Visualization of sound fields on vibrating steel beam using linear microphone array. In *Proceedings of 6th WSEAS Conference on signal processing, computational geometry and vision*, p. 1–4, Agios Nikolaos, Crete, Greece, 2006.

[25] HAVRÁNEK, Z. Modal analysis of vibrating steel beam by acoustic holography method. *WSEAS Transactions on signal processing*, vol. 1, p. 1–6, 2006.

[26] HAVRÁNEK, Z., JACOBSEN, F. Near-field acoustic holography with double layer array processing. In *Proceedings of EURONOISE 2006*, p. 1–6, Tampere, Finland, 2006.

[27] HAVRÁNEK, Z. Akustická holografie - prostředek pro bezkontaktní analýzu vibrací. *Elektrorevue - www.elektrorevue.cz*, vol. 1, p. 1–16, 2005.

[28] HAVRÁNEK, Z., BEJČEK, L. Local patch acoustic holography methods in enclosed spaces. In *Proceedings of the Acoustics'08 Paris Conference*, p. 1567–1572, Paris, France, 2008.

[29] HERRIN, D. W., MARTINUS, F., WU, W. T., SEYBERT, A. F. A new look at the high frequency boundary element and rayleigh integral approximation. Technical paper, University of Kentucky, Kentucky, USA, 2003.

[30] JACOBSEN, F., DE BREE, H.-E. A comparison of two different sound intensity measurement principles. *Journal of the Acoustical Society of America*, vol. 118, no. 3, p. 1510–1517, September 2005.

[31] JACOBSEN, F., DE BREE, H.-E. A comparison of $p - p$ and $p - u$ sound intensity measurement systems. In *Proceedings of the Eleventh International Congress on Sound and Vibration*, p. 3159–3166, Petersburg, Russia, July 2004. Noise and Vibration Control Society of Russia.

[32] JUHL, P., GOMES, J. A comparison of SONAH and IBEM for near-field acoustic holography. In *Proceedings of Acoustics'08 Paris Conference*, p. 1–6, Paris, France, July 2008.

[33] KIM, Y.-H. Can we hear the shape of a noise source?. In *Proceedings of International Congress on Acoustics ICA 2004*, p. 1–58, Kyoto, Japan, April 2004. The 18th International Congress on Acoustics.

[34] KWON, H.-S., KIM, Y.-H. Minimization of bias error due to windows in planar acoustic holography using a minimum error window. *Journal of the Acoustical Society of America*, vol. 98, no. 4, p. 2104–2111, October 1995.

[35] KWON, H.-S., KIM, Y.-H. Moving frame technique for planar acoustic holography. *Journal of the Acoustical Society of America*, vol. 103, no. 4, p. 1734–1741, April 1998.

[36] MARTINUS, F., HERRIN, D. W., SEYBERT, A. F. Practical considerations in reconstructing the surface vibration using inverse numerical acoustics. Technical paper, University of Kentucky, Kentucky, USA, 2003.

[37] NAM, K.-U., KIM, Y.-H. Errors due to sensor and position mismatch in planar acoustic holography. *Journal of the Acoustical Society of America*, vol. 106, no. 4, p. 1655–1665, October 1999.

[38] PARK, S.-H., KIM, Y.-H. An improved moving frame acoustic holography for coherent bandlimited noise. *Journal of the Acoustical Society of America*, vol. 104, no. 6, p. 3179–3189, December 1998.

[39] SAIJYOU, K., YOSHIKAWA, S. Reduction methods of the reconstruction error for large-scale implementation of near-field acoustical holography. *Journal of the Acoustical Society of America*, vol. 110, no. 4, p. 2007–2023, October 2001.

[40] SCHUHMACHER, A., HALD, J., RASMUSSEN, K. B., HANSEN, P. C. Sound source reconstruction using inverse boundary element calculations. *Journal of the Acoustical Society of America*, vol. 113, no. 1, p. 114–127, January 2003.

[41] SenSound technology - nearfield acoustical holography. Online paper, SenSound, www.sensound.com, 2005.

[42] Sound intensity probe kit - Type 3599. Product data, Brüel & Kjær, Nærum, Denmark, 2008.

[43] Spatial transformation of sound fields - Type 7780. Product data, Brüel & Kjær, Nærum, Denmark, 2005.

[44] WILLIAMS, E. G. *Fourier Acoustics: Sound radiation and Near-field Acoustical Holography.* Academic Press, San Diego, 1999.

[45] WILLIAMS, E. G. Regularization methods for near-field acoustical holography. *Journal of the Acoustical Society of America*, vol. 110, no. 4, p. 1976–1988, October 2001.

[46] WILLIAMS, E. G. Continuation of acoustic near-fields. *Journal of the Acoustical Society of America*, vol. 113, no. 3, p. 1273–1281, 2003.

[47] WILLIAMS, E. G., MAYNARD, J. D. Numerical evaluation of the Rayleigh integral for planar radiators using the fft. *Journal of the Acoustical Society of America*, vol. 72, no. 6, p. 2020–2030, December 1982.

[48] WU, S. F., RAYESS, N. E. Visualizing sound radiation from vehicle front end using the HELS method. *Journal of Sound and Vibration*, vol. 248, p. 963–974, 2001.

[49] WU, S. F., RAYESS, N., ZHAO, X. Visualization of acoustic radiation from a vibrating bowling ball. *Journal of the Acoustical Society of America*, vol. 109, no. 6, p. 2771–2779, June 2001.

[50] WU, S. F., ZHAO, X. Combined Helmholtz equation–least squares method for reconstructing acoustic radiation from arbitrarily shaped objects. *Journal of the Acoustical Society of America*, vol. 112, no. 1, p. 179–188, July 2002.

[51] WU, S. F. Hybrid near-field acoustic holography. *Journal of the Acoustical Society of America*, vol. 115, no. 1, p. 207–217, January 2004.

[52] ADS1278 quad/octal, simultaneous sampling, 24-bit analog-to-digital converters. Product datasheet, Texas Instruments, USA, 2007.

[53] DS2433 4kb 1-Wire EEPROM. Product datasheet, Maxim Integrated Products, USA, 1999.

[54] MAX4175, SOT23, Rail-to-Rail, Fixed-Gain Gainamps/Open-loop op amps. Product datasheet, Maxim Integrated Products, USA, 1999.

[55] NI PXI-7811R R series digital RIO with virtex-II 1M gate FPGA. Product datasheet, National Instruments, USA, 2008.

[56] SPM0405HD digital mini SiSonic^{TM} microphone specification. Product datasheet, Knowles Acoustics, Itasca, USA, 2008.

[57] ĎAĎO, S., KREIDL, M. *Senzory a měřicí obvody.* Vydavatelství ČVUT, Praha, 1996.

Symbols and Abbreviations

Symbols

a	[kg.s^{-1}]	surface acoustic admittance
ATM		acoustic transfer matrix in BEM calculation
ATV		acoustic transfer vector in BEM calculation
c	[m.s^{-1}]	speed of sound (343 m.s^{-1}
c_n		constant in SONAH algorithm
DIF	[%]	difference between results of algorithms
E	[Pa]	Young's module
f	[Hz]	time domain frequency
F	[N]	harmonic point force
G, G_p		Green's function (direct propagator of pressure field)
$G_p i$		inverse Green's function (inverse propagator of pressure field)
G_{pv}		modified Green's function (direct propagator of velocity field)
G		velocity transfer matrix in BEM calculation
H		pressure transfer matrix in BEM calculation
I	[W/m^2]	sound intensity
I		identity matrix
J_0		Bessel function of first kind, zero order
J_1		Bessel function of first kind, first order
k	[m^{-1}]	spatial angular frequency (wavenumber)
K		shape of the wavenumber filter function
K		coefficient/system matrix in GCV function
L	[m]	size of the hologram
$L_e rr$	[dB]	logarithmic error norm
MSE	[%]	error norm in percent
$p, \hat{p}$	[Pa]	complex sound pressure
p_{ent}	[Pa]	complex sound pressure of entering field
p_{inc}	[Pa]	complex sound pressure of incidence field
p_{scatt}	[Pa]	complex sound pressure of scattered field
P		image of sound pressure in wavenumber domain
SNR	[dB]	signal-to-noise ratio
SPL	[dB]	sound pressure level
u_m	[m.s^{-1}]	speed of movement of the array or object
v_n	[m.s^{-1}]	normal component of surface velocity
w	[-]	shape of the spatial window function
W	[-]	Wiener filter function

Δ	[m]	spacing between microphones in array
ε	[-]	regularization parameter for classical algorithms
λ	[m]	wavelength
λ		singular value of transfer matrix
μ	[-]	Poisson constant
∇^2		Laplace operator
ω	[rad.s^{-1}]	angular frequency in time domain
Φ_K		elementary wave
Ψ_j		basis (expansion) function of HELS method
ρ	[kg.m^{-1}]	density of medium (air 1.2 kg.m^{-1})
θ	[-]	regularization parameter for SONAH algorithm

Abbreviations

BEM	Boundary Element Method
CIC	Cascaded Integrator-Comb (filter)
DLA	Double Layer Array
DSP	Digital Signal Processing (Processor)
EEPROM	Electrically Erasable Programable Read Only Memory
FPGA	Field Programmable Gate Array
EI	Entering Intensity
GCV	Generalized Cross Validation
HELS	Helmholtz Equation Least Squares
IBEM	Inverse Boundary Element Method
LDV	Laser Doppler Vibrometry
MEMS	Micro Electro-Mechanical System
MSE	Mean Square Error
NAH	Near-field Acoustic Holography
NI	National Instruments
PXI	PCI Extension for Instrumentation
RIO	Reconfigurable Input Output
SLA	Single Layer Array
SNR	Signal to Noise Ratio
SONAH	Statistically Optimized Near-field Acoustic Holography
SVD	Singular Value Decomposition
TEDS	Transducer Electronic Data Sheet
TSVD	Truncated Singular Value Decomposition

Curriculum Vitae

Personal Information:

Name:	Zdeněk Havránek
Date and place of birth:	29th June 1980 in Třebíč, Czech Republic
Address:	Karlov 200, 595 01 Velká Bíteš, Czech Republic
E-mail:	havranek@feec.vutbr.cz

Education:

2003 - 2009	Brno University of Technology, Faculty of Electrical Engineering and Communication, Doctoral degree program Cybernetics, Automation and Measurement at Department of Control and Instrumentation,
1998 - 2003	Brno University of Technology, Faculty of Electrical Engineering and Computer Science, Master's degree program Electrical Engineering and Computer Science, specialization in Cybernetics, Automation and Measurement, completed in June 2003 with final state exam and thesis defence, awarded with the title Engineer. Study completed with honors and dean's prize,
1994 - 1998	SPŠE Brno, High School of Electrical Engineering, specialization in Automation and Measurement.

Internships & Work Experience:

2006 - present	Department of Control and Instrumentation, Faculty of Electrical Engineering and Communication, Brno University of Technology - technician and research assistant, partial work on european project CREDO - Cabin noise Reduction by Experimental and numerical Design Optimization.
2005 - 2006	half-year research fellowship at Denmark Technical University, Department of Acoustic Technology, under supervision of Assoc. Prof. Finn Jacobsen, project work in the field of Near-field Acoustic Holography.

Projects:

2006 - 2009	co-solver of the FP6 european project CREDO "Cabin noise reduction by Experimental and Numerical Design Optimization" development and testing of new acoustic holography methods,
2005 - 2008	co-solver of the grant GA 102/06/1617 "Modern approach to vibration measuremen",
2006	solver of the grant FRVS G1/3265 "Acoustical Holography - non-contact vibration analysis",
2005	co-solver of the industrial project "Software for automated data processing".

Professional Interest:

- Vibration and Noise Measurement,

- Near-field Acoustic Holography,

- Non-contact Technical Diagnostics,

- Measurement of Non-electrical Quantities,

- Smart Sensor Design and Interfacing,

- Data Acquisition, Measurement Hardware,

- Programming of Embedded Systems.